

REPRODUCTION COPY

2

GL-TR-89-0232

On Gravity Prediction Using Density and Seismic Data

Gunter W. Hein
Klaus Hehl
Bernard Eissfeller
Michael Ertel
Wolfgang Jacoby
Dirk Czerwek

AD-A231 896

University of the Federal Armed Forces, Munich
Institute of Astronomical & Physical Geodesy
Werner-Heisenberg-Weg 39
D-8014 Neubiberg
FEDERAL REPUBLIC OF GERMANY

1 July 1989

Final Report
June 1987-June 1989

DTIC
ELECTE
FEB 14 1990
S B D

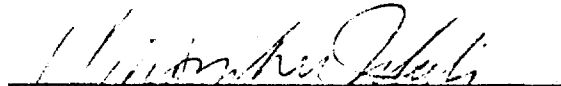
APPROVED FOR PUBLIC RELEASE; DISTRIBUTION UNLIMITED

GEOPHYSICS LABORATORY
AIR FORCE SYSTEMS COMMAND
UNITED STATES AIR FORCE
HANSCOM AIR FORCE BASE, MASSACHUSETTS 01731-5000

*Original contains color
plates; All DTIC reproductions
will be in black and
white*

91 2 13 023

"This technical report has been reviewed and is approved for publication"



CHRISTOPHER JEKELI

Contract Manager



THOMAS P. ROONEY

Branch Chief

FOR THE COMMANDER



DONALD H. ECKHARDT

Division Director

This report has been reviewed by the ESD Public Affairs Office (PA) and is releasable to the National Technical Information Service (NTIS).

Qualified requestors may obtain additional copies from the Defense Technical Information Center. All others should apply to the National Technical Information Service.

If your address has changed, or if you wish to be removed from the mailing list, or if the addressee is no longer employed by your organization, please notify GL/IMA, Hanscom AFB, MA 01731. This will assist us in maintaining a current mailing list.

Do not return copies of this report unless contractual obligations or notices on a specific document requires that it be returned.

REPORT DOCUMENTATION PAGE			Form Approved OMB No. 0704-0188	
<small>Instructions: This report is the property of the Government and is loaned to your agency; it and its contents are not to be distributed outside your agency. This report is to be maintained in accordance with the instructions in the report. This report is to be maintained in accordance with the instructions in the report. This report is to be maintained in accordance with the instructions in the report.</small>				
1. AGENCY USE ONLY (leave blank)	2. REPORT DATE 1 July 1989	3. REPORT TYPE AND DATES COVERED Final Report (June 1987-June 1989)		
4. TITLE AND SUBTITLE On Gravity Prediction Using Density and Seismic Data			5. FUNDING NUMBERS PE 61102F PR 2309 TA GI WU BU Contract AFOSR-87-0271	
6. AUTHOR(S) Gunter W. Hein Klaus Hehl Bernard Eissfeller			Michael Ertel Wolfgang Jacoby Dirk Czerwek	
7. PERFORMING ORGANIZATION NAME(S) AND ADDRESS(ES) University of the Federal Armed Forces, Munich Institute of Astronomical & Physical Geodesy Werner-Heisenberg-Weg 39 D-8014 Neuburg, FEDERAL REPUBLIC OF GERMANY			8. PERFORMING ORGANIZATION REPORT NUMBER	
9. SPONSORING/MONITORING AGENCY NAME(S) AND ADDRESS(ES) Geophysics Laboratory Hanscom AFB, MA 01731-5000			10. SPONSORING/MONITORING AGENCY REPORT NUMBER GL-TR-89-0232	
11. SUPPLEMENTARY NOTES				
12a. DISTRIBUTION AVAILABILITY STATEMENT APPROVED FOR PUBLIC RELEASE; DISTRIBUTION UNLIMITED			12b. DISTRIBUTION CODE	
13. ABSTRACT (Maximum 200 words) In the approximation of the earth's gravity field, in particular, in gravity prediction, geophysical information in the form of density and seismic data is mainly used indirectly in geodesy for gravity smoothing procedures. Moreover, mostly globally averaged model assumptions are used for density and Mohorovičić discontinuity. Following the need for an improved knowledge of the gravity field the study tries to outline possible models and algorithms how to use nowadays available digital (surface) density models as well as seismic velocities and displacements in unified prediction approaches. Central role hereby plays the establishment of a (numerically reasonable) mathematical/physical relationship between the geophysical observations and data, respectively, and the gravity (disturbing) potential. Since these considerations are closely				
14. SUBJECT TERMS Gravity prediction Crustal density models Seismic velocity models		Integrated prediction algorithms Inverse problem		15. NUMBER OF PAGES 154
				16. PRICE CODE
17. SECURITY CLASSIFICATION OF REPORT Unclassified	18. SECURITY CLASSIFICATION OF THIS PAGE Unclassified	19. SECURITY CLASSIFICATION OF ABSTRACT Unclassified	20. LIMITATION OF ABSTRACT SAR	

connected with the so-called gravimetric inverse problem, extended computations were carried out in the European Alps in order to verify already established (model) relationships.

After discussing various possibilities for the consideration of density in an integrated geodetic adjustment, a new approach is presented using the physical relationship, namely Newton's attraction integral, for the construction of the necessary auto- and crosscovariances when treating anomalous density as a stationary random process. Isostatic response theory as developed by Dorman/Lewis as a generalization of Vening Meinesz' isostasy model is introduced in the derivation and also proposed as deterministic predictor. The empirical relationship between seismic velocities and density as well as gravity is thoroughly investigated. Starting from the wave equation for an inhomogeneous medium seismological displacements are used forming a stochastic process.

For the various numerical investigations geophysical and geodetic/gravimetric data were collected in a local area as well as over the European Alps. Geophysical models of the Moho, the seismic basement, and the depth of the lithosphere as well as a threedimensional P wave velocity model are developed.

Numerical tests in gravity prediction are carried out mainly using the attenuated white noise gravity covariance model and quasi-harmonic inversion.

FOREWORD

This report was prepared by Günter W. Hein in cooperation with the research associates Dr. Bernd Eissfeller, Dipl.-Ing. Michael Ertel and Dipl.-Ing. Klaus Hehl. The geophysical parts were contributed by Prof. Dr. Wolfgang Jacoby and Dipl.-Geoph. Dirk Czerwek, Universität Mainz, Institut für Geowissenschaften. In particular, chap. 3 is based on their work. The final report was edited by Dipl.-Geogr. Monika Jennert.

The study was partially sponsored by the Air Force Office of Scientific Research, Air Force Systems Command, USAF, under grant AFOSR-87-0271. It is administrated by the Air Force Geophysics Laboratory, Hanscom Air Force Base, Massachusetts, with Dr. Christopher Jekeli, Scientific Program Officer.



Accession For	
NTIS GRA&I	<input checked="" type="checkbox"/>
DTIC TAB	<input type="checkbox"/>
Unannounced	<input type="checkbox"/>
Justification	
By _____	
Distribution/	
Availability Codes	
Dist	Avail and/or Special
A-1	

ACKNOWLEDGEMENTS

Several people and institutions contributed to this report in providing data. Especially the large amount of data over the European Alps could not have been used without the generous support and assistance of Univ.-Prof. Dr. techn. Dipl.-Ing. Hans Sünkel, Technische Universität Graz, Austria. Prof. Dr. K. Fahlbusch, Technische Hochschule Darmstadt (F.R. Germany) provided through own investigations and field work the density data in the "Rossdorf" test area. Discussions with Prof. Christian Tscherning, Copenhagen, are gratefully acknowledged. We are grateful to the Italian petrol company AGIP (Milano, Italy), Univ.-Prof. Dr. techn. Dipl.-Ing. K. Bretterbauer (Technische Universität Vienna, Austria), Bureau Gravimétrique Internationale (Toulouse, France), Deutsches Geodätisches Forschungsinstitut (Munich, F.R. Germany), Gruppe für Rüstungsindustrie (Bern, Switzerland), Industriebetriebe Betriebsgesellschaft (Munich, F.R. Germany), Institut für Angewandte Geodäsie (Frankfurt, F.R. Germany), Univ.-Prof. Dr. techn. Dipl.-Ing. B. Hofmann-Wellenhöf (Technische Universität Graz, Austria), Univ.-Prof. Dr. H.-G. Kahle (Eidgenössische Technische Hochschule, Zürich, Switzerland), Prof. Dr. S. Plaumann (Niedersächsisches Landesamt für Bodenforschung, Hannover, F.R. Germany), Prof. Dr. F. Sansò (Politecnico di Milano, Italy), Dr. G. Walach (Institut für Geophysik, Montanuniversität Leoben, Austria) for providing data.

The initial part of this research, in particular the isostatic investigations and computations for the inverse gravitational problem over the European Alps were supported by the German Research Foundation (Deutsche Forschungsgemeinschaft). Gravity prediction investigations were supported by Air Force Geophysics Laboratory, Hanscom, Mass.

TABLE OF CONTENTS

Page

1. Introduction	1
2. Definition of the problem	5
3. The influence of seismic structures on the gravity field: The geophysicist's view	8
3.1 Computation of the gravity effect of given model bodies	9
3.2 Computation of geoid undulations caused by model mass anomalies	11
3.3 Estimation of the normal values for crustal parameters	12
3.4 Two-dimensional model computations	15
3.5 Three-dimensional model computations	18
3.6 Velocity-density systematics	25
4. A brief survey of proposed (geodetic) approaches in the past	34
5. The integrated geodesy adjustment model	37
6. Density in an integrated geodetic approach	42
6.1 Minimum norm solutions	42
6.2 The attenuated white noise statistical gravity model	46
6.3 A new approach to link gravity and density	50
6.3.1 <i>Newton's attraction integral</i>	50
6.3.2 <i>The isostatic response function in space-domain representation</i>	51
6.3.3 <i>The isostatic response function in frequency-domain representation</i>	53
6.3.4 <i>The power spectral model for gravity anomalies (disturbances)</i>	53
6.3.5 <i>The gravity disturbance covariance model</i>	55
6.3.6 <i>Inferences for gravity prediction applications</i>	56
6.4 Reference (normal) density models	58
7. Seismic and seismological data in an integrated approach	61
7.1 Simple seismic velocity-density relationship in a homogeneous medium	61
7.2 Seismic wave motion in an inhomogeneous medium	63
7.3 A possibility of evaluating the autocovariance function of density anomalies from seismic observations	69

8. Test data	72
8.1 Test network "Rossdorf"	72
8.2 Test area "European Alps"	76
8.2.1 <i>Topography</i>	76
8.2.2 <i>Gravimetric observations</i>	78
8.2.3 <i>Astronomical observations</i> <i>(deflections of the vertical)</i>	81
8.2.4 <i>Seismic data</i>	81
8.2.5 <i>Depth of the seismic basement</i>	87
8.2.6 <i>Depth of the Mohorovičić discontinuity</i>	88
8.2.7 <i>Thickness of the lithosphere</i>	96
8.2.8 <i>Perturbations of seismic velocities</i>	97
8.2.9 <i>Digital density model</i>	103
9. Numerical investigations	106
9.1 Prediction of gravity anomalies in test area "Rossdorf"	106
9.2 Prediction of gravity anomalies in the European Alps	114
10 Conclusions	119
Appendix A	121
References	139

1. INTRODUCTION

The *determination of the gravity field* is one of the major tasks of geodesy besides precise positioning. Especially in the last two decades great progress could be achieved. On the one side *satellite observations* became available which contributed significantly to the construction and improvement of global earth models (*SZABO 1986*). The best of those are nowadays complete to degree and order $m = n = 360$ (*RAPP, CRUZ 1986*) corresponding to a resolution of $30' \times 30'$ mean gravity anomalies, say $50 \times 50 \text{ km}^2$. Satellite altimetry has reversed the state of global knowledge of the gravity field with respect to land and oceans. Whereas still in the 1960's the gravity field over land was much better known than over sea, now the opposite became true.

On the other side *integrated data processing* techniques were developed which are able to give best estimates by combining all available geodetic observations. Their field of application can be found more or less in the local or regional range. *Least-squares collocation* and *integrated geodesy adjustment*, first developed and proposed by *KRARUP (1969)*, *EEG, KRARUP (1979)*, are the key developments on this theoretical and data analysis side.

Despite of these great achievements on the observation recovery and the analysis side, the demands grow further for a better resolution and accuracy of the earth's gravity field. With respect to global aspects the needs are coming from satellite geodesy where most missions require an orbit determination in the submeter- or even decimeter level. They are coming from oceanic circulation investigations, sea-level variability studies and marine geophysics. Crustal dynamics and plate tectonic research has to be mentioned, too. On the regional or local scale the advent of the Global Positioning System has started a revolution in surveying techniques. Although the measurements yield threedimensional positions, the height problem cannot be solved due to its dynamical character. Thus, precise geoid heights - nothing else than a functional of the geopotential - have to be known in order to derive, for example, orthometric heights from GPS ellipsoidal heights. A method which can lead to a replacement of the traditional spirit levelling, so far physical geodesy is able to provide the geoid with sufficient accuracy. Prerequisite again is the precise knowledge of gravity (anomalies) and/or vertical deflections in those areas.

What is the state-of-the art in the knowledge of the gravity field? Although due to satellite altimetry nearly a complete gravity coverage over the oceans can be used for the construction of global earth models, there are still something like $5500 10^6 \times 10^6$ blocks over land where mean gravity values for certain reasons are not available. This corresponds to

approximately one third of the earth's land surface (see Fig.1.1). Those gaps have to be filled by so-called *geophysical anomalies*, that means that the gravity anomaly values have to be estimated on the basis of geophysical information and models. There is no doubt that an improvement in those procedures and gravity values, respectively, results in more accurate global geopotential models.

Approximation methods like collocation are able to combine different geodetic and gravimetric observations to determine the gravity field and its functionals with wavelengths smaller than the resolution of the global earth models. Mainly, gravity (anomalies) and astronomic latitudes and longitudes (deflections of the vertical) are combined. For gravity anomaly interpolation a certain reduction has to be carried out in order to perform the real numerical computations in a smooth field, often referred to as "remove-restore" technique. For the determination of the geoid as a boundary value problem, gravity and other data have to be reduced down to the geoid. For both purposes mentioned before digital terrain models have to be available and rock density assumptions are necessary. Although the gravity field is caused by mass irregularities within the earth – see Newton's law of gravitation – geodetic/gravimetric algorithms for the determination of the gravity field (prediction, interpolation, etc.) do not use geophysical data, like density and mass distribution to construct the gravitational potential,

$$V(\underline{x}) = G \iiint_{v_E} \frac{\rho(\underline{y})}{|\underline{x} - \underline{y}|} dv_E(\underline{y}) \quad (1-1)$$

where G is the gravitational constant, v_E is the volume of the earth E , ρ is the density and \underline{x} , \underline{y} are threedimensional position vectors.

The imperfect knowledge of the density distribution within the earth, however, results in the fact, that the gravitational potential outside the earth has to be determined by solving a boundary value problem with gravity anomalies as boundary data, for example.

For both methods, smoothing as well as reduction, density assumptions have to be made. In case of isostatic gravity anomalies even hypotheses on the model of isostatic compensation and the depths of the Mohorovičić-discontinuity are necessary to perform the necessary computations. Thus, the geophysical (model) data are used *indirectly* in geodesy. With increasing observations in seismics, geophysics is nowadays able to give reasonable density values or seismic velocity information for whole regions. An excellent example is the *digital surface density model* of WALACH (1987). Often also density values at discrete locations are available. This seems to be now the time to think about the *direct*

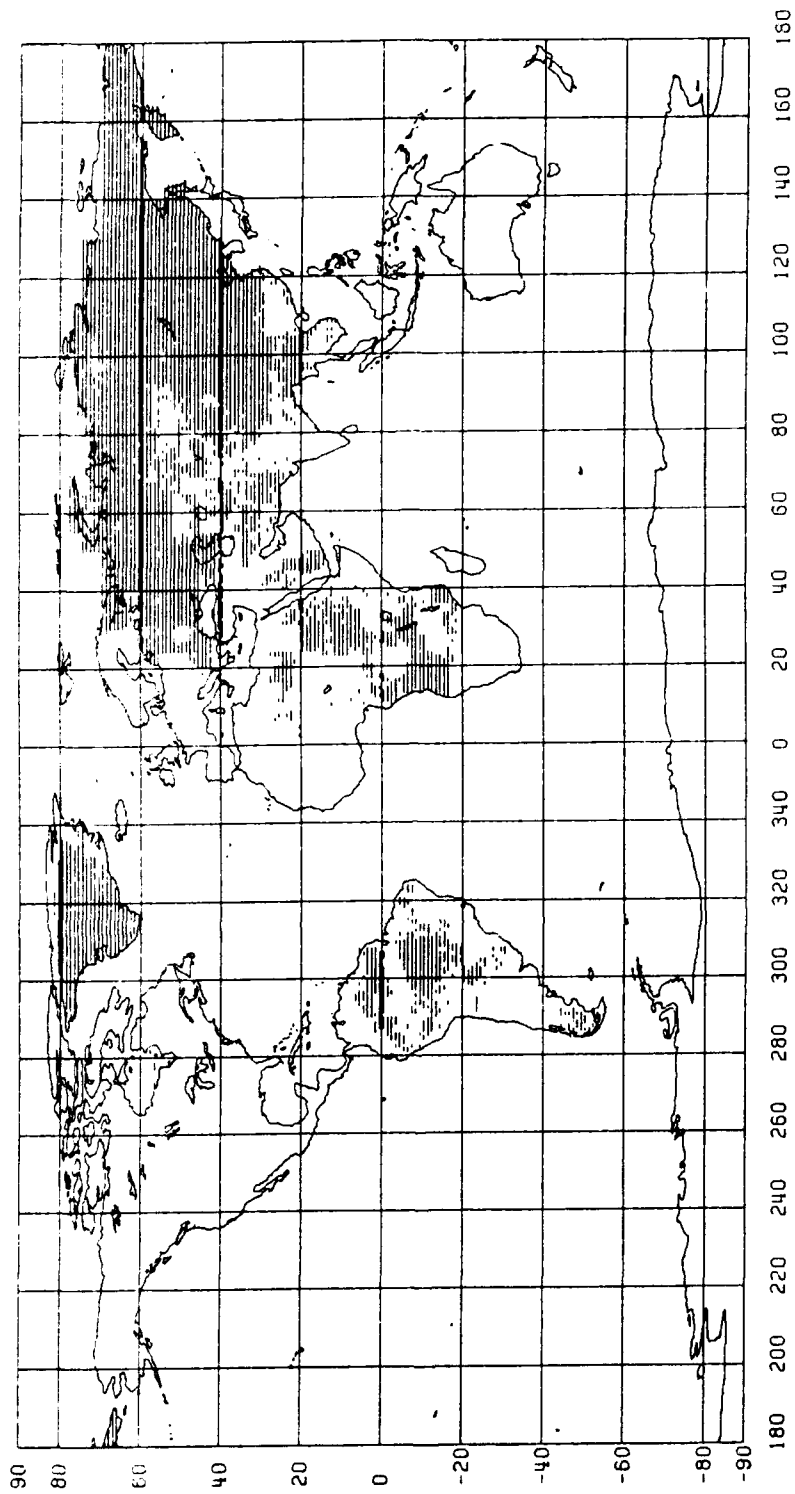


Fig. 1.1. Locations of the 6331 geophysically predicted $1^{\circ} \times 1^{\circ}$ mean gravity anomalies $\bar{\Delta}$ (File: JUN86.TUG87.DMAMOES7, RAPP 1989, pers. comm.).

use of geophysical data in geodetic approximation methods for the determination of the gravity field. First proposals in the last years are reviewed in chap. 4. Two warnings are always coming from geophysicists when we try to use those available density data and establish a certain mathematical/physical relationship between density and gravity (see also chap. 2).

Density is varying with depth and can change drastically also in lateral direction. Consequently, it is very hard to establish a density model. No doubt, it has to be threedimensional. The need of geodesy, to generalize the density information – both, laterally in the form of certain mean blocks, and vertically, in the form of a minimum of layers – implies a certain loss on geophysical information. It is, however, required for the sake of numerical handling of the problem in the computer. Insofar, a digital model of (surface) rock densities has its problem. What does surface density mean? Obviously, the first some hundred meters down to sea-level are characterized: a small distance compared to the earth's radius.

Due to the complexity of the earth's crust *a simple mathematical relationship between density ρ and gravity with sufficient accuracy exists only locally, $g = f(\rho)$.* However, the problem in opposite direction, $\rho = f(g)$ is *ambiguous* and usually called "*inverse problem*" in geophysics.

Nevertheless, (more details are outlined in the next chapter on the definition of the problem), in view of all those generalizations and approximations which have to be made, it is better to use such density information, for example, in gravity (anomaly) interpolation than to leave the gravity gaps white or to use globally averaged estimates like $\rho = 2.67 \text{ g cm}^{-3}$. Even probabilistic approaches are justified ("When in doubt, smooth", Sir Harold Jeffreys).

This report proposes some first (simple) ideas, proposals, and approaches how to use geophysical data in the determination of the earth's gravity field and its functionals (gravity, deflections of the vertical, geoid heights). Numerical investigations with real data are especially carried out in the field of gravity interpolation.

2. DEFINITION OF THE PROBLEM

We will assume that we have made the following *measurements on the earth's surface (or in space)*,

- gravity g , astronomic latitude Φ , astronomic longitude Λ , gravity gradients $\partial^2 W / \partial x_i \partial x_j$ (second-order derivatives of the gravity potential) or, in other form, after subtracting reference- or model-(normal) values:
gravity anomalies Δg , components of deflections of the vertical in north-south and in east-west direction (ξ, η) , resp., anomalous gravity gradients $\partial^2 T / \partial x_i \partial x_j$.

We further assume, that *geophysical information* is available, in detail,

- density data, characterizing as discrete point or mean block values over a certain lateral area a specified layer of the earth's crust,
- seismic velocities v , referring as representative values to certain portions or layers within the earth's crust,
- seismic displacements.

In the ideal case density and seismic velocities are given in the form of a three-dimensional digital model.

We are looking for a solution for the *gravity potential W* (or disturbing potential T) *outside the earth by combining all available geodetic and geophysical information* as mentioned above. From this representation of W (or T) we like to derive all functionals, like gravity anomalies, deflections of the vertical, geoidal heights, etc.

A good *example* for the problem stated above in the real world would be the prediction of gravity anomalies in unsurveyed areas (without gravity observations) where, however, density estimates and/or seismic velocities either from geophysical investigations are available, or where a reasonable guess of the density variation based on geological features can be made. In addition, gravity values in the surrounding areas are available which could be considered in a combination solution.

Central point in such a solution algorithm is the mathematical-physical foundation of the relationship

seismic velocity $v \mapsto$ density $\rho \mapsto$ gravity g (or gravity potential W).

It was already mentioned that the determination of internal masses from (surface) gravity data, $\rho = f(g)$, has no unique solution and is treated in geophysics as so-called *inverse problem*.

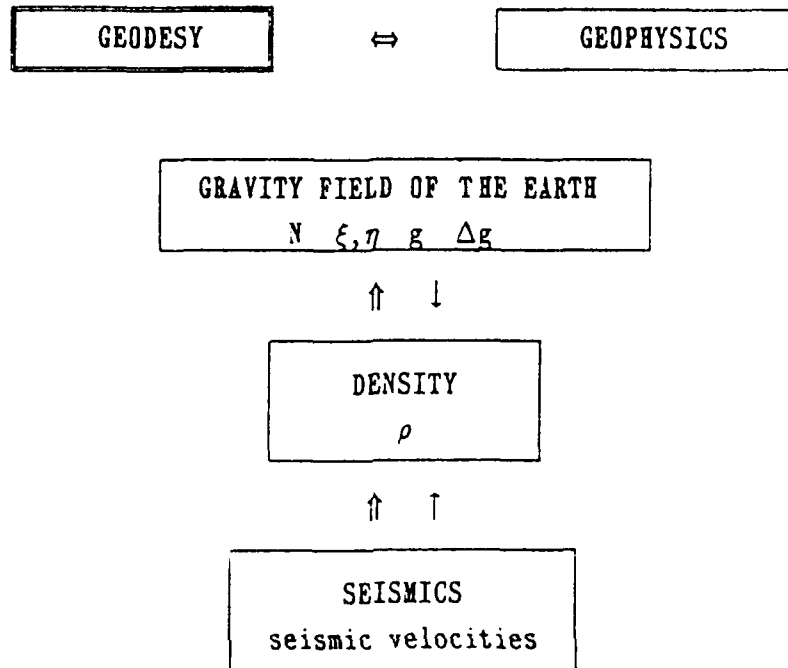


Fig. 2.1. Gravity, density, and seismic data in geodesy and geophysics (the corresponding arrows indicate the main goals and working directions of geodesy (\Rightarrow) and geophysics (\rightarrow)).

There are, however, two major differences to geophysics in our task which are also illustrated in Fig. 2.1. First, we are only interested in the solution in the one direction $v \rightarrow \rho \rightarrow g$. A fully established, mathematically and physically correct *inverse* relationship or solution is not of primary interest for us, since we are only interested in the improvement of the exterior gravity field. It may be possible, for example, that a certain relationship between ρ and g leads to a reasonable solution for $g = f(\rho)$; however, the inverse-relationship applied in the algorithm may yield unacceptable results. The second point which should be raised here when defining the problem is the following. If we are faced with the problem that *no* gravity observations are available in certain regions of the world even a guess of the geological/geophysical situation may help in the prediction of smoothed gravity values and may be better than to use zero-values in the spherical harmonics solution of an earth model. It is obvious, that for such a task some kind of generalization has to take place which may drastically smooth local geophysical features.

Finally, we have to decide on the character of the relationship $v \rightarrow \rho \rightarrow g$. Should we define it in the deterministic way or is it opportune to apply the concept of random processes in such a (prediction) algorithm. There are good reasons to vote for the last. Gravity field determination involves functions, or better functionals like geoid heights, gravity disturbances, deflections of the verticals, etc. which have to be evaluated from the same source. Our knowledge about the interior of the earth and the needed mathematical/physical relationships are limited. Thus, the concept of probability enters to some extent into our problem. Even from the (visual) distribution of the masses within the earth one might think of some irregular distribution which justifies the application of stochastic or random theory. No doubt, that it would also extend the already applied concept of geodetic collocation in integrated geodesy. These arguments all have led us to the decision to look – besides other deterministic methods – also for an (overall) stochastic concept.

3. THE INFLUENCE OF SEISMIC STRUCTURES ON THE GRAVITY FIELD: **THE GEOPHYSICIST'S VIEW**

In order to use geophysical data for gravity interpolation we have to understand more in detail the underlying mathematical/physical relationship between the corresponding observations. Since those relations often have model character or represent simplified physics it is worthwhile to verify them also with real data. Therefore this chapter mainly tries to investigate available models and includes also some inverse computations determining density contrasts between the different layers of the earth's crust.

The layer boundaries determined from seismic or seismological data are the most direct evidence for physical inhomogeneity within the earth's crust and upper mantle. Since density tends to correlate with seismic velocity, undulating layer boundaries are very likely to influence the gravity field. The recently released digital density models, see, e.g., *WALACH (1987)*, represent, however only surface densities. In spite of their rather exact knowledge they cannot be reliably continued downward. More knowledge about the density distribution at depth is necessary, if we want to compute and improve the gravity field and its functionals.

The most important and widely accepted way to determine the rock densities at depth is to apply the velocity-density systematics or relationships. They are based on experimental laboratory measurements (e.g., *BIRCH 1960, 1961; LIEBERMANN, RINGWOOD 1973*) or on solid state physical theory (e.g., *BIRCH 1979; ANDERSON 1973*). Another approach is the inversion of gravity data with the assumption of "known" geometrical structure, e.g., from seismic studies, and the additional assumption that bodies of constant seismic velocity are also uniform in density (e.g., *JACOBY 1973, 1975*).

We must note, however, that gravity, as any potential field, cannot be inverted unambiguously but that in principle there is an infinite number of solutions. Nevertheless the number can be drastically reduced by adding information, e.g., from geology, and seismic or other geophysical information. If the structure of the crust is sufficiently known, the gravity effect of finite parts, e.g., bodies or layers, can be computed at any surface points. If only their densities are unknown, one may determine them with the aid of the least-squares method by fitting the computed sum of the individual bodies to the observations. Subsequently one may relate the density variation found with the already known seismic velocities to determine the velocity-density systematics. From this, it is hoped, the physical state and the chemical and petrological composition of the earth's interior will be better understood.

In principle, it should be possible to extend this method to gravity prediction. If the gravity field is known incompletely, e.g., only in parts of a region or only in its long wavelength components, but published seismic models are fairly detailed, one may attempt the following approach. First find the best fitting densities as sketched above and then compute the gravity anomalies and/or geoid undulations that are caused by the seismic structure with the density variation determined. However, whether this approach is successful has to be tested with practical examples.

3.1 Computation of the gravity effect of given model bodies

The starting point for the computation of the gravity effect of given masses is the contribution of an infinitesimal mass element dm to the gravitational potential δV . It can be expressed as:

$$\delta V(\underline{x}) = G \iiint_V \frac{dm}{|\underline{x} - \underline{y}|} \quad (3-1)$$

where G is the universal gravitational constant ($(6.673 \pm 0.003) \times 10^{-8} \text{ g}^{-1} \text{ cm}^3 \text{ s}^{-2}$), and the vectors $\underline{y} = \{\xi, \eta, \zeta\}$ and $\underline{x} = \{x, y, z\}$ represent the coordinates of the mass element and the observation point (where the gravity effect is to be calculated), respectively (see Fig. 3.1).

Differentiating equation (3-1) with respect to z (vertical downward) assuming a local cartesian threedimensional coordinate system and expressing $|\underline{x}-\underline{y}|$ by their components renders the gravity effect δg of the mass body (density is denoted by ρ)

$$\delta g(\underline{x}) = \delta V_z(\underline{x}) = G \int_{\xi} \int_{\eta} \int_{\zeta} \frac{\rho(\xi, \eta, \zeta)(\zeta - z)}{[(\xi - x)^2 + (\eta - y)^2 + (\zeta - z)^2]^{1.5}} d\xi d\eta d\zeta. \quad (3-2)$$

The integral (3-2) can be most easily computed for two-dimensional masses. Such masses can be represented by a polygon (with j corners) in the normal section of the mass which is assumed to be infinite horizontally at the right angle to the section. According to *JUNG (1961)* the gravity effect at the point P of a triangular section with apex $P(\underline{x})$ is (see Fig. 3.2 for the notation and corresponding quantities):

$$\delta g(\underline{x}) = 2 G \rho (n - x) \sin \alpha \left[\sin \alpha \ln \frac{\sin(\alpha + \varphi_A)}{\sin(\alpha + \varphi_B)} + \cos \alpha (\varphi_B - \varphi_A) \right]. \quad (3-3)$$

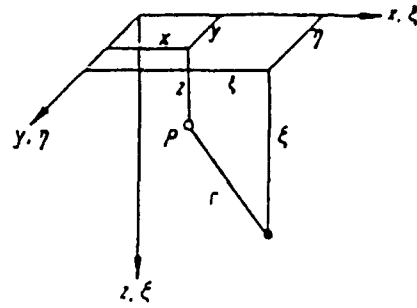


Fig. 3.1. Coordinate system for calculating gravity and geoid

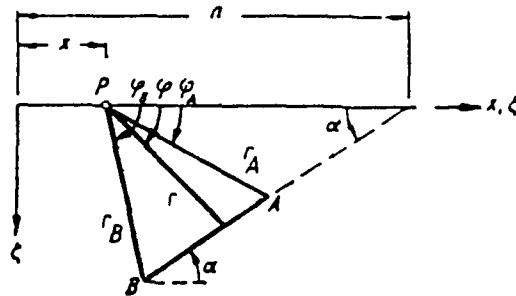


Fig. 3.2. Integration of a triangle (two-dimensional body)

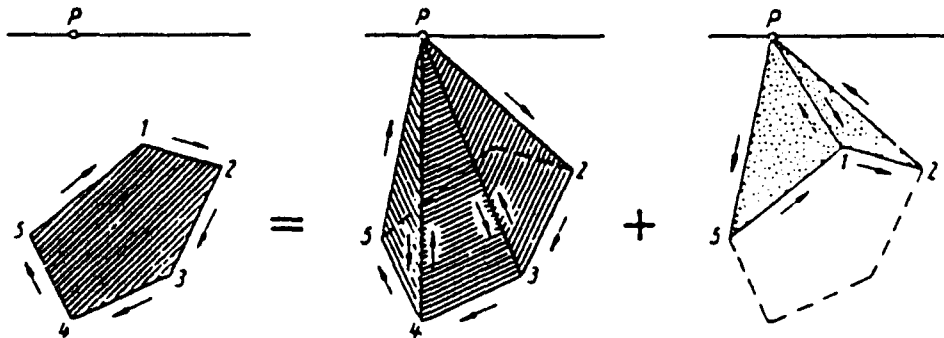


Fig. 3.3. The effect of two-dimensional bodies represented as a polygon calculated from the sum of triangles

The effect of a two-dimensional mass of an arbitrary polygonal cross section is calculated by dividing the polygon into j triangles between two neighbouring corner points and P as the apex. The total gravity effect is the sum of all triangle effects where the sign changes along the circumference of the polygon such that the effect of "external" triangles are subtracted and that the "interior" area (volume) is left (see Fig. 3.3).

For three-dimensional masses, more appropriate in reality, a similar approach is available. The surface of a body is divided into a finite number of triangles or one approximates the body by a polyhedron. Each triangle forms a tetrahedron with the observation point P . As in the two-dimensional case, the gravity effect of the whole body is the sum of the effects of all tetrahedra with a similar sign rule. Therefore one has again to follow strict rules when defining the orientation of the triangles at the body surface, e.g., by surrounding them always clockwise such that the surface normal always points out of the body. The analytical solution of the gravity integral (3-2) for this case, i.e., the gravity effect of just one tetrahedron is complicated and would fill several pages (ÇAVŞAK 1988). (A computer code in FORTRAN77 is available to the authors.)

3.2 Computation of geoid undulations caused by model mass anomalies

For the computation of potential anomalies or geoid undulations the solution has been described in detail by CHAPMAN (1979). It is extendable to the gravity effect without much difficulty. The gravity effect is obtained by differentiating the potential solution with respect to z . Computing the geoid means to determine the shape of an equipotential surface. Roughly speaking it is a rotational ellipsoid with small perturbations (undulations), which are related to the disturbing potential. If the disturbing potential T is known, the geoid undulation N is found from Bruns' formula (HEISKANEN, MORITZ 1967):

$$N = \frac{T}{\gamma}, \quad (3-4)$$

where γ is the normal gravity value at the reference ellipsoid vertically below (above) the observation point. The potential δT of a disturbing point mass m at a distance l is given by:

$$\delta T = \frac{Gm}{l}. \quad (3-5)$$

If this definition is extended to the expression (3-1) with the coordinates used there (Fig. 3.1) the integral expression for the geoid becomes

$$N(x,y,z) = \frac{G}{\gamma} \int_{\xi} \int_{\eta} \int_{\zeta} \frac{\rho(\xi,\eta,\zeta)}{[(\xi-x)^2 + (\eta-y)^2 + (\zeta-z)^2]^{0.5}} d\xi d\eta d\zeta. \quad (3-6)$$

3.3 Estimation of the normal values for crustal parameters

In gravimetric modelling of the crust it is necessary to extend bodies, as, e.g., layers not limited to the study area, beyond its margin in order to avoid edge effects. One may use a coarse grid to represent such "external" bodies if known, taking advantage of the "remote zone effect". If unknown, as often the case, the "external" crustal structures have to be extended anyway, but one may assume standard or normal models. Deviations of boundaries from their normal values are the cause of gravity and geoid anomalies and their knowledge is thus important as a reference. For gravity calculations the crustal model must extend several hundred kilometers beyond the limits, 200 – 500 km are generally sufficient. For geoid calculations the external extension must be greater, at least 600 – 1000 km, because of the slower decrease of the potential with distance.

In estimating the normal crustal values, e.g., of the Moho depth, one may make use of a standard functional relationship between elevation of the earth's surface and Moho depth. This is because the isostatic equilibrium of sufficiently large regions of the earth's crust is generally expected to exist. We may assume the average linear relationship, which has been reported by *TURCOTTE, SCHUBERT (1982)*, based on the Airy model of isostasy and the assumption of standard values of crustal thickness and crust as well as mantle densities.

$$Z_m \text{ [km]} = 33.0 + 6.60 * H \text{ [km]}. \quad (3-7)$$

Z_m is the depth of the Mohorovičić discontinuity and H is the average topographic elevation of a compartment.

If one has sufficient data for the study area, one may determine regionally more appropriate values of A and B in the model $Z_m = A + B * H$ by linear regression analysis. In order to determine this isostatic effect and the normal average crustal thickness one limits the investigation to elevations $H \geq 0.2$ km. Fig. 3.4 and Table 3.1 present the results of such an analysis on the basis of all compartments in the study area except those in the southern Rhine Graben, where the Moho is anomalously shallow, and the southeast part of the study

area where our Moho data are merely interpolated. Table 3.1 also includes the results of *GEISS (1987)* for comparison.

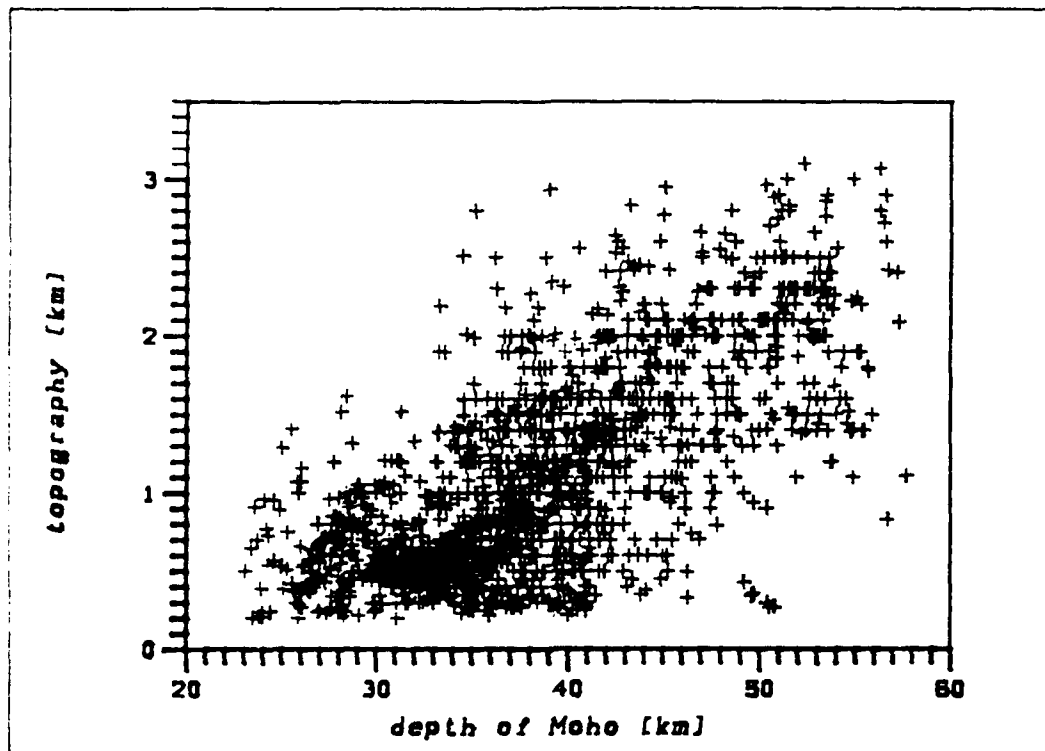


Fig. 3.4. The correlation of Moho depth and topographic elevation in the test area "European Alps".

Table 3.1. Regression of topography and crustal thickness
 Z_m [km] = $A + B \cdot H$ [km].

Model	n	A [km]	ΔA	B	ΔB	R	STDV
1	2036	28.20	± 0.20	9.00	± 0.26	0.61	6.40
2	332	26.20	± 0.74	4.40	± 0.32	0.60	7.20
3	1851	29.90	± 0.24	7.78	± 0.20	0.67	5.56
4	1587	30.03	± 0.26	7.79	± 0.20	0.69	5.26

n ... number of data dupletts,
 $\Delta A, \Delta B$... standard deviation of the coefficients A, B,
R ... correlation coefficient,
STDV ... standard deviation of the regression [km]

Model 1 ... crust ($H \geq 0.2$ km) Central Europe and Alps (GEISS 1987)
Model 2 ... Oceans ($H \leq -0.2$ km) (GEISS 1987)
Model 3 ... Alps, all data dupletts ($H \geq 0.2$ km)
Model 4 ... as Model 3, but without anomalous and uncertain values

The results are rather similar, but the correlation coefficients are a little larger, and the standard deviations are smaller than those of *GEISS (1987)*, whose investigation was based on much bigger compartments ($12' \times 20'$ and $10' \times 10'$). The regression shows also that the relationship between elevation and crustal thickness fit the data with remarkably little scatter in the Alpine region. An "isostatic" Mohorovičić discontinuity computed on the basis of the models 2 and 4 (Table 3.1) shows a good agreement with the seismically determined one (Fig. 8.13), in fact, it agrees within the reliability limits (Figs. 8.14 and 8.15). Note, however, that the dependence of Moho depth on elevation is greater in the seismic model than in the theoretical one of equation (3-7), based on Airy-isostasy and standard densities.

Similar regression analyses for the other boundaries (seismic basement Z_b and lithosphere/asthenosphere boundary Z_1) are not possible or sensible. The basement does not show any unique correlation with the topography and it is not the result of isostatic equilibrium. The same is true for the lithospheric root which may be a relic of subduction. Isostasy is the vertical mass equilibrium, or in other words, the tendency towards hydrostatic pressure at some depth with a laterally varying density distribution above the surface of pressure equilibrium. Experience with other large scale models (*JACOBY 1973, 1975*) have shown that this surface must lie below the deepest Moho depth, but it is not identical with the lithosphere/asthenosphere boundary. Thus, in estimating the normal Z_b and Z_1 values one can only rely on the literature.

The work of *MOSTAANPOUR (1984)* indicates that the depth of the seismic basement in large parts of Europe is close to 6.0 ± 0.1 km. The mean value of Z_b in our study area is only 5.5 km. The normal thickness of the "lid" or the thickness of the uppermost mantle part of the lithosphere between Moho and top of the asthenosphere is given by *SUHADOLC, PANZA (1988)* for the Mediterranean - Alpine region to be 70 - 80 km. With the normal crustal thickness added we get about 110 km for the normal lithosphere thickness. For our purposes this value is questionable since we are interested in the anomalous region of the Alps. The lithosphere thickness in marine areas (e.g., of the Mediterranean) is only 40 - 60 km, and in northern central Europe the values are also rather low. If the marginal regions of our models are assumed to follow the above normal values, the error introduced into the gravity computations is negligibly small because of the rapid gravity decrease with distance. In calculating the geoid, decreasing as $1/l$, the errors will still be noticeable. Generally, a given mass element (of the upper and lower crust as well as the uppermost mantle typical for an Alpine model, each with the same lateral

extent, directly below a station) at 13, 39 and 65 km depth has effects that vary as 1 : 0.3 : 0.02 for gravity and 1 : 1 : 0.1 for the geoid; for horizontally displaced elements the geoid effect decreases even less with depth. Table 3.2 summarizes the mean values, reference depth for computed values and depth of boundaries used as extensions beyond the model limits for the following gravimetric computations.

Table 3.2. Mean values and reference depth of layer boundaries.

Layer	MEAN	REF	F
Basement	5.53	5.50	6.00
Mohorovicic discontinuity	36.60	32.00	30.00
Lithosphere thickness	143.19	105.00	110.00

MEAN ... mean value for study area [km],
 REF ... reference depth [km],
 F ... extension depth outside study area [km].

3.4 Two-dimensional model computations

Although two-dimensionality is a gross deviation from the real geometry of the earth, two-dimensional models for profiles at right angles to the main strike of the geological structures are a simple and important means to estimate the density contrasts at boundaries. They can thus give an indication of how good the seismic models are. The advantage of two-dimensional modelling is that it requires much less computing time than three-dimensional models. If the depth extent is small as compared to the approximately linear horizontal extent, the errors caused by two-dimensionality are small. In the study area "European Alps" a profile was chosen that is perpendicular to the main axis of the Alps (see Fig. 3.5). The two-dimensionality is acceptable in view of the maximum model depth of less than 200 km and the radius of curvature of the Alpine axis of more than 400 km. The location of the profile is determined largely by the availability of gravity data (see chap. 8.2.2) and parallels the Swiss Geotraverse. The data bases are the area means of the Bouguer anomaly, i.e., a smoothed version of the gravity profile (see Fig. 3.5). The profile crosses the Ivrea body, which is possibly a high-density piece of oceanic crust and upper mantle (lithosphere) obducted onto continental lithosphere from the south. The Ivrea body was approximated by an additional model body dipping to the south as indicated in the seismic data (*BERCKHEMER 1968*). In fitting gravity, this assumption proved to be very important to reduce the residuals or "errors" and to improve the density estimation for the three layers of our general model, shown in Fig. 3.6 as a cross section through the

three-dimensional models (Figs. 8.11, 8.13, 8.16). Our experience is that the neglect of important geometrical model aspects will adversely influence the density estimates of the rest of the model.

In computing the densities we advanced from simple models to as complete ones as possible. In the sequence, we first (model 1) assumed only the Mohorovičić discontinuity to exist, then we added the seismic basement (model 2) and finally completed the model by adding the lithosphere/asthenosphere boundary. The Ivrea body was always included. The results, i.e., our estimates of the various density contrasts (across the boundaries relative to the mantle below the lithosphere) are presented in Table 3.3.

Table 3.3. Density contrasts from two-dimensional model calculations (fit of Bouguer anomaly) relative to sublithospheric mantle.

Model	C ₀	C ₁	C ₂	C ₃	C ₄	R	STDV
1	233.0±21.6		-0.24±0.02		0.13±0.05	0.93	17.4
2	310.3±30.9	-0.41±0.06	-0.27±0.02		0.12±0.04	0.95	15.3
3	129.2±23.5	-0.40±0.03	-0.27±0.01	0.06±0.02	0.09±0.01	0.99	7.45

C₀ ... constant gravity value [mGal], only formal,
 C₁ ... density contrast of lower crust [g/cm³],
 C₂ ... density contrast of upper (sedimentary) crust [g/cm³],
 C₃ ... density contrast of lithosphere [g/cm³],
 C₄ ... density contrast of Ivrea body [g/cm³],
 R ... correlation coefficient
 STDV ... standard deviation of model gravity anomaly [mGal],

Model 1 ... Moho and Ivrea body included,
 Model 2 ... Moho, seismic basement, Ivrea body,
 Model 3 ... Moho, seismic basement, Ivrea body, and lithosphere / asthenosphere boundary.

The results demonstrate that the models get better if more details (of seismic origin) are included, particularly the lithosphere/asthenosphere boundary; the fit is greatly improved (standard deviation less than half from model 1 to 3), and the density contrasts assume values that are very plausible in view of seismic velocities. If a reference density of 3.3 g/cm³ (KISSLING 1982) is assumed for the uppermost part of the earth's mantle below the Alps, the densities are similar to the densities in a north-south profile (part of the European Geotraverse) which was computed by SCHWENDENER, MÜLLER (1985). They found the following values: upper crust assumed and fixed at 2.73 g/cm³; middle crust 2.86 g/cm³, lower crust 2.957 g/cm³, and uppermost mantle 3.264 g/cm³. In our own

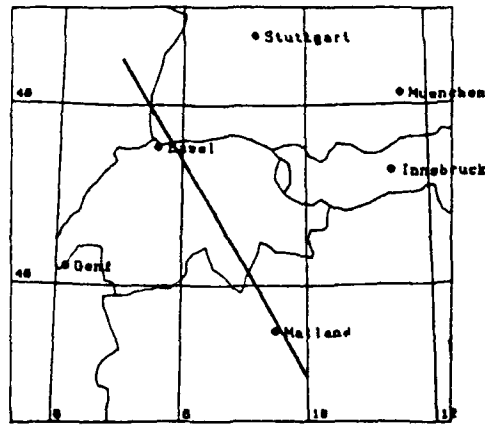


Fig. 3.5. The investigated two-dimensional profile parallel to the Swiss geotraverse.

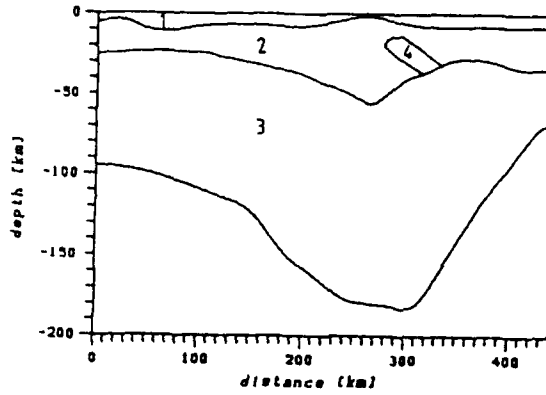


Fig. 3.6. Seismic cross section along the two-dimensional profile, (1) upper crust above seismic basement, (2) lower crust between seismic basement and Moho, (3) lithosphere, (4) Ivrea body

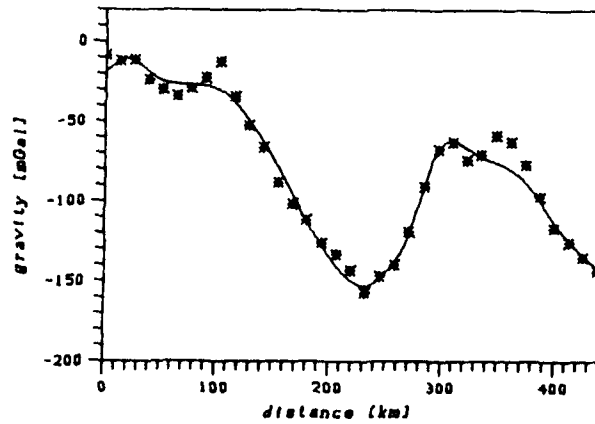


Fig. 3.7. Observed and calculated gravity along the two-dimensional profile in [mGal].

two-layer model the corresponding values are: upper crust: 2.845 g/cm³, middle and lower crust: 2.973 g/cm³, and uppermost mantle 3.30 g/cm³ (assumed).

The positive density contrast from the asthenosphere to the lithosphere is expected from geodynamic arguments and from the low seismic velocities in the asthenosphere. Similar values have been found by *JACOBY (1973, 1975)* and by *SUHADOLC, PANZA (1988)* for the Alps, who investigated gravimetrically the sub-Alpine lithospheric roots and obtained + 0.05 g/cm³. In contrast *GEISS (1987)* found a value of about - 0.01 g/cm³ which is insignificant, but surprising.

The density contrast of - 0.327 g/cm³ from the mantle to the crust falls into the frequently assumed range of - 0.30 to - 0.35 g/cm³ (*KISSLING 1982*). For the Ivrea body we found the density to be nearly that of the upper mantle. This was the result of a free fit of model gravity to the observations. These results give us some confidence into the model and we believe that this is an argument for the high quality of seismic data. There are still relative large residuals in the region of the Ivrea body and the northern Molasse (see Fig. 3.7); these are probably caused by shallow mass anomalies not sufficiently well incorporated into our model. The deviations from the two-dimensionality assumed will also contribute to the residuals.

3.5 Three-dimensional model computations

Two-dimensional models are always rather arbitrary and incomplete, though very simple. The above results are therefore to be verified by computing a three-dimensional model for the whole study area "European Alps". We computed both gravity effects and *geoid undulations on the basis of the shapes of the boundaries Z_b , Z_m , and Z_1* . In computing the geoid we must also take into account the effect of the topography. For simplicity we assumed the density of the "topographic masses" to be 2.67 g/cm³. The data to be fitted were the geoid undulations represented by a global spherical harmonic expansion to degree and order 360 (spatial resolution about 0.5 degree). For the gravity fit we again used the area means of the Bouguer anomaly (see Chapter 8.2.2). Compartments near the Ivrea body were excluded from density estimation by least-squares gravity fit so that we could avoid the introduction of an additional complicated and uncertain three-dimensional model of this structure. The geoid representation also includes no effect of the Ivrea body.

The results of gravity fitting on the basis of 1660 compartments are presented in Table 3.4. The standard deviations are much greater than in the 2-d cases. The density contrasts

Table 3.4. Density contrasts at the layer boundaries from three-dimensional model computations (fitting of gravity).

Model	C_0	C_1	C_2	C_3	R	STDV
1	-28.23 ±1.39		-0.207 ±0.005		0.71	33.94
2	-15.96 ±1.48	-0.191 ±0.011	-0.253 ±0.005		0.76	31.37
3	-36.39 ±4.80	-0.176 ±0.012	-0.278 ±0.008	0.029 ±0.006	0.77	31.19

- C_0 ... constant of fitting [mGal],
 C_1 ... density contrast at the seismic basement [g/cm³],
 C_2 ... density contrast at the Moho [g/cm³],
 C_3 ... density contrast at the lithosphere / asthenosphere boundary [g/cm³],
 R ... correlation coefficient
 STDV ... standard deviation of the model [mGal],
 Model 1 ... only Moho included,
 Model 2 ... Moho and the seismic basement included,
 Model 3 ... Moho, basement, and lithosphere / asthenosphere boundary.

computed are, however, much the same. The density contrasts relative to the sub-lithospheric mantle and the absolute values (if 3.3 g/cm³ is assumed for the lithosphere) are: lithosphere + 0.029 (3.30) g/cm³; lower crust above the Moho: - 0.249 (3.022) g/cm³; and upper crust above the seismic basement: - 0.425 (2.846) g/cm³. Note that the density contrast between the lithosphere and asthenosphere is much smaller, only about one half of that computed for the two-dimensional profile. The introduction of the lithosphere/asthenosphere boundary does also no longer reduce the standard deviation that much. It is suspected that the model assumptions - mainly the homogeneity of the layers between the boundaries - are not exactly true and that this becomes more serious the larger the region included in the modelling (2-d profile towards 3-d model). This may be especially so in the case of the lithosphere and asthenosphere, perhaps the lithospheric roots. The two-dimensional profile exactly crosses the root below the western Alps. In other regions the density contrast may be lower; an indication is also the result of *GEISS (1987)* - see above.

The effects of the three boundaries with the density contrasts of model 3 and the computed effect resulting from the fit of the original data are shown in Figs. 3.8 a,b,c and 3.9. The computed gravity map for the region of Switzerland is already quite similar to that of *KISSLING (1982)* in which the effects of the Ivrea body and of the superficial sediments at the northern Alpine margin have been removed from measured gravity data. The gravity minimum in the central Alps is about 40 mGal lower in our map. The gravity high in the Po plain is well approximated. The gravity fit is worse in Austria as compared to detailed

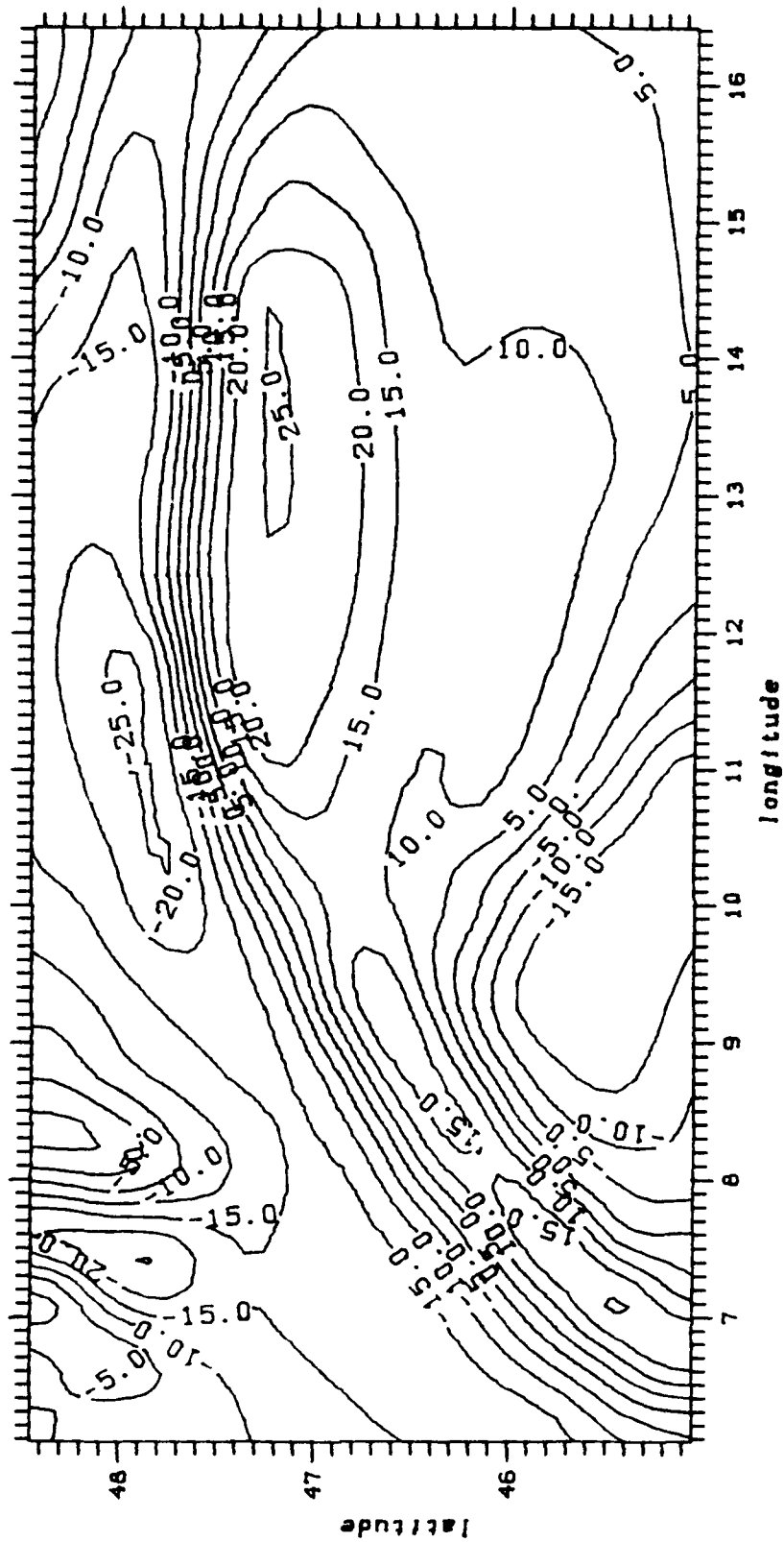


Fig. 3.8a. Gravity effect [mGal] of the variation of the seismic basement due to a density contrast of -0.176 g/cm^3 , in relationship to a normal seismic basement of 5.5 km depth.

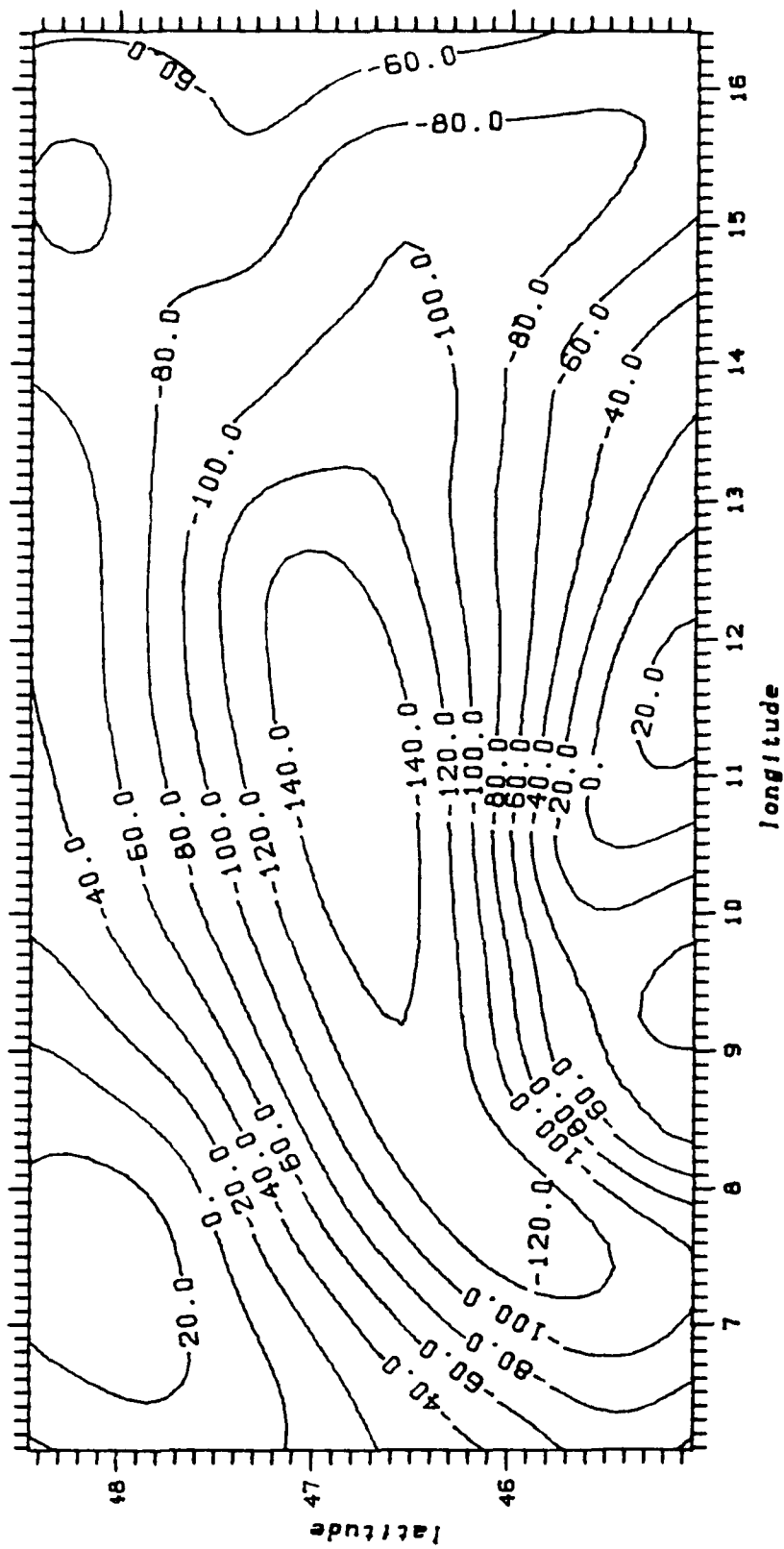


Fig. 3.8b. Gravity effect [mGal] of the variation of the Moho due to a density contrast of -0.278 g/cm^3 , in relationship to a normal crustal thickness of 30.0 km.

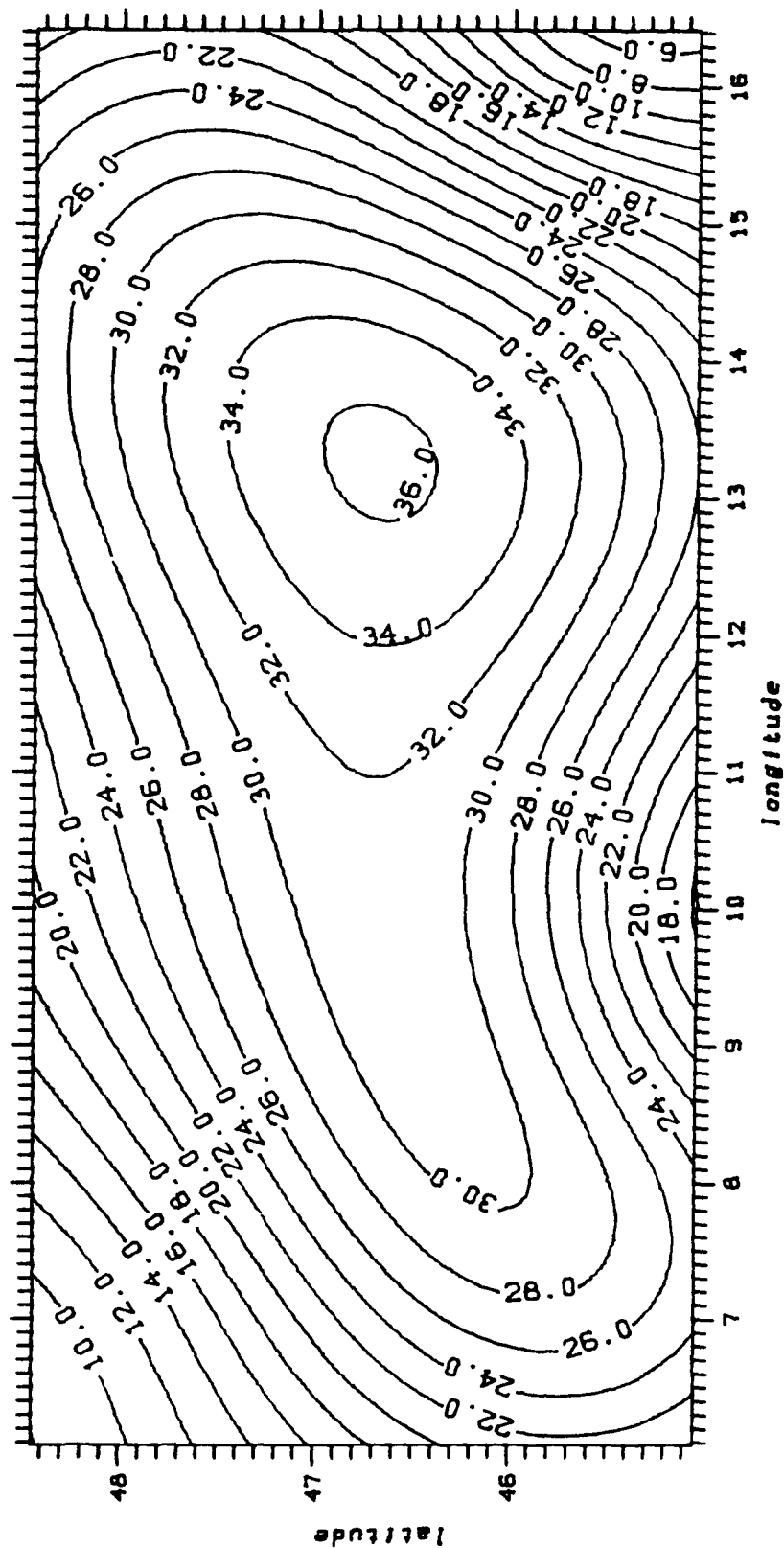


Fig. 3.8c. Gravity effect [mGal] of the variation of the lithosphere/asthenosphere boundary due to a density contrast of $+0.029 \text{ g/cm}^3$, in relationship to a normal lithospheric thickness of 105 km.

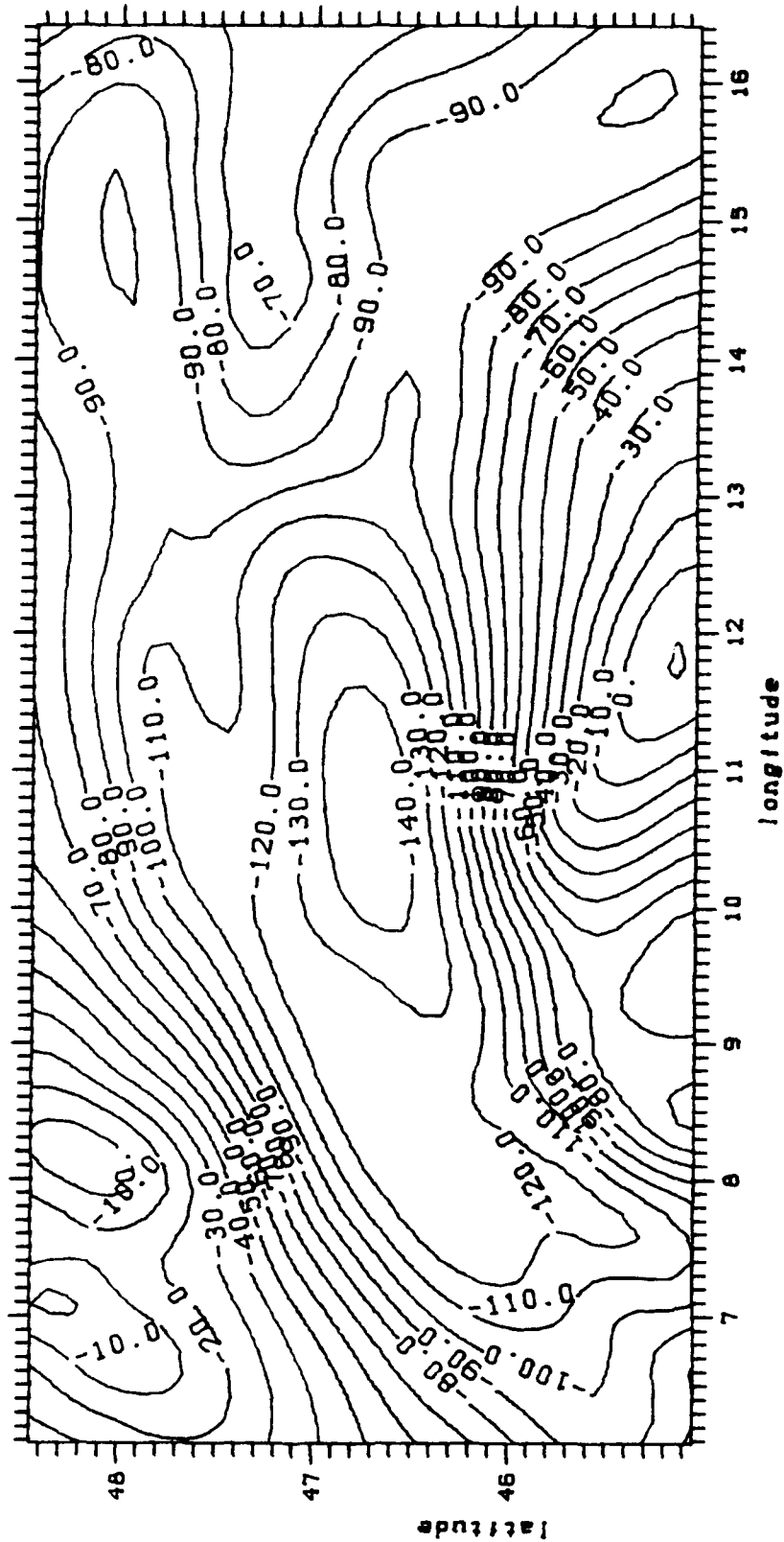


Fig. 3.9. Total calculated gravity [mGal] of the three-dimensional model 3.

gravity maps (e.g., STEINHAUSER, PUSTIZEK 1987); the reason for this is probably the poorer crustal model in this region. To the north in the foreland of the Alps the interpretation of PLAUMANN (1987) is confirmed.

The greatest contribution to the total gravity effect is that of the Moho variation. It is the exclusive cause of the Alpine gravity minimum. This confirms the statistically inferred aspect of the good isostatic compensation of the Alpine structure. The mismatch of 40 mGal in the axial region cannot be explained by changing the Mohorovičić discontinuity within the limits of confidence (Figs. 8.14, 8.15). A rock layer of 1 km thickness at 40 km depth with a density contrast of 0.3 g/cm³ will have a gravity effect of less than 10 mGal at the surface and a change of Moho depth within the permissible limits will not explain more than 50 % of the residuum.

Fitting the geoid data (see Fig. 3.10) in the same manner how it was done with the mean Bouguer anomalies leads to the density contrasts represented in Table 3.5. The density of the topographic masses was fixed to 2.67 g/cm³ as mentioned above.

Table 3.5. Density contrasts at the layer boundaries from three-dimensional model computations (fitting of geoid).

Model	C ₀	C ₁	C ₂	C ₃	R	STDV
4	41.32 ±0.69		-0.234 ±0.005		0.74	3.315
5	67.42 ±0.75	-0.453 ±0.010	-0.342 ±0.004		0.88	2.369
6	80.19 ±0.70	-0.421 ±0.008	-0.197 ±0.005	-0.071 ±0.002	0.77	1.898

- C₀ ... constant of fitting [mGal],
 C₁ ... density contrast at the seismic basement [g/cm³],
 C₂ ... density contrast at the Moho [g/cm³],
 C₃ ... density contrast at the lithosphere / asthenosphere boundary [g/cm³],
 R ... correlation coefficient
 STDV ... standard deviation of the model [mGal],
 Model 4 ... only Moho included,
 Model 5 ... Moho and the seismic basement included,
 Model 6 ... Moho, basement, and lithosphere/asthenosphere boundary.

The density contrasts relative to the sub-lithospheric mantle and the absolute values (again with the assumption of 3.3 g/cm³ for the lithosphere) are as follows: lithosphere: - 0.071 (3.30) g/cm³; lower crust above the Moho: - 0.268 (3.103) g/cm³; and the upper crust above the seismic basement: - 0.689 (2.682) g/cm³. The densities derived from geoid inver-

sion are also quite reliable but they differ, however, from those derived from gravity inversion mainly in two points. First the significant negative density contrast at the lithosphere/asthenosphere boundary has to be noticed, secondly the strong negative density contrast at the seismic basement. In Table 3.5 one could see, that the densities in the different models are even more dependent on the number of influencing boundaries.

The effects of topography and the boundaries with the density contrasts of model 6 and the total geoid effect resulting from the best fit of the input data are shown in Figs. 3.11 a,b,c,d and 3.12. The greatest contribution to the calculated geoid is that of the topography; the variation of the Moho has not the strong effect on geoid as on gravity. Although the geoid is well fitted (comparison of Figs. 8.17 and 8.19 and the correlation coefficient of 0.92 corroborate this fact) the density contrasts found *do not lead to a linear velocity-density systematics*. About the reasons one can only speculate. Our opinion is that edge effects of the seismic model are not entirely eliminated and that the geoid data resolution calculated from a spherical harmonic expansion up to order and degree 360 is too coarse to include the effect of such small areas like the Alpine lithospheric roots with its positive density contrast. Such geoid data are not suitable to deduce velocity-density systematics, but its inversion could be used to consider the results of gravity inversion. If the seismic model is good, the geoid inversion should give results of the same order of magnitude. This is true in case of our model.

3.6 Velocity-density systematics

The term "systematics" for the relationship between density and seismic velocity is used to indicate that there is only a trend with much real scatter. Solid state theory cannot yet establish unequivocal relationships. Velocity and density are influenced by the material as such (composition, mean atomic weight) and by the packing and bonding of the atoms (crystallography, mineralogy), i.e., by many parameters. Thus in order to connect gravity and seismic data via density-velocity systematics one tries to establish them empirically. Mostly one refers to laboratory results, e.g., by *BIRCH (1960, 1961)*.

It is, however, also possible to take the reversed route. If we compare the density contrasts found with the two- and three-dimensional gravity models (density contrasts found from geoid inversion are excluded) and the average seismic velocities \bar{v}_p in the layers of our models, *we find a nearly linear relationship* (Fig. 3.13). The density contrasts in this case have been transformed to absolute densities with the assumption of a value of 3.3 g/cm³

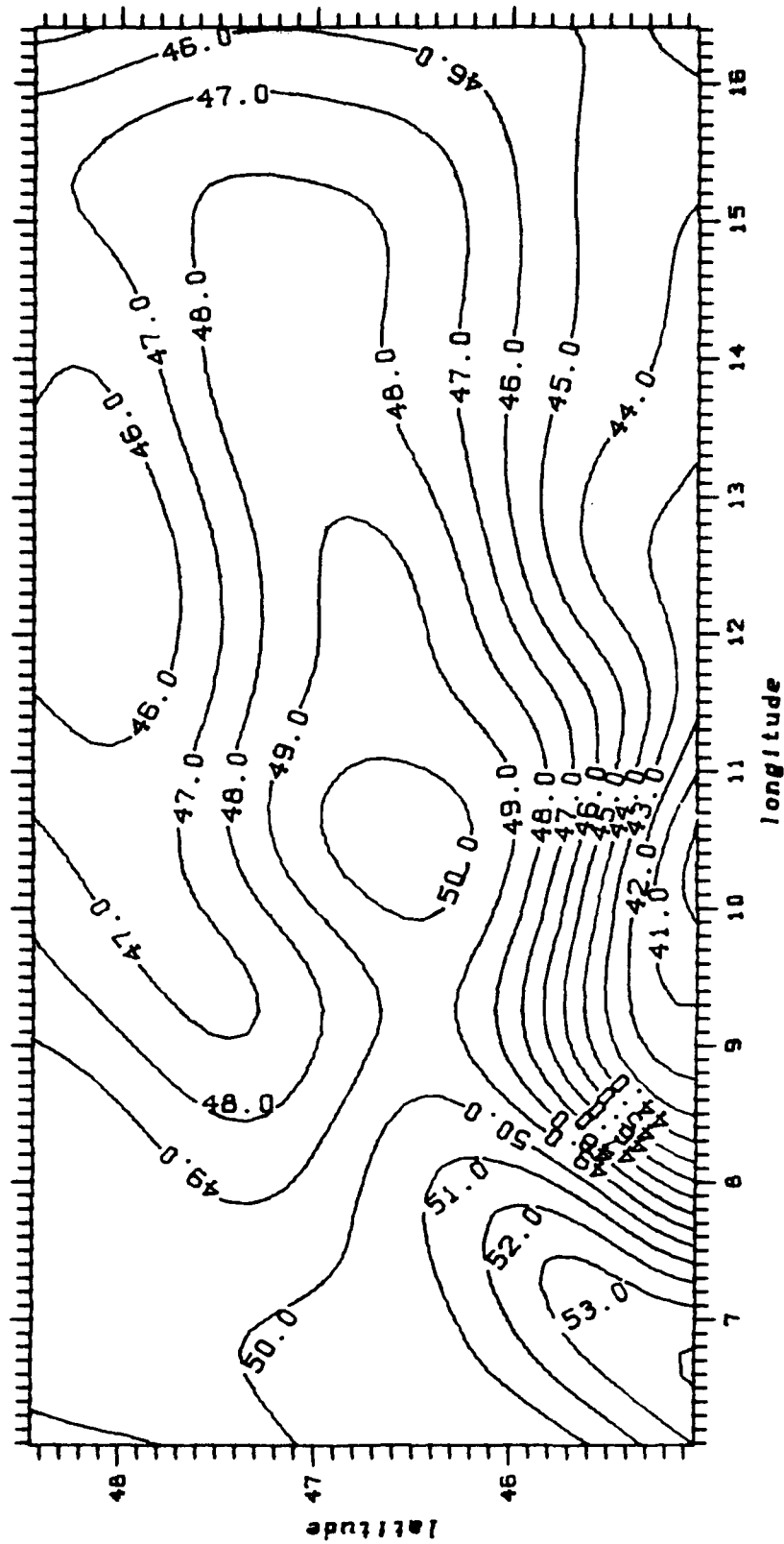


Fig. 3.10. Geoid undulation [m] calculated from a spherical harmonical expansion up to order and degree 360 in the Alpine area.

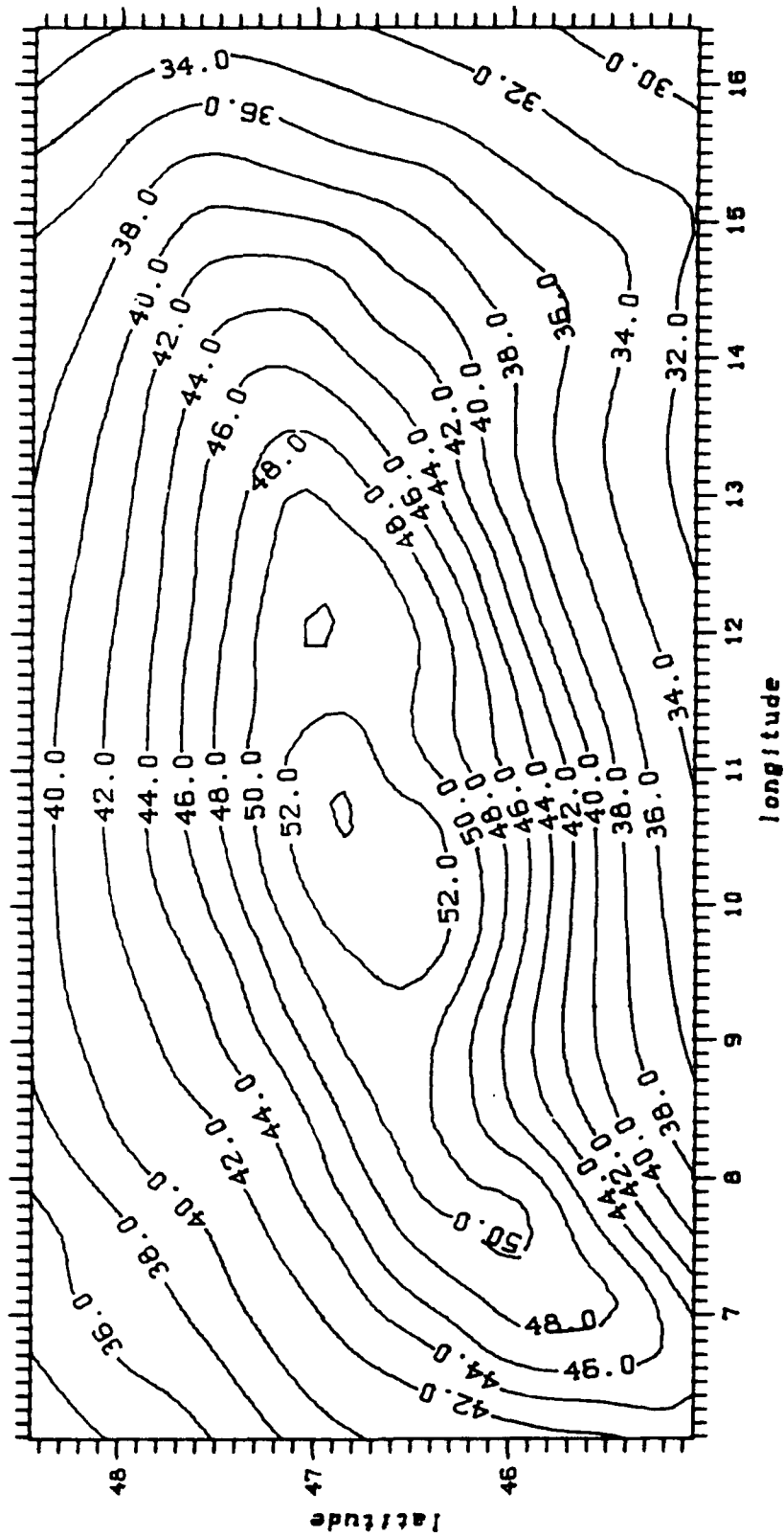


Fig. 3.11a.

Geoid effect [m] of the topography due to a density of surface rocks of 2.67 g/cm^3 .

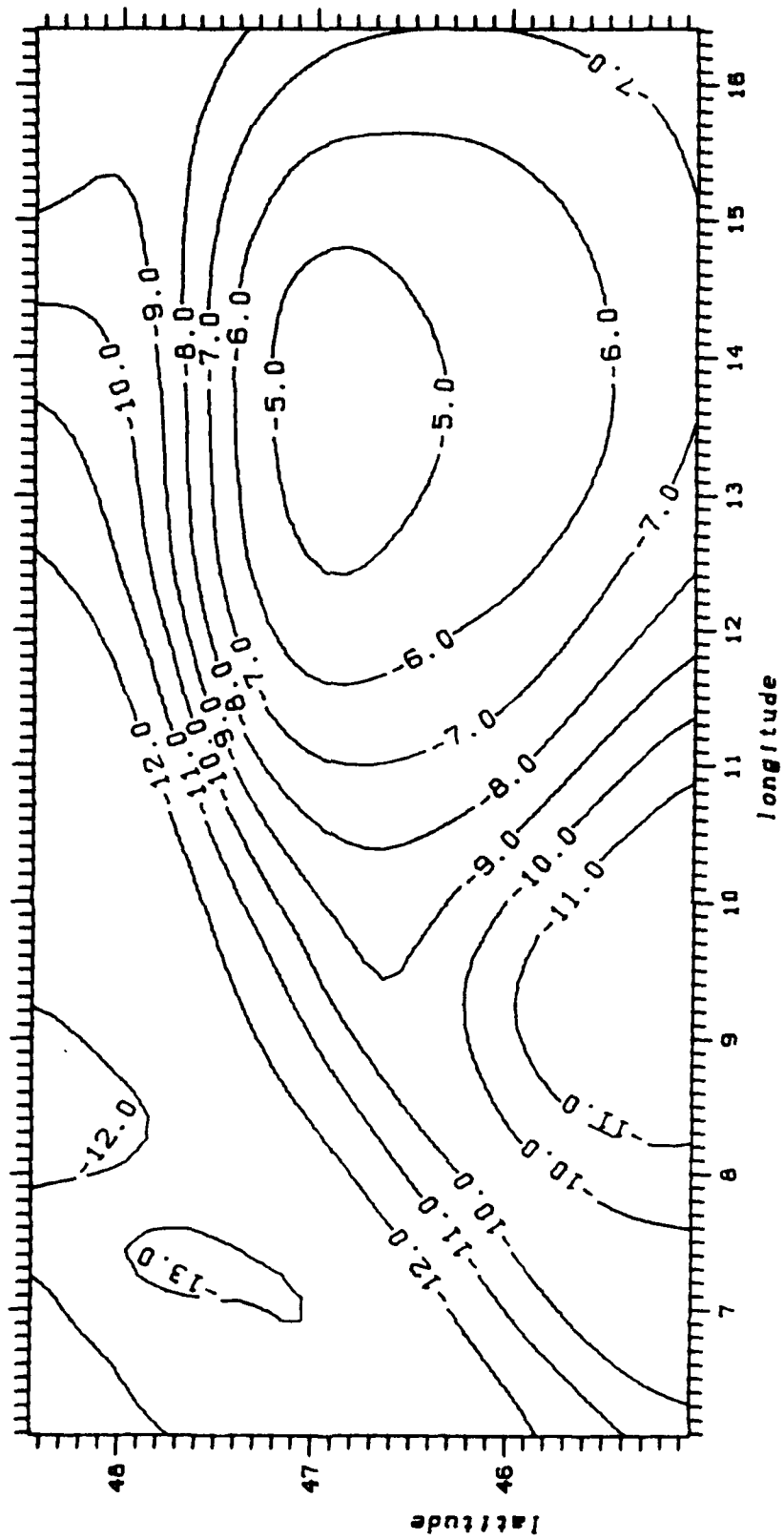


Fig. 3.11b.

Geoid effect [m] of the variation of the seismic basement due to a density contrast of -0.421 g/cm^3 in relationship to a normal seismic basement of 5.5 km depth.

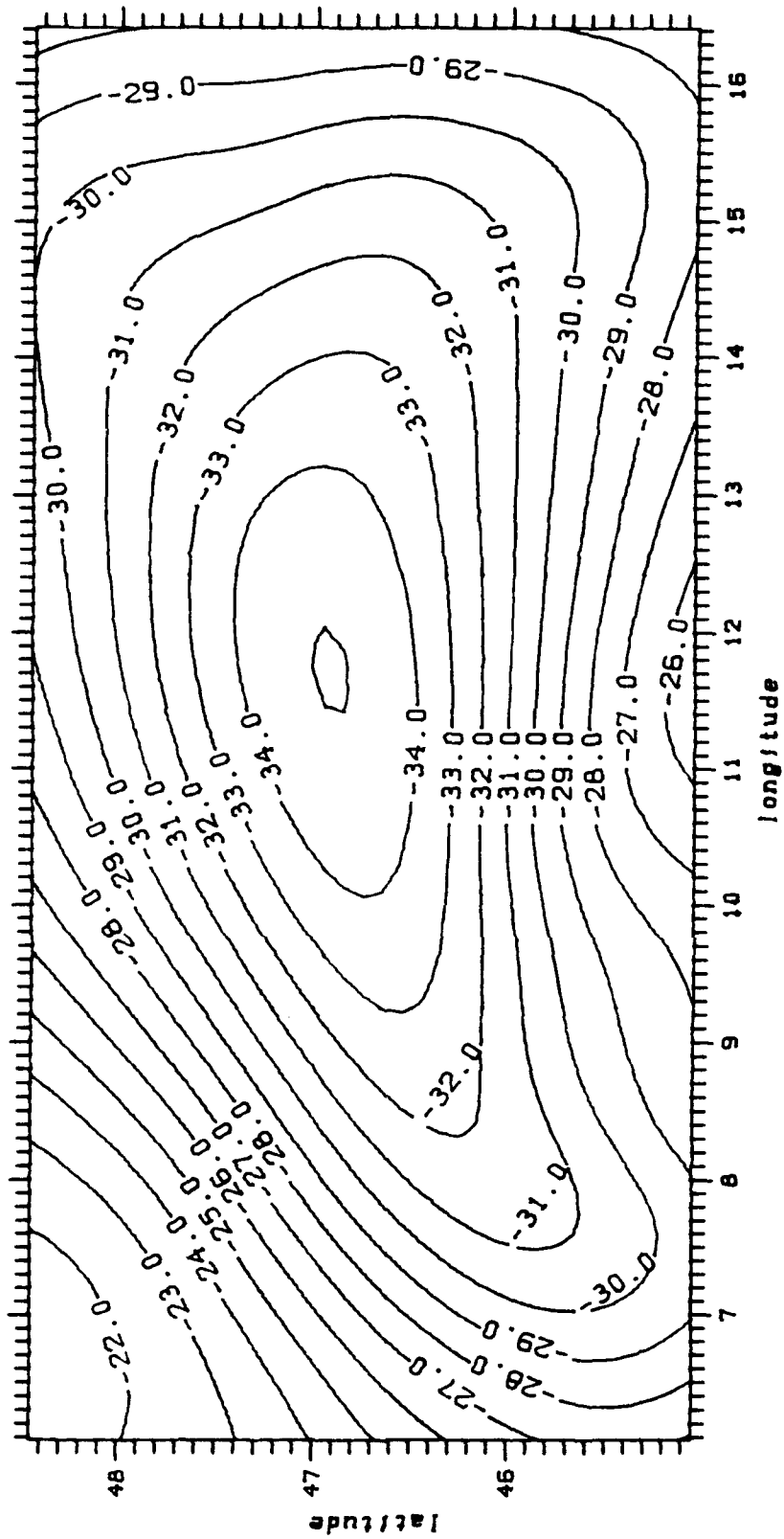


Fig. 3.11c.

Geoid effect [m] of the variation of the Moho due to a density contrast of -0.197 g/cm^3 in relationship to a normal crustal thickness of 30.0 km.

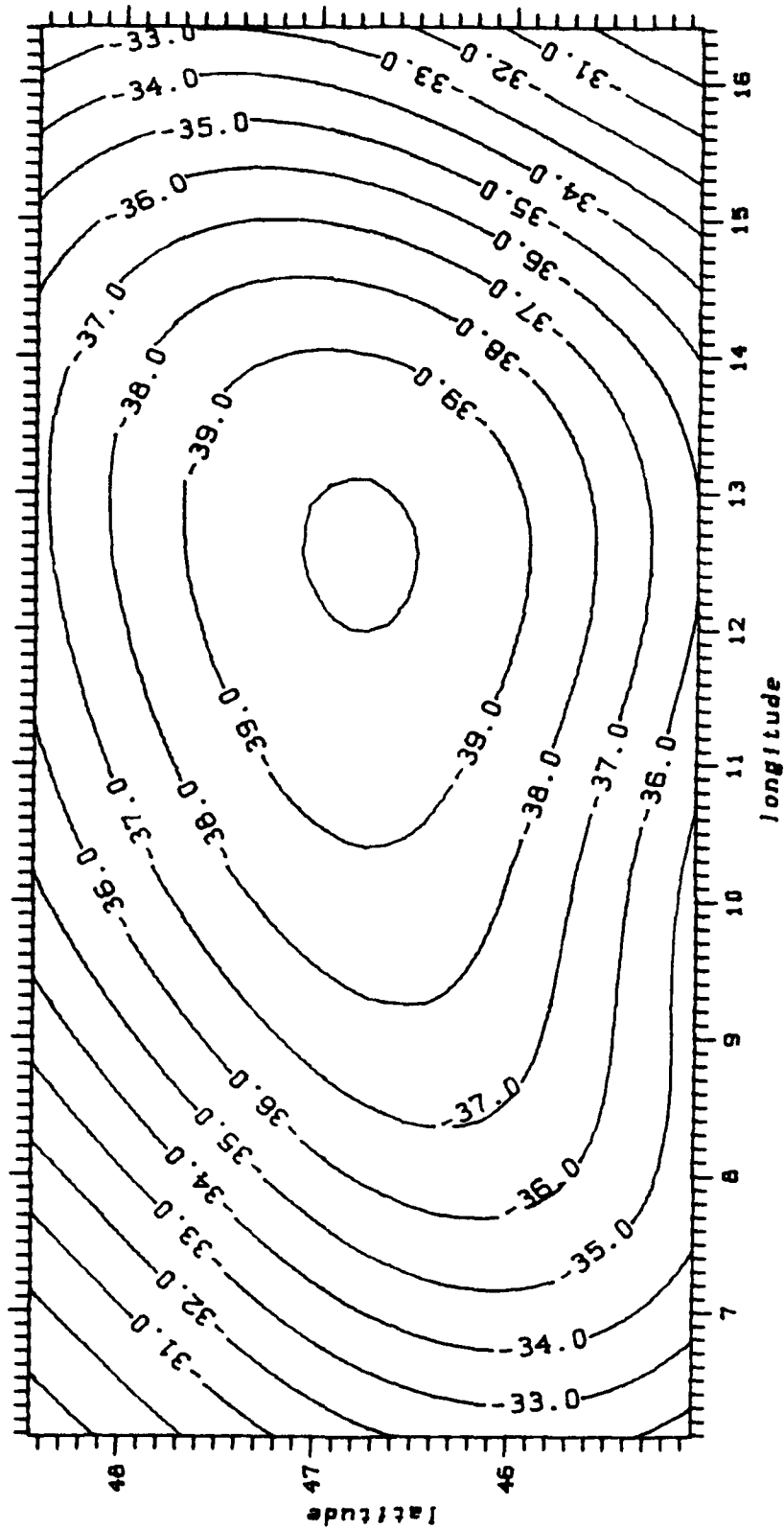


Fig. 3.11d.

Geoid effect [m] of the variation of the lithosphere/asthenosphere boundary due to a density contrast of -0.071 g/cm^2 in relationship to a normal lithospheric thickness of 105 km.

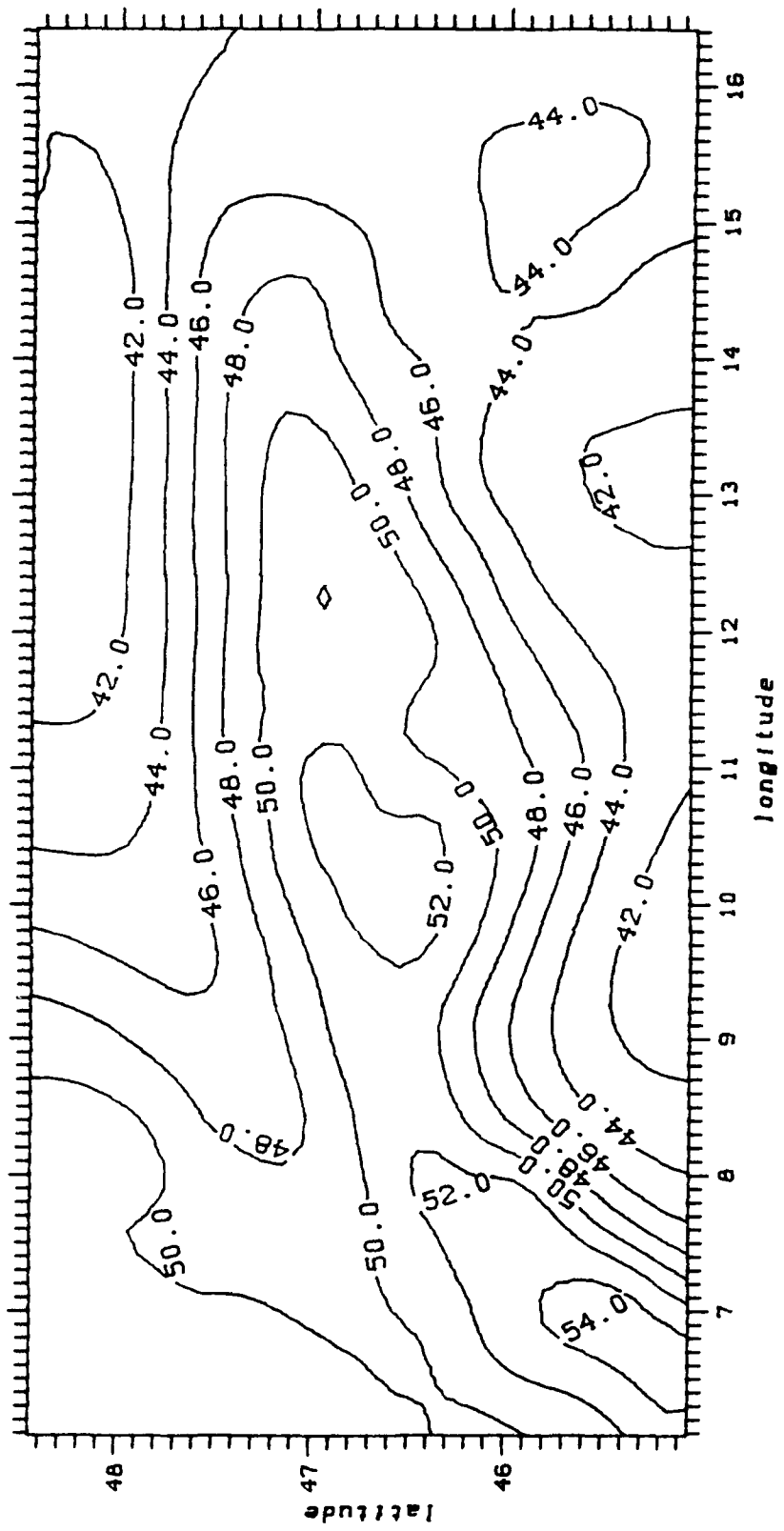


Fig. 3.12. Total calculated geoid [mGal] of the three-dimensional model 6.

within the uppermost mantle. We find the coefficient $b = \partial v_p / \partial \rho$ to be about 5.4 ± 0.4 [km/s]/[g/cm³]. This result is relatively high as compared to other investigations. For example, *JACOBY (1975)* - Fig. 3.15 - found values about 4.8 ± 0.8 [km/s]/[g/cm³] for long range models or profiles in North and South America. Laboratory investigations (*BIRCH 1960, 1961*) have given somewhat lower values of, for example, about 3.5 [km/s]/[g/cm³] for basalt-type rocks. We therefore shall not overemphasize our linear relationship.

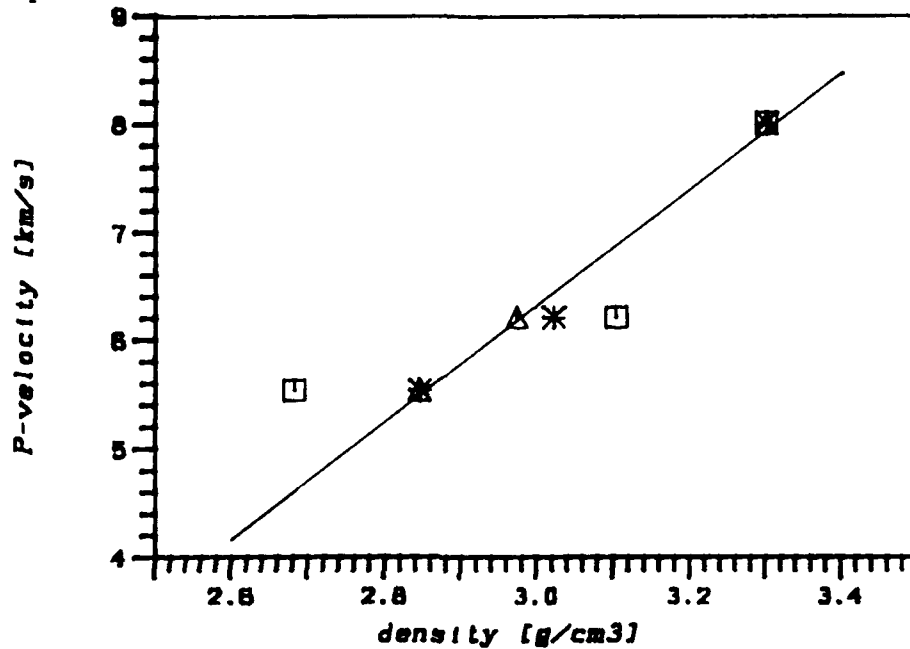


Fig. 3.13. Velocity-density systematics from two- and three-dimensional gravity inversion; triangles: two-dimensional models; asterixes: three-dimensional models; quadrangles: three-dimensional geoid model (for comparison), the gradient $\partial v_p / \partial \rho = 5.39$ [km/s]/[g/cm³]

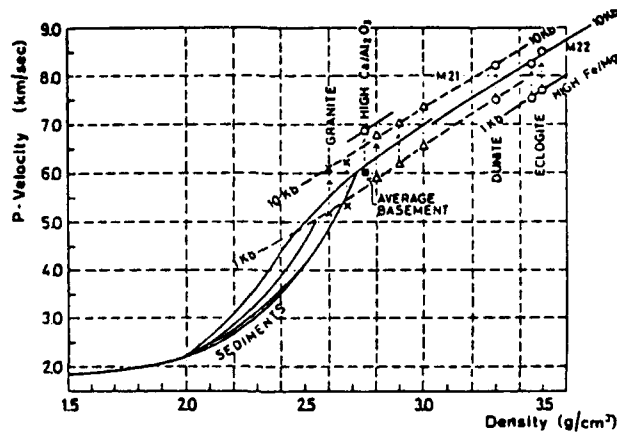


Fig. 3.14. Experimental velocity-density systematics after *WOOLLARD (1975)*.

However, the gravimetric results as ours principally suffer from their insensitivity to purely depth-dependent density variations in the earth. It is quite likely that there is generally such a component of purely vertical density increase in the real density variation of the crust and upper mantle; this component may differ from region to region and thus explains the deviation of our result from others obtained by similar methods and from laboratory measurements.

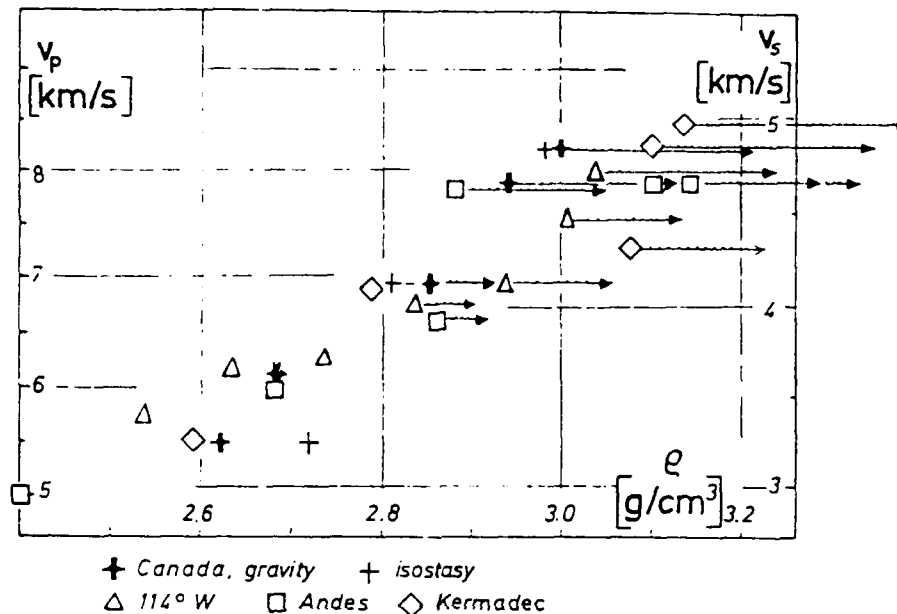


Fig. 3.15: Velocity-density systematics from gravity studies after JACOBY (1975).

This is no real handicap for the present investigation and for the aim of regional gravity prediction, since the component of vertical density variation does not influence the gravity variation in a region where this component is approximately constant. If it changes on larger regional scale the corresponding gravity variations will be of about the same length scale. If the studies are applied to large regions, the vertical density variation common to such regions may be smaller. If smaller and larger scale studies are combined it should be possible to link the gravity prediction scheme to the scale (wavelength, harmonics) of gravity field representations of sufficient reliability. In any case, the approach to the question of gravity prediction as proposed here is probably best for scales of order of $10^2 - 10^3$ km and not good on very large scales ($\geq 10^3$ km). If the seismic data are good and the gravimetric data are good in parts or for relatively long wavelength two- and three-dimensional modelling as presented in this chapter, we believe we can advance to a finer spatial resolution of the gravity field with a reliability comparable to that of seismic data. The method can also be used to interpolate or to some extent even to extrapolate the gravity field.

4. A BRIEF SURVEY OF PROPOSED (GEODETIC) APPROACHES IN THE PAST

Special emphasis in this brief survey is put on approaches relevant for geodesy. It may be by no means complete. The idea of using geophysical information when predicting gravity anomalies is not new, see (WILCOX 1974). It is obvious, that the solution of the "inverse problem" plays an important role in geophysics. A mathematically-oriented overview of possible methods can be found, e.g., in TARANTOLA (1987).

Consequently, we may categorize the work done up till now into three groups:

(1) *Geophysical treatment of inverse problem theory.* As mentioned before, one can find chapters on inverse problem theory, e.g., the determination of the internal structure of the crust from other data like seismic and gravity measurements in every textbook. From the large variety we only like to mention BOTT (1971), BULLEN (1975), MEISSNER (1986), or the handbook of LANDOLT-BÖRNSTEIN (1982). Recently, the complex relationships between mass heterogeneities and surface observables such as topography, gravity, etc. were treated by various authors (see e.g., FLEITOUT, FROIDEVAUX 1982; KHAN 1977; VIGNY, FROIDEVAUX 1988; WOODHOUSE, DZIEWONSKI 1984). Especially in seismics, the term "3D-tomography" is now used with respect to studies of the earth's internal structure. Quite recently, MORITZ (1989) presented a (geodetic) approach to the gravimetric inverse problem.

(2) *Indirect use of geophysical data in geodetic methods.* Since the determination of the gravity potential in geodesy is considered to be a boundary value problem, where the boundary data like gravity anomalies etc., have to be given on the geoid, it is necessary to reduce the observations from the physical surface of the earth to the geoid. For gravity field interpolation a certain smoothing is anticipated in order to reduce the prediction errors.

For these purposes a simple density model, eventually in connection with isostatic compensation hypotheses and a digital terrain model are used to take into account some kind of geophysical evidence. Thereby the density between the surface of the earth and the Mohorovičić discontinuity is simplified as global constant, $\rho_0 = 2.67 \text{ g cm}^{-3}$. In the frequently-used Airy-Heiskanen isostasy model (see, e.g., HEISKANEN, MORITZ 1967, p. 135f.) the mountains of constant density ρ_0 float on a dense underlayer of constant density $\rho_1 = 3.17 \text{ g cm}^{-3}$. The condition of floating equilibrium is (in flat earth approximation)

$$t \Delta \rho = h \rho_0 \quad (4-1)$$

where $\Delta \rho = \rho_1 - \rho_0$, h is the topographic height. The thickness of the corresponding root, starting at the compensation depth T , is defined by t . Assuming standard values ($\Delta \rho = 0.6 \text{ g/cm}^3$; $\rho_0 = 2.67 \text{ g/cm}^3$) leads to the "rule of thumb" $t = 4.45 h$. The crustal thickness under mountains is $T + h + t$, where the normal thickness (\rightarrow Moho depth, to some extent) is generally assumed to be $T = 30 \text{ km}$. These short descriptions illustrate more or less the (poor) consideration of geophysical data in geodetic methods.

The recent developments of digital (surface) density models, see for example WALACH (1987), and also the construction of Moho models (see chapter 8.2.6) will lead to a significant improvement in near future in the indirect use of geophysical quantities in geodetic algorithms (SÜNKEL 1986; TSCHERNING 1979). High-resolution global isostatic earth models were presented by SÜNKEL (1986), see also RUMMEL et al (1988). More detailed investigations on "experimental isostasy" can be found in (DORMAN, LEWIS 1970; LEWIS, DORMAN 1970).

In a more general sense, one can understand those smoothing approaches with respect to mixed models (or collocation) also in such a way, that the more the deterministic part is increasing the stochastic treatment of the rest will become smaller and smaller.

Quite recently, GRAFAREND (1989) proposed to replace the standard topographic mass reduction by a volume integral over the datum-dependent internal Neumann kernel and anomalous masses $\delta \rho$ plus a surface integral over the surface-reduced internal Neumann kernel and the anomalous boundary data of gravimetric type.

- (3) *Direct use of geophysical data in geodetic computations.* Direct use in this context means that we (i) either use the geophysical data as some kind of (pseudo-) observations in our geodetic algorithms, or (ii) set it into correlation/regression to gravity field functionals like geoidal heights, etc., or (iii) use it in the construction of earth gravity models consistent with internal mass distributions. The last is often also a prerequisite for methods (i).

With regard to (i) attempts were made to incorporate density into a stochastic concept using the theory of random processes (JORDAN 1978, MORITZ 1977, TSCHERNING 1976, 1977). SANSO (1980) proposed the application of the collocation principle to the internal densities (*internal collocation*). Later on SANSO,

TSCHERNING (1982) represented the anomalous gravity field by a combination of an anomalous potential T_s harmonic down to some Bjerhammar sphere S_0 and an anomalous potential T_t , generated by a layer of topographic masses between the sphere S_0 and the topographic surface S (*mixed collocation*). Recently, the so-called "*quasi-harmonic inversion*" of gravity field data was tested (*TSCHERNING, STRYKOWSKI 1987; HEIN et al 1988*). The central problem in those approaches, the choice of norm for the density distribution - earlier treated by *KRARUP (1970), SANZO et al (1986), TSCHERNING (1974)* - was solved in such a way that density $\delta\rho$ is supposed to be a solution of a partial differential equation, $\Delta(\delta\rho/p(r))$ where $p(r)$ is a polynomial only dependent on the distance from the origin r , and Δ is the well-known Laplace-Operator. In addition, indicator functions with overlapping support were proposed as covariance functions (*HEIN et al 1988; TSCHERNING 1989*). *VASSILIOU, SCHWARZ (1987)* discussed different methods out of the variety of the geophysical literature for the combination of gravity with other geophysical data for the solution of the inverse problem. *STRYKOWSKI (1989)* presented density autocovariance functions from North Sea density logs.

With respect to category (ii) example-wise we like to mention studies of *COLIĆ et al (1988), FOTIOU et al (1988), GEISS (1987), LAMBECK (1976), McNUTT (1980), RICARD et al (1984)*.

The construction of reference (normal) density models consistent with the outer gravity potential and vice versa is discussed in chap. 6.4 (*MARTINEC, PĚČ 1986a,b; MATYSKA 1987; MESHCHERYAKOV et al 1986; PĚČ, MARTINEC 1984, 1988; TSCHERNING, SÜNKEL 1981*).

5. THE INTEGRATED GEODESY ADJUSTMENT MODEL

As mentioned before, our goal is to incorporate the data types *density*, *seismic velocities* and *displacements* in the *direct* way into geodetic algorithms for the approximation of the gravity field outside the earth. For the sake of an unified theory we will try to derive (pseudo-) observation equations fitting into the general scheme of integrated geodesy adjustment. The mixed model approach is therefore also suited, since precise relationship between density and gravity, for example, can often only be found locally. Necessary generalizations for regional areas imply that besides such an (attempt of a) deterministic mathematical/physical relation (more or less local) residuals may remain which can be considered as forming a random process. This is in correspondence also with geophysical proposals and investigations, to consider, for example, seismic wave propagation and density perturbations in a random medium (*CHERNOV 1960, KORN 1987*).

We review here the general principle of integrated geodesy (*EEG, KRARUP 1973, HEIN 1986*). Every geodetic and geophysical measurement l can be expressed as a nonlinear functional depending on one or several position vectors $\underline{x} = (x,y,z)$ in space and on the gravity field of the earth, symbolically written

$$l = F(\underline{x}, W) \quad (5-1)$$

where W is the gravity potential

$$W = V + \omega^2(x^2 + y^2)/2 \quad (5-2)$$

V is the potential of the gravitational force and ω is the angular velocity of the earth's rotation. By (x,y,z) or (x_1,x_2,x_3) we denote the Cartesian coordinates of the geocentric system \hat{E} defined as follows: the origin is at the earth's center of mass, the z -axis coincides with the (mean) rotation axis, and the x -axis goes through the (mean) Greenwich meridian. We presume further that the observations are corrected for time-dependent geodynamic effects.

The scope of geodesy is now to determine the coordinates of material points on the surface of the earth (and in space) *and* the gravity potential including its functionals by the relation (5-1). Since our measurements are nonlinear functionals we have to introduce approximate values for the linearization process.

$$\underline{x} = \underline{x}_0 + \delta\underline{x} \quad (5-3)$$

$$W(\underline{x}) = U(\underline{x}) + T(\underline{x}) \quad (5-4)$$

\underline{x}_0 is the approximate position vector, $U(\underline{x})$ is some kind of trial value for the actual gravity potential at \underline{x} . This could be a so-called normal potential belonging to an arbitrary ellipsoid or any other reference potential, e.g., a low-order harmonics expansion derived from satellite geodesy. For the sake of comparison of the results with those of other computations one can use one of the adopted reference systems of the International Association of Geodesy. As done hitherto we will call $T(\underline{x})$ the disturbing potential and we will assume further that both, $T(\underline{x})$ and $\delta\underline{x} = (\delta x, \delta y, \delta z)^T = (\delta x_1, \delta x_2, \delta x_3)^T$ are small quantities, which allow us to work with a linear model.

Thus we get for (5-1)

$$l = F(\underline{x}_0 + \delta\underline{x}, U + T) \quad (5-5)$$

Applying Taylor's theorem at $\underline{x}_0 = [x_1^0, x_2^0, x_3^0]^T$ and restricting ourselves to first-order terms in the series it follows

$$l = F(\underline{x}_0, U) + \sum_{i=1}^3 F_{x_i}(\underline{x}_0, U) \delta x_i + L(T) \quad (5-6)$$

where $L(T)$ is a linear operator applied on T . By the substitutions

$$\delta l = l - F(\underline{x}_0, U) \quad (5-7)$$

$$a_i = \frac{\partial F}{\partial x_i}(\underline{x}_0, U) \quad (5-8)$$

we get the general linear observation equation of the form

$$\delta l = \underline{a}^T \delta\underline{x} + L(T), \quad \text{or} \quad (5-9)$$

considering noise \underline{n} , in matrix form (\underline{A} and \underline{R} are corresponding design matrices),

$$\delta l = \underline{A} \delta\underline{x} + \underline{R}t + \underline{n} \quad (5-10)$$

where the first expression of the right hand side represents the *metric coordinates* part and the second the (functionals of the) *disturbing potential*, in detail

$$\underline{t} = [T, \partial T / \partial x_i, \partial^2 T / \partial x_i \partial x_j]^T \quad i, j = \{1, 2, 3\} . \quad (5-11)$$

Simple mapping and scaling of the quantities in (5-11) yields

- *geoidal heights* $N = T / \gamma$, (γ is normal gravity),

- *gravity disturbances* $\delta g = - \frac{\partial T}{\partial h}$,

- *gravity anomalies* $\Delta g = - \frac{\partial T}{\partial h} + \frac{1}{\gamma} \frac{\partial \gamma}{\partial h} T$

(h indicates (approximately) the direction of the normal to the ellipsoid),

- *deflections of the vertical*,

north-south component $\xi = - \frac{1}{R \gamma} \frac{\partial T}{\partial \varphi}$,

east-west component $\eta = - \frac{1}{R \gamma \cos \varphi} \frac{\partial T}{\partial \lambda}$

where R is the mean earth's radius, and (φ, λ) are spherical latitude and longitude,

- *anomalous gravity gradients*.

The observation equation system (5-10) can be solved using the hybrid minimum norm condition

$$\underline{n}^T \underline{C}_{nn}^{-1} \underline{n} + \underline{t}^T \underline{K}_{tt}^{-1} \underline{t} = \min \quad (5-12)$$

where \underline{C}_{nn} and \underline{K}_{tt} are the covariance matrices of \underline{n} and \underline{t} . The covariance matrix \underline{K}_{tt} can be derived from a (global) covariance model.

The solution of a general collocation model of type (5-10) can be found, e.g., in (MORITZ 1980, p. 111f.). The unknown *coordinates* are given by

$$\delta \underline{x} = (\underline{A}^T \underline{D}^{-1} \underline{A})^{-1} \underline{A}^T \underline{D}^{-1} \delta \underline{t} \quad (5-13)$$

and the functionals of the disturbing potential at the observation points are

$$\hat{\mathbf{t}} = \underline{\mathbf{K}}_{tt} \underline{\mathbf{R}}^T \underline{\mathbf{D}}^{-1} (\underline{\mathbf{d}} - \underline{\mathbf{A}} \underline{\delta\mathbf{x}}). \quad (5-14)$$

Since in the collocation model an interpolation of the stochastic part is implicitly built in, (5-14) can be also used for the determination of *any other functional s* of the gravity disturbing potential at *any other station* when knowing the corresponding crosscovariances $\underline{\mathbf{K}}_{st}$

$$\hat{\mathbf{s}} = \underline{\mathbf{K}}_{st} \underline{\mathbf{R}}^T \underline{\mathbf{D}}^{-1} (\underline{\mathbf{d}} - \underline{\mathbf{A}} \underline{\delta\mathbf{x}}). \quad (5-15)$$

The error statistics are given by

$$\underline{\mathbf{E}}_{xx} = (\underline{\mathbf{A}}^T \underline{\mathbf{D}}^{-1} \underline{\mathbf{A}})^{-1} \quad (5-16)$$

and

$$\underline{\mathbf{E}}_{ss} = \underline{\mathbf{K}}_{ss} - \underline{\mathbf{K}}_{st} \underline{\mathbf{D}}^{-1} [\underline{\mathbf{I}} - \underline{\mathbf{A}} (\underline{\mathbf{A}}^T \underline{\mathbf{D}}^{-1} \underline{\mathbf{A}})^{-1} \underline{\mathbf{A}}^T \underline{\mathbf{D}}^{-1}] \underline{\mathbf{K}}_{ts} \quad (5-17)$$

where $\underline{\mathbf{I}}$ is the identity matrix and

$$\underline{\mathbf{D}} = \underline{\mathbf{C}}_{nn} + \underline{\mathbf{R}} \underline{\mathbf{K}}_{tt} \underline{\mathbf{R}}^T. \quad (5-18)$$

For the estimation process above there are certain assumptions necessary, as

$$\overline{\mathbf{E}}\{\underline{\mathbf{n}}\} = 0 \quad (5-19)$$

$$\overline{\mathbf{E}}\{\underline{\mathbf{t}}\} = 0 \quad (5-20)$$

$$\overline{\mathbf{E}}\{\underline{\mathbf{s}}\} = 0 \quad (5-21)$$

where $\overline{\mathbf{E}} = \mathbf{E}\mathbf{M}$ is the *total average*. \mathbf{E} is the expectation operator, and \mathbf{M} describes a homogeneous and isotropic average over the sphere.

In case, that we assume the positions $\underline{\mathbf{x}}$ to be known where our measurements are taken, the observation equation (5-10) reduces to

$$\underline{\mathbf{d}} = \underline{\mathbf{R}} \underline{\mathbf{t}} + \underline{\mathbf{n}} \quad (5-22)$$

and

$$\underline{\mathbf{A}} \underline{\delta\mathbf{x}} = \underline{\mathbf{0}} \quad (\underline{\mathbf{A}} = \underline{\mathbf{0}}) \text{ in (5-13) to (5-17).}$$

Central point in a possible inclusion of density ρ and seismic velocities v in the approach above (consideration in t eventually) is the definition of the necessary covariance matrix \underline{K}_{tt} which is based on the autocovariance functions $\text{cov}(\rho, \rho)$ and $\text{cov}(v, v)$ as well as the necessary crosscovariances $\text{cov}(\rho, t)$, $\text{cov}(v, t)$. The fulfillment of the necessary conditions (5-20), (5-21) assumes that density as well as seismic velocities are considered to be random which they are, of course, in reality not! But for the application of the theory of random processes it can be artificially derived through trend elimination; in other words, subtracting an *approximate* deterministic model leads to the corresponding anomalous (random) quantities $\delta\rho$, δv .

For the deterministic relations underlying the crosscovariance propagation we have to find some (simple) formulation which, obviously, concerns the so-called inverse problem. As a consequence, possible constraints have to be considered in order to achieve uniqueness of the solution. However, the reader should be reminded to the discussion in chapter 2, in particular, see Fig. 2.1.

The application of mixed model approaches can be nowadays found in many scientific disciplines. It is always just suited when the deterministic relationships for the explanation of mathematical/physical phenomena are insufficiently known, so that no other choice is than to live with large model discrepancies or to treat those residuals in a random way.

6. DENSITY IN AN INTEGRATED GEODETIC APPROACH

6.1 Minimum norm solutions

In the following we like to discuss (simple) models for the relationship between density and the gravity potential using a random approach. Some of them are already applied or in the context of this work numerically tested.

Generalized Poisson equation

One of the simplest models would be to start from the generalized Poisson equation (HEISKANEN, MORITZ 1967, p. 47)

$$\Delta W = -4 \pi G \rho + 2 \omega^2 \quad (6-1)$$

where Δ is the Laplace operator, W the gravity potential, G the gravitational constant, and ω is the angular velocity of the earth's rotation. The potential of gravity W is the sum of the potential of the gravitational force V and the potential of the centrifugal force Φ .

$$W = V + \Phi \quad (6-2a)$$

with

$$\Phi = 0.5 \omega^2 (x^2 + y^2) \quad (6-2b)$$

where (x,y,z) are the cartesian coordinates in a global geocentric system.

We linearize by introducing (see also chap. 5)

$$W = U + T, \quad (6-3)$$

$$\rho = \rho_0 + \delta\rho. \quad (6-4)$$

U is a *model* or *normal potential* which has to be *consistent* with the corresponding *model* or *normal density*. T is the anomalous (disturbing) potential and $\delta\rho$ the *anomalous density* function. We choose U and ρ_0 in such a way that the anomalous quantities, $\delta\rho$ and T , can be considered to be random or stochastic. Inserting (6-3), (6-4) into (6-1) and solving for $\delta\rho$ we get

$$\delta\rho = -(4\pi G)^{-1}(\Delta U + \Delta T) - \rho_0 \quad (6-5)$$

where the *anomalous density* function is given by

$$\delta\rho = -(4\pi G)^{-1}\Delta T = -(4\pi G)^{-1}\sum_{i=1}^3\partial^2 T/\partial x_i^2 \quad (6-6)$$

and the *normal density* is

$$\rho_0 = -(4\pi G)^{-1}\Delta U = -(4\pi G)^{-1}\sum_{i=1}^3\partial^2 U/\partial x_i^2 \quad (6-7)$$

Considering (6-6) as a linear observation equation where $\Delta T = \sum_{i=1}^3\partial^2 T/\partial x_i^2$ is part of the signal vector \underline{t} , see (5-11), we can define the necessary covariance function by crosscovariance propagation from those of the second-order derivatives of the potential, for example,

$$\text{cov}(\delta\rho, \delta\rho) = -(4\pi G)^{-2}\text{cov}(\Delta T, \Delta T) \quad (6-8)$$

The main drawback, however, lies in the fact that the *generalized Poisson equation is valid only in the interior of the earth*, but we are interested in the determination of the gravity potential *outside* the earth. The potential inside the earth is *not* harmonic. Second-order derivatives have jumps at discontinuities of density. Thus, (6-6) can be considered only as one possible solution out of the solution space, a so-called *zero-potential density* (MORITZ 1989).

Density as quasi-harmonic function

In order to overcome the difficulties mentioned above a proposal was made (TSCHERNING, STRYKOWSKI 1988) to consider density as a quasi-harmonic function using the condition

$$\Delta(\delta\rho/\rho(r)) = 0 \quad (6-9)$$

$p(r)$ is a polynomial only dependent on the radius of the point under consideration. Assuming $p(r) = r^n$ and considering (6-4) we get using a spherical harmonic expression,

for the *covariance function* (or reproducing kernel) of the *disturbing potential*

$$C_{TT}(P,Q) = \sum_{i=2}^{\infty} \sigma_i^2 \left[\frac{R^2}{r r'} \right]^{i+1} P_i(\cos\psi) \quad (6-10)$$

with the degree variances σ_i^2

$$\sigma_i^2 = \left[\frac{GM}{R} \right]^2 \sum_{j=0}^i (\bar{C}_{ij}^2 + \bar{S}_{ij}^2) \quad (6-11)$$

\bar{C}_{ij} , \bar{S}_{ij} are the normalized coefficients of the spherical harmonics expansion, P_i are the Legendre's polynomials, ψ is the spherical distance between points P, Q. GM is the product of the gravitational constant and the mass of the earth, R the mean radius of the earth, and $r = r(P)$, $r' = r(Q)$ are the radial distances of P, Q.

For the *covariance function of the (anomalous) density function* we get

$$C_{\delta\rho\delta\rho}(P,Q) = \sum_{i=2}^{\infty} (r r')^n \tau_i^2 \left[\frac{r r'}{R^2} \right]^i P_i(\cos\psi) \quad (6-12)$$

with

$$\tau_i^2 = \sigma_i^2 \left[\frac{M}{4\pi R^3} \right]^2 \frac{(2i+1)^2 (2i+3+n)^2}{R^{2n}} \quad (6-13)$$

and the *crosscovariance function between the disturbing potential T and $\delta\rho$* is

$$C_{T\delta\rho}(P,Q) = \sum_{i=2}^{\infty} \sigma_i^2 \tau_i^2 \frac{(r^i)^2}{r^{i+1}} P_i(\cos\psi) \quad (6-14)$$

The cross- (or auto-) covariances of all other functionals of the disturbing potential, s_i , s_j , can be derived by (the inner product)

$$\text{cov}(s_i, s_j) = s_i(P) s_j(Q) C_{TT}(P, Q) . \quad (6-15)$$

As easily verified, the use of $p(r) = r^n$ in the so-called quasi-harmonic inversion results in anomalous density values which attain their maxima and minima at the boundary of the earth. Density values at deeper localities within the earth are just a smooth mirror of the corresponding situation at the earth's surface. *This is in contradiction of the physical reality where density increases with depth.*

Density as harmonic function

Quite recently MORITZ (1989) has given a general solution for the (global) gravitational inverse problem. A general set of *continuous density distributions* for the sphere consistent with the gravitational potential outside the earth was represented using radius-dependent polynomials, spherical harmonics, and generalized matrix inverses. Based on geophysical evidence appropriate radius-dependent functions may be found which allow to determine the anomalous density (after subtracting a reference density model, see chap. 6.4) within the earth. Although still much more work has to be done in applying this model in numerical studies, it seems that the approach is suited for the construction of a global density-gravity covariance model which could be an extension of the well-known Tscherning/Rapp spherical harmonics covariance model (TSCHERNING, RAPP 1974).

Other choice-of-norm proposals

In (SANSONO *et al* 1986) different minimum norms are discussed for the density distribution of the earth. The generally used L^2 -norm (5-12) implies further that blocks of constant density are uncorrelated. If *base functions with overlapping support* are used this problem could be overcome. It leads to a reproducing kernel

$$C_{\delta\rho\delta\rho}(P, Q) = \sum_{i=1}^n I_i(P) I_i(Q) / v_i \quad (6-16)$$

where I_i is the indicator function of the i -th block with volume v_i (TSCHERNING 1989). However, the drawback there is that the density covariance function has values equal to one and zero at the earth's surface (HEIN *et al* 1988). In addition, crosscovariance propagation between density and gravity field functionals was only done numerically using Newton's attraction integral instead of (needed) analytical solutions for practical applications.

Thus, stronger norms or combination of different criteria have to be tried. The $H^{1,2}$ -norm as proposed by *SANSO et al (1986)* seems to be more realistic

$$\int_{\Omega} a \delta\rho^2 + b |\nabla(\delta\rho)|^2 d\Omega = \min \quad (6-17)$$

since it can take into account lateral variations of density within the earth's crust using the *horizontal* gradient operator ∇ in (6-17).

This principle can be extended using the so-called *mixed collocation* proposed by *SANSO, TSCHERNING (1982)*. They propose to split-up the gravity disturbing potential into a part associated with an internal sphere Ω_0 of the earth and a topographic layer including, for example, all masses between the topographic surface and the Moho. At the first part the L^2 -norm could be applied whereas to the second a Sobolev-type of norm like in (6-17) could be tried,

$$\int_{\Omega_0} a \delta\rho^2 d\Omega_0 + \int_{\Omega - \Omega_0} b |\nabla(\delta\rho)|^2 d(\Omega - \Omega_0) = \min . \quad (6-18)$$

6.2 The attenuated white noise statistical gravity model

A self consistent covariance model was developed 1976 by Heller (*HELLER, JORDAN 1979; JORDAN 1978; JORDAN, HELLER 1978*) which is able to consider also *topography* and *density contrasts* within the earth.

The *spherical* model for the autocovariance function of the disturbing potential T has the form

$$C_{TT}(r, r', \psi) = \frac{D^3 (R-D/4)^3 C_{0T} [r^2 r'^2 - (R-D/2)^4]}{[R^4 - (R-D/2)^4] [r^2 r'^2 + (R-D/2)^4 - 2(R-D/2)^2 r r' \cos\psi]^{1.5}} \quad (6-19)$$

where $\psi = |P-Q|$ is the spherical distance between two points P, Q on the earth's surface, R is the mean radius of the earth, and $r = r(P)$, $r' = r(Q)$ are the radii of P, Q . The *two free parameters* (besides ψ) scaling the model are the *variance* C_{0T} of the disturbing potential and the *characteristic depth* D .

Model (6-19) was derived from Poisson's integral for upward continuation, assuming that the disturbing potential is uncorrelated for any arbitrary small neighbourhood on the surface, so that its *white noise process distribution* looks like

$$C_{TT}(\psi') = \frac{A \delta(\psi')}{2\pi R^2 \sin \psi'} \quad (6-20)$$

where $\delta(\psi')$ is the Dirac delta function and A is the spectral density of the impulse. Because of this property (6-20) the name "*attenuated white noise*" was given to the model (6-19), since the surface integral of (6-20) over the sphere with radius R yields the value A.

For *local applications plane approximations* of (6-19) are useful. Thus, the corresponding *asymptotic relation* is obtained by considering $R \rightarrow \infty$ or $(D/R) \rightarrow 0$, $\psi \rightarrow 0$ in (6-19) resulting in

$$C_{TT}(u,v,z,z') = \frac{4D^2 (2D+z+z') C_{0T}}{[u^2+v^2+(2D+z+z')^2]^{1.5}} \quad (6-21)$$

where

$$u = x' - x = R \psi \cos \alpha \quad (6-22)$$

$$v = y' - y = R \psi \sin \alpha \quad (6-23)$$

The points under consideration have the three-dimensional orthogonal plane coordinates $P(x,y,z)$, $Q(x',y',z')$ which are related by (6-22), (6-23) to their spherical counterpart. α is the azimuth.

JORDAN (1978) has also proposed to superimpose many models of type (6-19) for more or less global applications each representing an additional white noise shell (layer) of the earth's interior. This explains also why he denotes $\delta\rho$ as density contrasts. As long as we are working only with *one shell (layer)* the density contrast between outside the earth and the first (surface) density layer corresponds to *anomalous density* $\delta\rho$ used throughout this report.

The auto- and crosscovariances of the other gravity field functionals can be derived by common covariance propagation using the well-known potential relations between them. For the reader who is interested in them, we refer to Appendix A.

Interesting in this context is how the link to density (contrasts) is established. It is founded by the theorem of Chasles (*HEISKANEN, MORITZ 1967, p. 19*) which states that *the potential V, at any point P outside the equipotential surface S, of a surface layer of density*

$$\rho = -(4\pi G)^{-1} \partial V / \partial n, \quad (6-24)$$

is the same as that of the attracting body itself. n is the outer normal. Thus, the corresponding relation with respect to the density contrast $\delta\rho$ and the disturbing potential T , at a point $P(\theta, \lambda, r)$, with spherical coordinates co-latitude θ , longitude λ , radius r ,

$$\delta\rho(\theta, \lambda, r) = -(4\pi G)^{-1} \frac{\partial}{\partial R_1} T(\theta, \lambda, r) \delta(r - R^*) \quad (6-25)$$

where

$$R^* = R - \tau. \quad (6-26)$$

By δ the Dirac delta function is denoted, and τ is the depth of the considered density contrasts (in the case of many layers). The derivative in (6-25) is evaluated at $R_1 = R^*$.

The *density contrast autocovariance function* corresponding to (6-25) and the autocovariance of the disturbing potential C_{TT} is

$$C_{\delta\rho\delta\rho}(r, r', \psi) = (4\pi G)^{-2} \frac{\partial^2}{\partial r \partial r'} C_{TT} \cdot \delta(r - R^*) \delta(r' - R^*) \quad (6-27)$$

For gravity field determination using density information the *crosscovariance between free-air gravity anomalies Δg_F and density contrasts $\delta\rho$* necessary to apply least-squares prediction is defined by

$$C_{\delta\rho\Delta g}(r, r', \psi) = (4\pi G)^{-1} \frac{\partial}{\partial r} \left[\frac{\partial}{\partial r'} + \frac{2}{r'} \right] C_{TT} \delta(r - R^*). \quad (6-28)$$

Note: When considering in the expressions above *only one density layer*, the inversion of matrix \underline{D} in the prediction formula (5-15) becomes *instable*, in the asymptotic form even *singular* in case that gravity anomalies and density data as observations are introduced. From appendix A we can easily deduce that the covariances $C_{\delta\rho\delta\rho}$ and $C_{\Delta g\delta\rho}$ as well as $C_{\delta\rho\Delta g}$ and $C_{\Delta g\Delta g}$ are linear dependent then:

$$C_{\delta\rho\delta\rho}(z, z', \psi) = (4\pi G)^{-1} \delta(z) C_{\Delta g\delta\rho}(z, z', \psi)$$

$$C_{\delta\rho\Delta g}(z, z', \psi) = (4\pi G)^{-1} \delta(z) C_{\Delta g\Delta g}(z, z', \psi)$$

Thus, the processing of a combined data set is not possible. One possibility to overcome these difficulties when considering only one layer could be the replacement of the Dirac delta function $\delta(z)$ by a function decreasing linearly or even exponentially with increasing height or height difference ($z'-z$).

As mentioned by JORDAN (1978) the model above is appropriate for density contrasts which are *not compensated isostatically*. He has therefore developed also regional isostatic compensation models for terrain and crust-mantle contrasts based on a floating elastic crust and its mean (numerical) material constants (Lamé's parameters, etc.). Starting point of this derivation is an equation for the displacement z_M of the Moho under loading which looks like the one treated by TURCOTTE, SCHUBERT (1982, p. 122). The resulting autocovariance model for gravity anomalies considering regional isostatic compensation is

$$C_{\Delta g\Delta g}(r, \Delta, \psi) = C_{\delta\rho} 4\pi^2 G^2 \left[\frac{(1-1.5 r^2/\Delta^2)}{(1+r^2/\Delta^2)^{3.5}} - \frac{2\Delta^4 (1-1.5 r^2/\Delta^2)}{\Delta^4 (1+r^2/\Delta^2)^{3.5}} + \frac{\Delta^4 (1-1.5 r^2/\Delta^2)}{\Delta^4 (1+r^2/\Delta^2)^{3.5}} \right] \quad (6-29)$$

where $r = R \psi$. Δ is a free parameter (characteristic distance) in (6-29) which has to be determined from the empirical covariance function. $C_{\delta\rho}$ is the variance of the terrain density contrasts. Further, we have

$$\Delta_1 = \Delta + 0.693 d + H \quad (6-29a)$$

$$\Delta_3 = \Delta + 1.386 d + 2H \quad (6-29b)$$

where H is the average thickness of the crust, and d is an elastic parameter which can be computed from

$$d^4 = \frac{c}{g (\rho_m - \rho_c)} \quad (6-29c)$$

with

$$c = \frac{1}{3} \frac{\mu (\lambda + \mu)}{\lambda + 2\mu} H^3 \quad (6-29d)$$

where λ , μ denote the Lamé's constants of the crust, ρ_m is the mantle density, and $\rho_0 = 1.03$ [g cm⁻³] for oceans, $\rho_0 = 0$ for continents.

6.3 A new approach to link gravity and density

As the reader might have realized from the preceding chapters, in particular 6.1, an optimal approach can only be found when considering also the *physical* relationship between gravity and density. The following proposal is mainly based on the theory of the earth's isostatic response to a concentrated load as used in (DORMAN, LEWIS 1970; LEWIS, DORMAN 1970).

For the derivations afterwards we recall, that the *Fourier transform* of $f(\underline{x})$ is defined by

$$\mathfrak{F}[f] = F(\underline{s}) = \int_{-\infty}^{\infty} f(\underline{x}) e^{-2\pi i (\underline{s}\underline{x})} d\underline{x} \quad (6-30)$$

and its inverse transform by

$$\mathfrak{F}^{-1}[F] = f(\underline{x}) = \int_{-\infty}^{\infty} F(\underline{s}) e^{2\pi i (\underline{s}\underline{x})} d\underline{s} \quad (6-31)$$

where \underline{x} , \underline{s} can be also two- or three-dimensional vectors, and consequently, the integration two- or threefold.

Convolution (denoted by $*$) of two functions $f(\underline{x})$, $g(\underline{x})$ is defined by

$$h(\underline{x}) = f(\underline{x}) * g(\underline{x}) = \int_{-\infty}^{\infty} g(\underline{u}) \cdot f(\underline{x} - \underline{u}) d\underline{u} \quad (6-32)$$

The convolution itself is also a function of \underline{x} .

6.3.1 Newton's attraction integral

We start with the gravity-density relationship by Newton's attraction integral,

$$W(\underline{x}) = G \int_{V_E} \rho(\underline{y}) l^{-1} dv_E(\underline{y}) + \Phi(\underline{x}) \quad (6-33)$$

where W is the gravity potential, G is the gravitational constant, ρ is the density, v_E is the volume of the earth, $\underline{x} = (x_1, x_2, x_3)$ and $\underline{y} = (y_1, y_2, y_3)$ are threedimensional vectors, and $l = |\underline{x} - \underline{y}|$ is their distance. The potential of the centrifugal force is given by

$$\Phi(\underline{x}) = 0.5 \omega^2 r^2 \cos^2 \varphi, \quad (6-34)$$

where ω is the angular velocity of the earth's rotation, $r = r(\underline{x})$ is the radius of a spherical earth, and $\varphi = \varphi(\underline{x})$, $\lambda = \lambda(\underline{x})$ are the spherical latitude and longitude, resp. As already mentioned we decompose density (6-4) in a reference or model part ρ_0 and an anomalous (irregular) term $\delta\rho$, the last forming a scalar stationary random process with zero mean,

$$\rho(\underline{x}) = \rho_0(\underline{x}) + \delta\rho(\underline{x}). \quad (6-35)$$

For example, the model density ρ_0 can be defined by a laterally homogeneous function as done in some earth density models (see chap. 6.4),

$$\rho(\varphi, \lambda, r) = \rho_0(r) + \delta\rho(\varphi, \lambda, r). \quad (6-36)$$

This leads to a split-up of (6-33) into

$$W(\underline{x}) = G \int_{v_E} \rho_0(\underline{y}) l^{-1} dv_E(\underline{y}) + G \int_{v_E} \delta\rho(\underline{y}) l^{-1} dv_E(\underline{y}) \quad (6-37)$$

where the first integral of the right hand side has to be consistent with the normal or reference potential U (see also 6.1) including Φ , and the second one with the disturbing or anomalous potential T . We will further assume that the kernel of the second part behaves in such a way that the integration has to be carried out only in a local region with limited volume v , so that

$$T(\underline{x}) = G \int_v \delta\rho(\underline{y}) l^{-1} dv(\underline{y}). \quad (6-38)$$

6.3.2 The isostatic response function in space-domain representation

The gravity disturbance (or also gravity anomaly in flat-earth approximation) is the vertical derivative of T

$$\delta g(\underline{x}) = \frac{\partial T}{\partial r}(\underline{x}) = G \int_V \delta \rho(\underline{y}) \mathcal{G}(\underline{x}, \underline{y}) dv(\underline{y}) \quad (6-39)$$

where $\mathcal{G}(\underline{x}, \underline{y})$ is a Green's function

$$\mathcal{G}(\underline{x}, \underline{y}) = \frac{\partial}{\partial r} (r^{-1}) = \frac{\partial}{\partial r} (|\underline{x} - \underline{y}|^{-1}) \quad (6-40)$$

and r is the earth's radius.

In the further approach we assume (using spherical coordinates φ, λ, r) that the change in density $\delta \rho(\varphi, \lambda, r)$ at a given depth under a point due to isostatic response is a function of depth alone and location alone,

$$\begin{aligned} \delta \rho(\varphi, \lambda, r) &= \iint h(\varphi', \lambda') \delta \rho(r, \varphi - \varphi', \lambda - \lambda') \cos \varphi' d\varphi' d\lambda' \\ \delta \rho(\varphi, \lambda, r) &= h * \delta \rho(r, \varphi - \varphi', \lambda - \lambda') = h * \delta \rho(r, \psi) \end{aligned} \quad (6-41)$$

where $*$ denotes the convolution (6-32) of the functions based on the coordinates φ, λ . ψ is here the central angle between (φ, λ) and (φ', λ') , defined by

$$\cos \psi = \cos \theta \cos \theta' + \sin \theta \sin \theta' \cos(\lambda - \lambda') \quad (6-42)$$

with $\theta = 90^\circ - \varphi$. Thus, the (isostatic) density changes are now expressed as a product of a function of depth alone and function of position alone. $\delta \rho(r, \psi)$ is the characteristic density change due to a unit load, and $h = h(\varphi, \lambda)$ is the elevation.

Considering (6-41) in (6-39) we get (in spherical approximation)

$$\delta g(\varphi, \lambda, r) = h * q(r, \psi) \quad (6-43)$$

where $q(r, \psi)$ is the isostatic response function,

$$q(r, \psi) = G \int_0^{r_E} \delta \rho(r', \psi) * \mathcal{G}(r', \psi) dr' \quad (6-44)$$

Looking more in detail to (6-43) δg must be the Bouguer anomaly Δg_B minus the gravity effect due to variations in density, Δg_ρ ,

$$\delta g = \Delta g_B - \Delta g_\rho \quad (6-45)$$

6.3.3 The isostatic response function in frequency-domain representation

As done in other methods recently – see, e.g., terrain correction determination – we like to use the advantages of transforming the formulas in the frequency domain by means of the Fourier transform. We will assume that due to the local applications having in mind a plane approximation is sufficient (possibly supplied by small corrections).

Considering (6-45) in (6-43) the isostatic response function in frequency-domain representation is given by (6-43) using (6-30),

$$Q = \mathfrak{F}[q] = \frac{\mathfrak{F}[\Delta g_B] - \mathfrak{F}[\Delta g_\rho]}{\mathfrak{F}[h]} \quad (6-46)$$

Since Δg_ρ is the gravity effect due to variations of density it can be assumed that the crosscorrelation between Δg_ρ and topography tends to zero. Thus, the real part of the isostatic response function in frequency-domain representation is

$$Q (|Q|) \doteq \text{Re} \frac{\mathfrak{F}[\Delta g_B]}{\mathfrak{F}[h]} \quad (6-47)$$

6.3.4 The power spectral model for gravity anomalies (disturbances)

The autocovariance function for δg forming a scalar random field is given by

$$C_{\delta g \delta g}(\underline{x}) = M \{ \delta g(\underline{y}) \delta g(\underline{x} + \underline{y}) \} \quad (6-48)$$

where M is a suitable averaging operator. Analogously, we have for the density anomalies $\delta \rho$

$$C_{\delta \rho \delta \rho}(\underline{x}) = M \{ \delta \rho(\underline{y}) \delta \rho(\underline{x} + \underline{y}) \} \quad (6-49)$$

Using the Wiener-Khinchine theorem we can express the covariance functions above in terms of their power spectral densities $C_{\delta g \delta g}$, $S_{\delta \rho \delta \rho}$

$$C_{\delta g \delta g}(\underline{x}) = \int_{-\infty}^{\infty} S_{\delta g \delta g}(\underline{s}) e^{2\pi i (\underline{s} \cdot \underline{x})} d\underline{s} \quad (6-50)$$

$$C_{\delta\rho\delta\rho}(\underline{x}) = \int_{-\infty}^{\infty} S_{\delta\rho\delta\rho}(\underline{s}) e^{2\pi i(\underline{s}\underline{x})} d\underline{s} \quad (6-51)$$

where $S_{\delta g\delta g}$, $S_{\delta\rho\delta\rho}$ are defined by the Fourier transform (6-30). Of course, the inverse relations, expressing the power spectra in terms of their covariance functions hold too, using the (inverse) Fourier transform (6-31).

We are starting our derivation now using (6-48) and inserting Newton's attraction integral (6-33). After reordering the integration we have

$$C_{\delta g\delta g}(\underline{x}) = G^2 \int_{\underline{v}} \int_{\underline{v}'} d\underline{y} d\underline{y}' \mathcal{G}(\underline{x}, \underline{y}) \mathcal{G}(\underline{x}', \underline{y}') M \{ \delta\rho(\underline{y}) \delta\rho(\underline{x} + \underline{y}') \} \quad (6-52)$$

where $M\{ \delta\rho(\underline{y}) \delta\rho(\underline{x} + \underline{y}') \} = C_{\delta\rho\delta\rho}(\underline{x})$ represents the autocovariance function of the density anomalies (6-49). We now insert in (6-52) the corresponding relation in terms of its power spectrum (6-51) and get

$$C_{\delta g\delta g}(\underline{x}) = G^2 \int_{\underline{v}} \int_{\underline{v}'} d\underline{y} d\underline{y}' \mathcal{G}(\underline{x}, \underline{y}) \mathcal{G}(\underline{x}', \underline{y}') \int_{\mathbb{R}^3} S_{\delta\rho\delta\rho}(\underline{s}) e^{2\pi i \underline{s}(\underline{y}' - \underline{y} + \underline{x})} d\underline{s} \quad (6-53)$$

The two-dimensional power spectral density of (6-53)

$$S_{\delta g\delta g}(\underline{s}) = \mathfrak{S}[C_{\delta g\delta g}(\underline{x})] \quad (6-54)$$

is of the form (* means here conjugate complex)

$$S_{\delta g\delta g}(\underline{s}_0) = G^2 \int_{\mathbb{R}^3} S_{\delta\rho\delta\rho}(\underline{s}) I(\underline{s}', \underline{x}, \underline{y}) I^*(\underline{s}', \underline{x}, \underline{y}') d\underline{s} \quad (6-55)$$

where

$$I(\underline{s}', \underline{x}, \underline{y}) = \int_{\underline{v}} \mathcal{G}(\underline{x}, \underline{y}) e^{-2\pi i \underline{s}' \cdot \underline{y}} d\underline{y} \quad (6-56)$$

$$I(\underline{s}', \underline{x}, \underline{y}') = \int_{\underline{v}} \mathcal{G}(\underline{x}, \underline{y}') e^{-2\pi i \underline{s}' \cdot \underline{y}'} d\underline{y}' \quad (6-57)$$

and

$$s' = (s'_1, s'_2, s_3)$$

Solving the integrals (6-56), (6-57) analytically, e.g., with software like REDUCE, and considering that the special Green's function (6-40) used here is defined by $\mathcal{G}(\underline{x}, \underline{y}')$ similarly)

$$\mathcal{G}(\underline{x}, \underline{y}) = \frac{-(y_3 - x_3)}{[(y_1 - x_1)^2 + (y_2 - x_2)^2 + (y_3 - x_3)^2]^{0.5}} \quad (6-58)$$

we get for (6-56), (6-57) the expressions

$$I = \frac{(i-1)s_3}{s_1'^2 + s_2'^2 + s_3^2} \quad (6-59)$$

$$I^* = \frac{(-i-1)s_3}{s_1'^2 + s_2'^2 + s_3^2} \quad (6-60)$$

Thus, expression (6-55) represents a gravity disturbance power spectral model as function of the power spectral density anomaly.

6.3.5 The gravity disturbance covariance model

As always done in geodesy we choose an analytical model for an autocovariance function whose free parameters are determined by a best approximation to the empirical derived covariance values. In this case we take the well-known *Gauss' function* to describe the *autocovariance function of density anomalies*,

$$C_{\delta\rho\delta\rho}(\underline{x}) = C_{\delta\rho}^0 (2\pi)^{-0.5} e^{-|\underline{x}^2|/2a} \quad (6-61)$$

The free parameters are the density variance $C_{\delta\rho}^0$ and the length scale parameter a . (6-61) has the power spectral density

$$S_{\delta\rho\delta\rho}(\underline{s}) = C_{\delta\rho}^0 (2\pi)^{-0.5} \int e^{-|\underline{x}^2|/2a} e^{-2\pi i \underline{s}' \cdot \underline{x}} d\underline{x} \quad (6-62)$$

After solving the integral in (6-62) we get

$$S_{\delta\rho\delta\rho}(\underline{s}) = C_{\delta\rho}^0 a^3 \pi e^{-2\pi^2 a^2 (s_1^2 + s_2^2 + s_3^2)} \quad (6-63)$$

which is inserted in the gravity disturbance power spectral model (6-55) using (6-59), (6-60)

$$S_{\delta g\delta g}(\underline{s}) = 2G^2 C_{\delta\rho}^0 a^3 \pi \int_{\mathbb{R}^3} e^{-2\pi^2 a^2 \underline{s}^2} \frac{s_3^2}{s_1'^2 + s_2'^2 + s_3'^2} d\underline{s}, \quad (6-64)$$

resulting in the analytical expression

$$S_{\delta g\delta g}(\underline{s}) = G^2 C_{\delta\rho}^0 a \pi \frac{[1 + 4\pi^2 a^2 (s_1'^2 + s_2'^2)] e^{-2\pi^2 a^2 (s_1'^2 + s_2'^2)}}{16 (s_1'^2 + s_2'^2)^{0.5}} \quad (6-65)$$

Considering the Wiener-Khinchine theorem (6-50) we can derive from (6-65) the covariance function of gravity anomalies (disturbances) as function of the variances $C_{\delta\rho}^0$ of the density autocovariance function $C_{\delta\rho\delta\rho}$, a , and the distance. Thus, we have a *consistent* model to *predict gravity anomalies* (disturbances) *using density information* on the basis of the theory of *stochastic processes*.

6.3.6 Inferences for gravity prediction applications

In the application of the theory mentioned above the assumption has to be made that the regional mechanism of compensation is of the same or similar nature in the whole area under consideration. Several approaches are now possible to use the density information for gravity field approximation.

Let us assume that after subtracting a certain (e.g., laterally homogeneous) density reference model anomalous density values $\delta\rho$ are available forming a scalar stationary random process with zero mean. Then we are able to determine the empirical anomalous density autocovariance function (6-49) which can then be fitted to the corresponding model (6-61) using adjustment techniques resulting in the determined free parameters, the variance $C_{\delta\rho}^0$ and the length scale factor a . Using these quantities the gravity anomaly power spectrum (in flat-earth approximation), see (6-65), is determined. By applying the Wiener-Khinchine

theorem (6-50) the gravity autocovariance function is defined. In a similar way as outlined in 6.34 we can also derive the crosscovariance $\text{cov}(\delta g, \delta \rho)$. Thus, we are able to define the necessary covariance matrix \underline{C}_{tt} needed to apply the prediction approach described in chapter 5 (possibly in combination with other geodetic / geometric observations).

It would be also possible to use the isostatic response function itself as gravity predictor. The spectral form (6-46) could be either determined from a Bouguer gravity anomaly field and applied in unsurveyed areas showing the same compensation mechanism. In this case the Wiener-Khinchine theorem has to be used and the convolution (6-43) carried out with the actual topography. If density information is available in the area, the isostatic response function can be determined numerically by (6-44), in addition, resulting most likely in a more improved and detailed resolution which reflects the local compensation.

If namely the compensation is assumed to be due to a change of density as a function of depth $\Delta\rho(r)$ occurring directly beneath the load, then the transfer function Q (6-46) can be directly constructed by

$$Q(\underline{s}) = G \int_0^{r_E} \Delta\rho(r) e^{-2\pi r s} dr. \quad (6-66)$$

This follows from applying Hankel's transform to (6-44).

Some available gravity data in the area would be useful to transform the gravity anomalies derived via (6-43) into the right frame (adding a trend, for example).

Estimating the isostatic response function is widely applied now in modern geophysics. A survey is found, e.g., in (LAMBECK 1988; p.425). The corresponding transfer function (6-46) can be used to estimate the mean density of the topography, similar to the Nettleton approach, see LEWIS, DORMAN (1970, p.3373).

$$\rho = \frac{1}{2\pi} \left[\left\langle \text{Re} \frac{\mathfrak{F}(\Delta g_F(\underline{s}))}{\mathfrak{F}(H(\underline{s}))} \right\rangle + \left\langle \text{Re} \frac{\mathfrak{F}(\Delta g_T(\underline{s}))}{\mathfrak{F}(H(\underline{s}))} \right\rangle \right] \quad (6-67)$$

$$\rho = \frac{1}{2\pi} \left[Q'(\underline{s}) + \left\langle \text{Re} \frac{\mathfrak{F}(\Delta g_T(\underline{s}))}{\mathfrak{F}(H(\underline{s}))} \right\rangle \right] \quad (6-68)$$

$$\rho = \frac{1}{2\pi} \left[Q(\underline{s}) + 2\pi G \rho - \left\langle \text{Re} \frac{\Delta g_T(\underline{s})}{H(\underline{s})} \right\rangle \right] \quad (6-69)$$

where Δg_F are free-air gravity anomalies, Δg_T are the terrain corrections, and H is the elevation. The brackets $\langle \cdot \rangle$ indicate averaging. The transfer function $Q'(s)$ is related to the gravity field of the compensation and topography.

One remark to the type of available density data: In general those data come from borehole investigations and characterize only the parts of the earth's crust near the earth's surface. In constructing the isostatic response function according to (6-44) the integration has to be carried out between the center of mass and the surface. Thus, for the interior of the earth certain density earth models have to be used. If the stochastic approach (see chapter 5) is applied as mentioned before those models can be used also to achieve the zero mean of density anomalies as required for the application of the theory of random processes.

On the other hand it might be worthwhile to consider the possibility of constructing always first the isostatic response function (6-44) in order to use it as some kind of (pseudo-) observation in least-squares prediction. The advantage of using it instead of (anomalous) density values lies in the fact that the isostatic response is a function depending only on the horizontal distance $f(\varphi-\varphi', \lambda-\lambda')$, and no more on the depth (or radius, resp.) as it is the case with density. Insofar, such a quantity fits better to an integrated adjustment of geodetic/geophysical observations using least-squares collocation (or prediction).

6.4 Reference (normal) density models

In chapter 6.1 – see (6-3) or (6-37), resp. – the reference or normal potential was introduced

$$U(\underline{x}) = G \int_{V_E} \rho_0(\underline{y}) l^{-1} dv_E(\underline{y}) \quad (6-70)$$

where ρ_0 is the so-called *normal* or *model density*. Due to the integration of different type of observations in the least-squares collocation model of integrated geodesy, ρ_0 has to be consistent with U , e.g., $U = f(\rho_0)$. Thus, assuming that we usually work with a normal potential model adapted by the International Association of Geodesy, the corresponding earth density model has, in principle, to come from the inverse gravimetric problem, $\rho_0 = f(U)$, which has no unique solution (MATYSKA 1987; MORITZ 1989).

Thus, the *reference density model* has to fulfill the following conditions:

- (1) The mass of the earth M has to be reproduced by ρ_0

$$M = \int_{v_E} \rho_0(\underline{y}) dv_E(\underline{y}) \quad (6-71)$$

- (2) The normal density distribution should have ellipsoidal or spherical geometry consistent with the normal potential. Analogously, the geometry of the different layers of shells should be of the same form.

Thus we have (with respect to an ellipsoidal normal potential of the earth) to fulfill the relation

$$J_{20} = \frac{C - (A+B)/2}{M a^2} \quad (6-72)$$

where J_{20} is the underlying coefficient of the spherical harmonic expansion (dynamic flattening). A , B , C are the moments of inertia defined in (*HEISKANEN, MORITZ 1967, p. 62*)

$$A = \int_{v_E} (y_2^2 + y_3^2) \rho_0(\underline{y}) dv(\underline{y}) \quad (6-73)$$

$$B = \int_{v_E} (y_1^2 + y_3^2) \rho_0(\underline{y}) dv(\underline{y}) \quad (6-74)$$

$$C = \int_{v_E} (y_1^2 + y_2^2) \rho_0(\underline{y}) dv(\underline{y}) \quad (6-75)$$

where $\underline{y} = (y_1, y_2, y_3)$ are geocentric cartesian coordinates.

- (3) If the density distribution is within a sphere with mean radius R

$$R = \sqrt[3]{a^2 b} \quad (6-76)$$

and the reference potential generating body is rotating with angular velocity ω , our density earth model is consistent with the normal potential. a , b in (6-76) are the two axes of the ellipsoid. For a spherical earth model we have to set $a = b$.

It might be possible, in particular with respect to very local applications, that a simple geometric trend function can be used, too, in order to generate our anomalous densities $\delta\rho$.

Various models and proposals are already developed in the geodetic / geophysical literature. The reader is referred to *BULLEN (1975)*, *KHAN (1982)*, *MARTINEC, PĚČ (1986 a,b)*, *MESHCHERYAKOV et al (1986)*, *MORITZ (1989)*, *PĚČ, MARTINEC (1984)*, *RUMMEL et al (1988)*, *SÜNKEL (1986)*, *TSCHERNING, SÜNKEL (1981)*.

7. SEISMIC AND SEISMOLOGICAL DATA IN AN INTEGRATED APPROACH

In the following a first attempt is made to use seismic data in gravity prediction. The outlined approaches are rather possible proposals than fully developed algorithms. Still more work has to be done in that field since geophysicists started to develop three-dimensional digital seismic velocity models of (parts of) the earth which will be available in near future. In our study a corresponding model was developed for the European Alps (see chap. 8).

7.1 Simple seismic velocity-density relationship in a homogeneous medium

Through seismic experiments artificial shocks (or explosions) are generated to which the earth responds by releasing part of the energy in form of *elastic waves* which travel through rocks with a certain velocity *depending on density and elastic moduli*. The same happens when earthquakes occur. The types of *body waves* (there are also *surface waves*) follow the laws of geometrical optics being reflected and refracted at layer boundaries where the velocity (and consequently, the material constants) changes.

Assuming a *homogeneous* medium we observe the so-called *P waves, longitudinal waves*, due to transmission of compressions and rarefactions, whose velocities v_p are given by

$$v_p = \left[\frac{\lambda + 2\mu}{\rho} \right]^{0.5} \quad (7-1)$$

where λ , μ are the *Lamé* elastic parameters characterizing the material, and ρ is the *density*. In seismology, it is convenient to replace the parameter λ by the so-called *bulk modulus* k ,

$$k = \lambda + \frac{2}{3}\mu \quad (7-2)$$

so that we get for *P waves*

$$v_p = \left[\frac{k + \frac{4}{3}\mu}{\rho} \right]^{0.5} \quad (7-3)$$

μ is also called the *rigidity modulus*.

The *S* (shear) wave velocities (transverse wave motion) are given by

$$v_s = (\mu/\rho)^{0.5} . \quad (7-4)$$

Thus, (7-3) and (7-4) represent the relationship between seismic velocities and density, so far the bulk and rigidity moduli are known and a homogeneous medium is assumed. The non-linear relations can be linearized and - at least theoretically - observation equations can be built up as a function of the disturbing gravity potential using Poisson's equation (6-1). Remember, however, the implications with it discussed in chap. 6. By doing so, we get (Δ is here the Laplace operator)

$$\delta v_p = (8\pi G)^{-1} (k_0 + \frac{4}{3}\mu_0)^{0.5} \rho_0^{-1.5} \Delta T \quad (7-5)$$

and

$$\delta v_s = (8\pi G)^{-1} \mu_0 \rho_0^{-1.5} \Delta T \quad (7-6)$$

where ΔT indicates that the relations to second order derivatives $\Delta T = \sum_{i=1}^3 \partial^2 T / \partial x_i^2$ are established. $\delta v_p = v_p - v_{p_0}$, $\delta v_s = v_s - v_{s_0}$ are the residual observations, and k_0 , μ_0 , ρ_0 are known (approximate) values.

As extensively discussed in chap. 3 and verified by own calculations, we can find a *linear empirical relationship* between densities and P wave velocities of the form (BIRCH 1961)

$$\rho = \bar{a} + \bar{b} v_p \quad (7-7)$$

or, expressed as $v_p = f(\rho)$, we get

$$v_p = -a + b \rho \quad (7-8)$$

where

$$b = \bar{b}^{-1} = \partial v / \partial \rho, \quad a = b \bar{a} \quad (7-9)$$

BIRCH (1961) has published for $a = 0.41$ [g cm⁻³] and for $\bar{b} = 0.3597$ [(g cm⁻³)/(km sec⁻¹)] corresponding to approximately $b = 2.8$ [(km sec⁻¹)/(g cm⁻³)] which he found from laboratory experiments. It is well known from studies with actual data, that those coefficients b

found are somewhat higher in the range 4 ... 5.5 [(km sec⁻¹)/(g cm⁻³)]. Our own experiment showed a mean value of 5.4 ± 0.4 for the European Alps. Even more complex relationships can be established; see, e.g., ANDERSON (1967, 1970), BUNTEBARTH (1982), RYBACH, BUNTEBARTH (1982).

Thus, assuming that a sufficient trend (or constant) with respect to the v_p velocities is subtracted from the data, so that we can work with *residual or anomalous velocities* δv forming a scalar stationary random process, the coefficient b (7-9) can be used for constructing the relevant covariance propagation which is needed to consider it in the integrated model for gravity prediction.

We further think that *digital three-dimensional seismic velocity models* will be available in near future – we have one constructed over the European Alps, see chap. 8 – so that those informations can be used to determine and/or to improve the gravity field. In this context, also proposals and developments for global P velocity models in the form of spherical harmonic models are already made (DZIEWONSKI 1984; PĚČ, MARTINEC 1985; WOODHOUSE, DZIEWONSKI 1984).

7.2 Seismic wave motion in an inhomogeneous medium

Since density ρ and elastic Lamé parameters λ , μ (or bulk and rigidity moduli, respectively) are *very irregular functions of position*, they may be treated as *randomly distributed in space* forming a *stochastic process*. These statements refer to the famous work of CHERNOV (1960). Meanwhile among geophysicists the theory was successfully applied, see, e.g. AKI (1973), CAPON (1974), KNOPOFF, HUDSON (1964), KORN (1987) – to mention also some.

Thus, KNOPOFF, HUDSON (1964) introduced six correlation functions of the form

$$C_{\lambda\lambda} = \text{cov}(\delta\lambda(P), \delta\lambda(Q)) \quad (7-10)$$

$$C_{\mu\mu} = \text{cov}(\delta\mu(P), \delta\mu(Q)) \quad (7-11)$$

$$C_{\rho\rho} = \text{cov}(\delta\rho(P), \delta\rho(Q)) \quad (7-12)$$

$$C_{\lambda\mu} = \text{cov}(\delta\lambda(P), \delta\mu(Q)) \quad (7-13)$$

$$C_{\lambda\rho} = \text{cov}(\delta\lambda(P), \delta\rho(Q)) \quad (7-14)$$

$$C_{\mu\rho} = \text{cov}(\delta\mu(P), \delta\rho(Q)) \quad (7-15)$$

and treated the quantities $\delta\rho$, $\delta\lambda$, $\delta\mu$ as signals which perfectly fit to our proposed integrated approach in conformity to least-squares collocation.

Following *KNOPOFF, HUDSON (1964)* the basic equation of wave motion in an inhomogeneous elastic medium is given by the following partial differential equation

$$\begin{aligned} \rho \frac{\partial^2 \underline{u}}{\partial t^2} = & \nabla \{(\lambda + 2\mu) \nabla \cdot \underline{u}\} - \nabla \times \mu \nabla \times \underline{u} \\ & + 2(\nabla \mu \cdot \nabla) \underline{u} - 2(\nabla \mu) \nabla \cdot \underline{u} + 2(\nabla \mu) \times \nabla \times \underline{u} \end{aligned} \quad (7-16)$$

where

- \underline{u} ... seismic displacement vector (observed by seismographs),
- ρ ... density,
- μ, λ ... elastic parameters (Lamé constants),
- t ... time,
- ∇ ... gradient operator,
- $\nabla \cdot$... divergence operator,
- $\nabla \times$... rotation operator.

For the sake of simplicity we want to discuss *only* the effect of *density anomalies* on *wave motion*. Thus, we assume, that λ and μ are (known) constants. This assumption does not always conform with reality, but simplifies the discussion. We are mainly interested in density anomalies, since their relationship to gravity was discussed in the chapters before.

The generalization with respect to all three parameters ρ, λ, μ can be done using the work of *KNOPOFF, HUDSON (1964)* and *CHERNOV (1960)*. The formal solution already exists.

Starting point is again the decomposition

$$\rho = \rho_0 + \delta\rho \quad (7-17)$$

$$\lambda = \lambda_0 \quad (7-18)$$

$$\mu = \mu_0 \quad (7-19)$$

where ρ_0 , λ_0 , μ_0 are approximate values and constants, and $\delta\rho$ are density anomalies. In the same way we decompose the displacement vector \underline{u} in

$$\underline{u} = \underline{u}_0 + \delta\underline{u} \quad (7-20)$$

where

\underline{u}_0 is the approximate value, and

$\delta\underline{u}$ is the variation of the displacement vector due to density anomalies.

As a consequence of (7-17) to (7-19) the gradients are $\nabla\lambda_0 = \underline{0}$, $\nabla\mu_0 = \underline{0}$, and $\nabla\rho_0 = \underline{0}$, which enter the basic equation of motion (7-16). It can be linearized resulting in

$$\frac{\partial^2 \underline{u}_0}{\partial t^2} = \frac{\lambda_0 + 2\mu_0}{\rho_0} \nabla (\nabla \cdot \underline{u}_0) - \frac{\mu_0}{\rho_0} \nabla \times (\nabla \times \underline{u}_0) \quad (7-21)$$

$$\frac{\partial^2 \delta\underline{u}}{\partial t^2} = \frac{\lambda_0 + 2\mu_0}{\rho_0} \nabla (\nabla \cdot \delta\underline{u}) - \frac{\mu_0}{\rho_0} \nabla \times (\nabla \times \delta\underline{u}) + \underline{f} \quad (7-22)$$

where

$$\underline{f} = -\frac{\partial^2 \underline{u}_0}{\partial t^2} \delta\rho \quad (7-23)$$

(7-21) defines the approximate wave motion, if the medium would be homogeneous. (7-22) is the inhomogeneous elastic wave equation which relates the variation $\delta\underline{u}$ of the displacement vector to the density anomalies $\delta\rho$, where \underline{f} is the disturbing force.

It is further common to introduce the wave velocities α and β defined by

$$\alpha^2 = \frac{\lambda_0 + 2\mu_0}{\rho_0} \quad (7-24)$$

$$\beta^2 = \frac{\mu_0}{\rho_0} \quad (7-25)$$

For the solution of wave equations like (7-21), (7-22) we decompose the displacement vector in one part, which is due to a compression (P) wave, and in another part, which is due to a shear (S) wave. Thus, introducing

$$\delta\phi = \nabla \cdot \delta\underline{u} \quad (7-26)$$

$$\delta\underline{w} = \nabla \times \delta\underline{u} \quad (7-27)$$

we find from (7-22)

$$\frac{\partial^2 \delta\phi}{\partial t^2} = \alpha^2 \Delta \delta\phi + \nabla \cdot \underline{f} \quad \text{P wave} \quad (7-28)$$

$$\frac{\partial^2 \delta\underline{w}}{\partial t^2} = \beta^2 \Delta \delta\underline{w} + \nabla \times \underline{f} \quad \text{S wave} \quad (7-29)$$

where Δ is the Laplace operator.

Assuming we have solved (7-28), (7-29) the displacement vector variation $\delta\underline{u}$ is given by

$$\delta\underline{u} = \nabla \delta\phi + \nabla \times \delta\underline{w} \quad (7-30)$$

Under the assumption that the incident wave \underline{u}_0 is harmonic, that means time-dependent with $e^{-i\omega t}$, the solutions for $\delta\phi$ and $\delta\underline{w}$ can be found in *KNOPOFF, HUDSON (1964)*.

$$\delta\phi = -\frac{1}{4\pi\rho_0\omega^2} \int_{\underline{v}} (\nabla' \cdot \underline{f}) \frac{e^{ik_\alpha l}}{l} dv \quad (7-31)$$

$$\delta\underline{w} = +\frac{1}{4\pi\rho_0\omega^2} \int_{\underline{v}} (\nabla' \times \underline{f}) \frac{e^{ik_\beta l}}{l} dv \quad (7-32)$$

where (r, θ, λ) are spherical coordinates (radius, co-latitude, longitude) and ψ is the spherical distance (P,Q)

$$l = [r^2 + r'^2 - 2rr' \cos\psi]^{0.5}, \quad r = r(P), \quad r' = r(Q) \quad (7-33)$$

$$dv = r'^2 \sin\theta' dr' d\theta' d\lambda \quad (7-34)$$

$$k_\alpha = \omega/\alpha \quad (7-35)$$

$$k_\beta = \omega/\beta \quad (7-36)$$

$$\nabla' = \frac{\partial}{\partial r'} \underline{e}_r + \frac{1}{r' \sin\theta'} \frac{\partial}{\partial r'} \underline{e}_\lambda + \frac{\partial}{\partial \theta'} \underline{e}_\theta \quad (7-37)$$

(gradient operator in spherical coordinates)

ω is the frequency of the incident wave, and using (7-31), (7-32) we find for the displacement vector variation $\delta\underline{u}$ (7-30)

$$\begin{aligned} \delta\underline{u} = & -\frac{1}{4\pi\rho_0\omega^2} \int_{\underline{v}} (\nabla' \cdot \underline{f}) \cdot \nabla \left[\frac{e^{ik_\alpha l}}{l} \right] dv \\ & + \frac{1}{4\pi\rho_0\omega^2} \int_{\underline{v}} \left[\nabla \frac{e^{ik_\beta l}}{l} \right] \times (\nabla' \times \underline{f}) dv \end{aligned} \quad (7-38)$$

We notice the *important* fact, that the integral solution for $\delta \underline{u}$ (7-38) is in principle of the same form as the expressions for the gravity field functionals using Newton's attraction integral. The variation $\delta \underline{u}$ of the displacement vector is also given as an integral over the volume v , where v should coincide with the volume in which we have density anomaly data. The density anomalies enter in (7-38) via the disturbing vector \underline{f} .

The incident wave \underline{u}_0 is assumed to be harmonic, e.g., \underline{u}_0 is a function of the form

$$\underline{u}_0(P,t) = e^{-i\omega t} \underline{u}_0(P) \quad (7-39)$$

with time-dependence $e^{-i\omega t}$ and $P(r, \theta, \lambda)$. Considering (7-39) we find for \underline{f} (7-23)

$$\underline{f}(P,t) = \omega^2 e^{-i\omega t} \delta\rho(P) \underline{u}_0(P) . \quad (7-40)$$

In order to evaluate the integrals for the displacement vector $\delta \underline{u}$ we have to insert \underline{f} at the integration point $Q(r', \theta', \lambda')$ into the integrals and to compute the divergence and rotation. Thus,

$$(\nabla' \cdot \underline{f}) = \omega^2 e^{-i\omega t} [\nabla' \delta\rho(Q) \underline{u}_0(Q) + \delta\rho(Q) \nabla' \cdot \underline{u}_0(Q)] \quad (7-41)$$

$$(\nabla' \times \underline{f}) = \omega^2 e^{-i\omega t} [\nabla' \delta\rho(Q) \times \underline{u}_0(Q) + \delta\rho(Q) \nabla' \times \underline{u}_0(Q)] \quad (7-42)$$

We can see from (7-41), (7-42) that *the displacement vector variation $\delta \underline{u}$ is not only a function of $\delta\rho$ itself, but also a function of the density gradient $\nabla' \delta\rho$* . This means that a change of density in the volume v will cause an effect on the displacement vector, a physically realistic model.

For the components of $\nabla \left[\frac{e^{icl}}{r} \right]$, $c = \{k_\alpha, k_\beta\}$, we get the following expressions using spherical coordinates:

$$\frac{\partial}{\partial r} \left[\frac{e^{icl}}{r} \right] = \frac{e^{icl}}{r^2} \left[icl \frac{\partial l}{\partial r} - \frac{\partial}{\partial r} \left[\frac{1}{r} \right] \right] \quad (7-43)$$

$$\frac{\partial}{\partial \theta} \left[\frac{e^{icl}}{r} \right] = \frac{e^{icl}}{r^2} \left[icl \frac{\partial l}{\partial \theta} - \frac{\partial}{\partial \theta} \left[\frac{1}{r} \right] \right] \quad (7-44)$$

$$\frac{\partial}{\partial \lambda} \left[\frac{e^{icl}}{r} \right] = \frac{e^{icl}}{r^2} \left[icl \frac{\partial l}{\partial \lambda} - \frac{\partial}{\partial \lambda} \left[\frac{1}{r} \right] \right] \quad (7-45)$$

$$\frac{\partial l}{\partial r} = \frac{r - r' \cos \psi}{l} \quad (7-46)$$

$$\frac{\partial l}{\partial \theta} = \frac{r r' \sin \psi \cos \alpha}{l} \quad (7-47)$$

$$\frac{\partial l}{\partial \lambda} = \frac{r r' \sin \psi \cos \phi \sin \alpha}{l} \quad (7-48)$$

The derivatives of $(1/l)$ are

$$\frac{\partial}{\partial r} \left[\frac{1}{l} \right] = \frac{r - r' \cos \psi}{l^2} \quad (7-49)$$

$$\frac{\partial}{\partial \theta} \left[\frac{1}{l} \right] = \frac{r r' \sin \psi \cos \alpha}{l^3} \quad (7-50)$$

$$\frac{\partial}{\partial \lambda} \left[\frac{1}{l} \right] = \frac{r r' \sin \psi \cos \phi \sin \alpha}{l^3} \quad (7-51)$$

$$\left[\frac{\partial}{\partial r} + \frac{2}{r} \right] \left[\frac{1}{l} \right] = \frac{r^2 - r r' \cos \psi - 2 l^2}{r \cdot l^3} \quad (7-52)$$

where $P(r, \varphi, \lambda)$, $Q(r', \varphi', \lambda')$, $\varphi = 90^\circ - \theta$, and α is the azimuth.

For the evaluation of the volume integrals in (7-38) we have again to apply a discretisation, e.g., replacing integration by summation over small volume elements.

If we assume, that an observed set of displacement vectors $\underline{u}(P_i, t_j)$ at stations P_i and at different times t_j are available reduced with regard to $\underline{u}_0(P_i, t_j)$, we get from (7-38) in connection with (7-41), (7-42) the following observation equations in matrix form

$$l = \underline{A} \underline{\rho} + \underline{B} \nabla \underline{\rho} + \underline{n} \quad (7-53)$$

where

$$l \dots (\delta u(P_i, t_j)) \quad (7-54)$$

$$\underline{\rho} \dots (\delta \rho(Q_i)) \quad (7-55)$$

$$\nabla \underline{\rho} \dots (\nabla \delta \rho(Q_i)) \quad (7-56)$$

\underline{n} is the observational noise and \underline{A} , \underline{B} are design matrices consisting of the kernels of (7-38).

7.3 A possibility of evaluating the autocovariance function of density anomalies from seismic observations

The concept of solution assumes that we know the autocovariance function of density anomalies $C_{\delta\rho\delta\rho}$. The computation can be done using available density data as outlined in chap. 6 and done numerically in this study (see chap. 8, 9).

Another method of determination of $C_{\delta\rho\delta\rho} = \text{cov}(\delta\rho, \delta\rho)$ is outlined in (*KNOPOFF, HUDSON 1964*) which is similar to variance-component estimation. The method is based on the analysis of seismic observations $\underline{l} = (\delta\underline{u}(P,t))$ providing an a priori base function representation of $C_{\delta\rho\delta\rho}$ with unknown constants. *KNOPOFF, HUDSON (1964)* have used a Gauss' function in their approach.

$$C_{\delta\rho\delta\rho}(P,Q) = C_{\delta\rho}^0 e^{-\alpha_p^2 |P-Q|} \quad (7-57)$$

But we may also think of a spherical harmonic representation of $C_{\delta\rho\delta\rho}$:

$$C_{\delta\rho\delta\rho}(P,Q) = \sum_{n=0}^N c_n(P,Q) \cdot P_n(\cos\psi) \quad (7-58)$$

In (7-58) the factors $c_n(P,Q)$ may be treated as constants (in very local investigations); they may be some functions of radial distances, considering the variations of density with depth.

Let us assume now, that we have a network of seismic stations P_i at the earth's surface. At each seismic station P_i , it is possible to observe the displacement vector $\underline{l} = (\delta\underline{u}(P_i,t))$ as a function of time for a seismic event.

With \underline{l} we start the covariance analysis by computing for each station P_i the covariance matrix $\underline{C}_{11} = (P_i, P_i)$

$$\underline{C}_{11} = E \{ \underline{l} \underline{l}^* \} \quad (7-59)$$

Note, that $*$ denotes here the conjugate-complex transposition, because we deal with complex operators and observations.

Using (7-53) in (7-59) we get

$$\underline{C}_{11}(P_i, P_i) = \underline{A} \underline{C}_{\delta\rho\delta\rho} \underline{A}^* + \underline{A} \nabla \underline{C}_{\delta\rho\delta\rho} \underline{B}^* + \underline{B} \nabla \underline{C}_{\delta\rho\delta\rho} \underline{A}^* + \underline{A} \nabla \nabla \underline{C}_{\delta\rho\delta\rho} \underline{B}^* + \underline{C}_{nn} \quad (7-60)$$

Having assumed that the incident wave \underline{u}_0 is harmonic with time-dependence $e^{-i\omega t}$ we notice, that for a station P_i \underline{l} is now no more any longer time-dependent because of $e^{-i\omega t} \cdot e^{i\omega t} = 1$.

The computation of \underline{C}_{11} is obtained by evaluation of the seismograms in vertical and horizontal direction.

The matrix $\underline{C}_{\delta\rho\delta\rho}$ consists of all covariances between the discrete points in the volume v . The further way is to substitute a model for a covariance function like (7-57) or (7-58) into the covariance matrix $\underline{C}_{\delta\rho\delta\rho}$. For example, the covariance function (7-57) is a function of the distance $|P-Q|$ with two free parameters, the variance $C_{\delta\rho}^0$ and the distance-scale parameters α_p to be determined.

Under the assumption, that we know some approximate values for $C_{\delta\rho}^0$, α_p , we may expand \underline{C}_{11} , see (7-60), into a Taylor series, neglecting all higher-order terms,

$$\underline{C}_{11}(P_i, C_{\delta\rho}^0, \alpha_p) = \underline{C}_{11}^0(P_i, C_{\delta\rho}^0, \alpha_p) + \frac{\partial \underline{C}_{11}}{\partial C_{\delta\rho}^0} \delta C_{\delta\rho}^0 + \frac{\partial \underline{C}_{11}}{\partial \alpha_p} \delta \alpha_p \quad (7-61)$$

Using the observation vector \underline{l} , we may compute the so-called *mean square fluctuation* (KNOPOFF, HUDSON 1964), that is the variance $C_0(\underline{l})$.

$$C_0(\underline{l}) = \underline{l}^* \underline{C}_{11} \underline{l} \quad (7-62)$$

Considering (7-61) together with (7-62) it should be possible to *minimize* the difference $\delta C_1(P_i)$

$$\delta C_1(P_i) = C_0(\underline{l}) - C_0^0(\underline{l}) = \underline{l}^* \underline{C}_{11} \underline{l} - \underline{l}^* \underline{C}_{11}^0 \underline{l} + \underline{l}^* \frac{\partial \underline{C}_{11}}{\partial C_{\delta\rho}^0} \underline{l} \delta C_{\delta\rho}^0 + \underline{l}^* \frac{\partial \underline{C}_{11}}{\partial \alpha_p} \underline{l} \delta \alpha_p \quad (7-63)$$

with respect to $\delta C_{\delta\rho}^0$ and $\delta \alpha_p$ (the unknown parameters of the covariance function (7-57) for all seismic stations P_i , $i = \{1, \dots, N\}$).

In this way we may obtain improved parameters for the autocovariance function $C_{\delta\rho\delta\rho}$. Eqs. (7-59) to (7-63) are in principle a discrete approach to the discussions of *KNOPOFF, HUDSON (1964)*. Here an integral expression for the mean square fluctuation (7-62) is derived. Subsequently, the covariance function (7-57) is inserted into the integral and the integration is performed. The result of integration yields also the mean-square fluctuation as a function of $C_{\delta\rho}^0$ and α_ρ .

8. TEST DATA

8.1 Test network "Rossdorf"

The test area Rossdorf is located around 50 km south of Frankfurt/F.R. Germany. It has an extension of $26 \times 23 \text{ km}^2$ and is especially well-suited because of large variations in (surface) density. This is due to the fact that part of the area belongs to the Rhinegraben whose upper layer consists of sedimentary fillings. The eastern part of the test area belongs to the so-called "Odenwald", a low mountain range. For the investigations 78 (point) gravity observations were available. At these stations, at least in the near neighbourhood, also surface densities were determined by a geologist (*FAHLBUSCH 1987, pers. comm.*). The density data are estimates coming from laboratory investigations, boreholes, and descriptions found in corresponding archives. They should be representative for a cylinder of about 150 m in diameter around the gravity station and a depth of approximately 1 km.

The coverage of the area with observational points cannot be described to be homogeneous, because they follow more or less levelling lines, see Fig. 8.1. The density values vary largely from 2.48 g/cm^3 to 3.02 g/cm^3 . The area has only height variations of a few hundred meters. The topography is plotted in Fig. 8.2 and a contour-line plot of surface densities is given in Fig. 8.3.

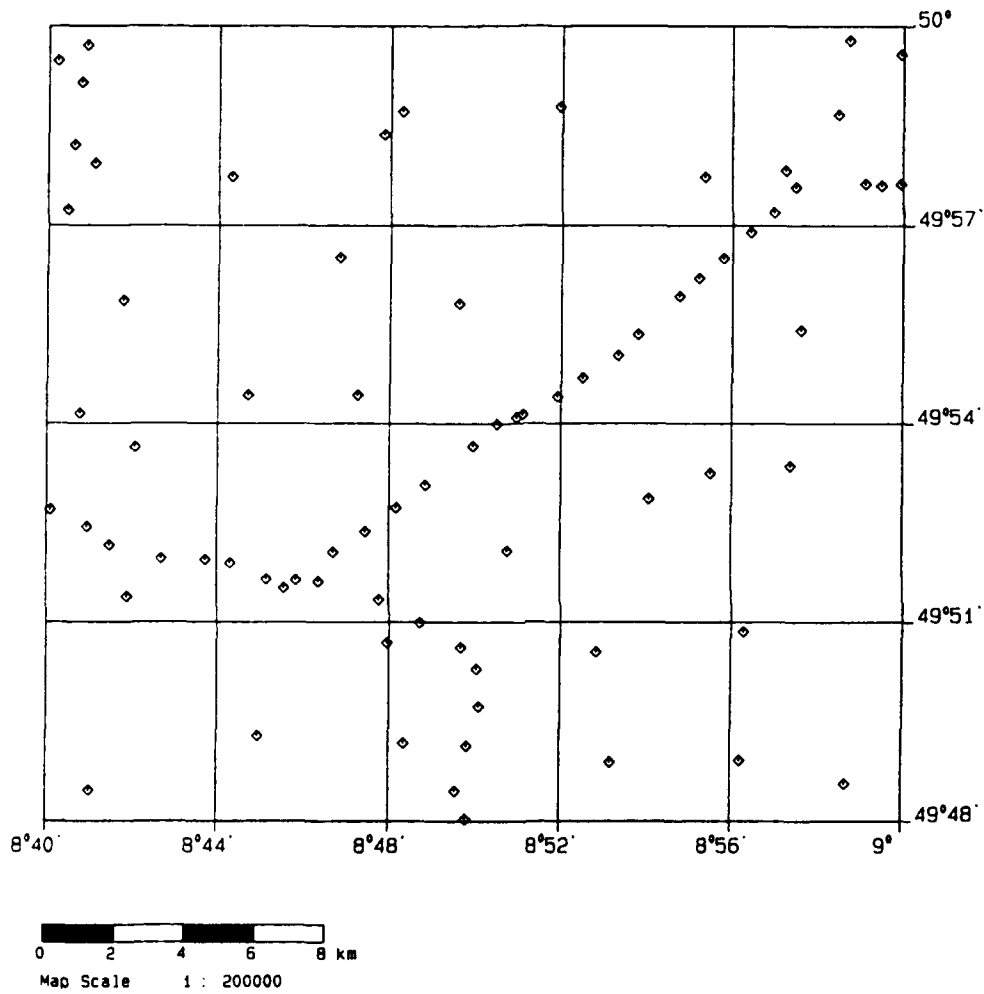


Fig. 8.1. Stations in test network "Rossdorf".

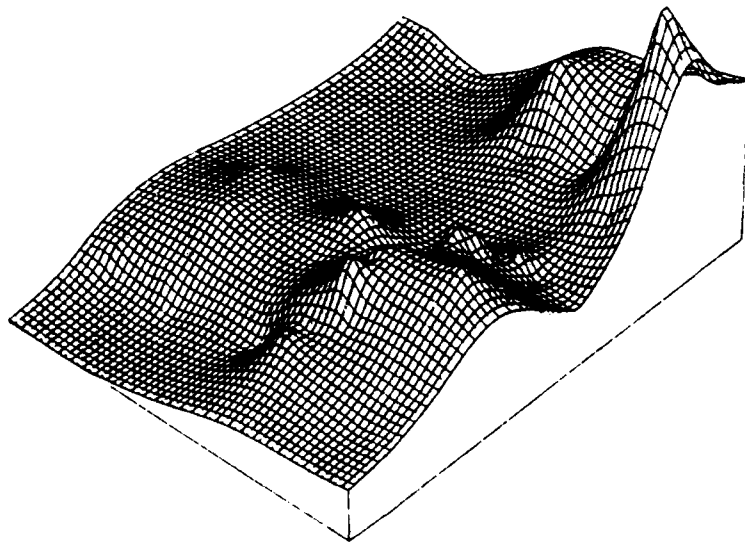
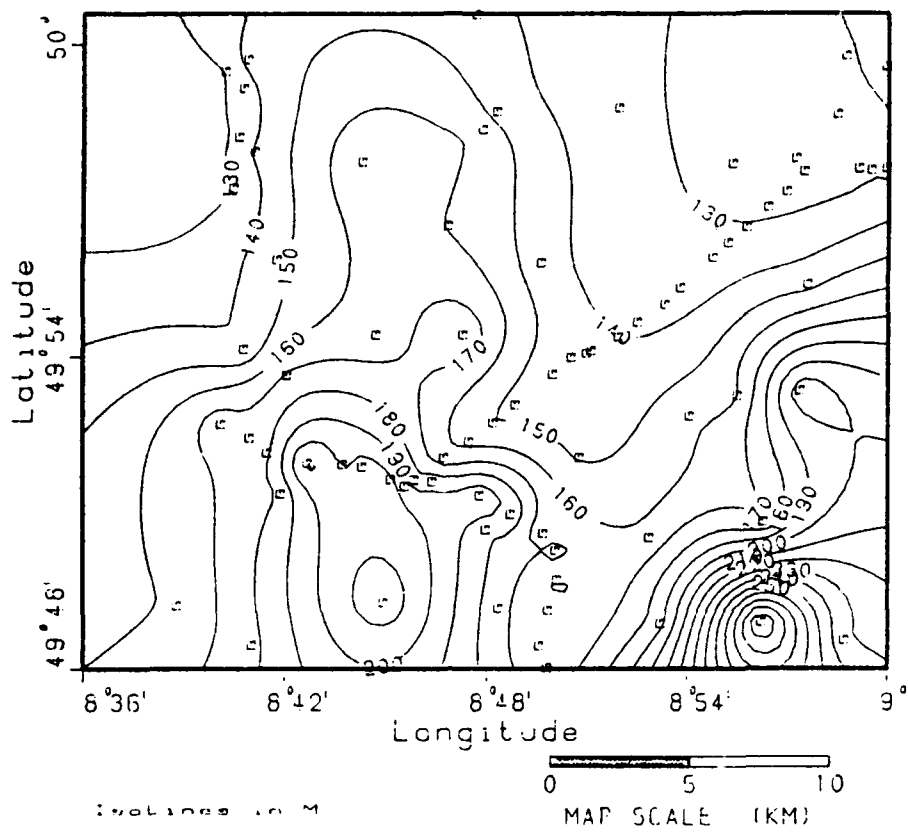


Fig. 8.2. Orthometric heights in test network "Rossdorf".

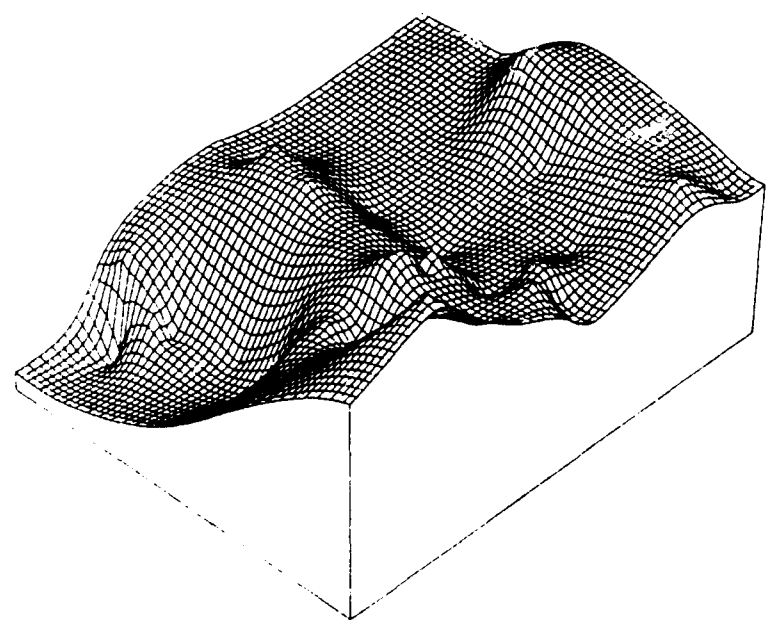
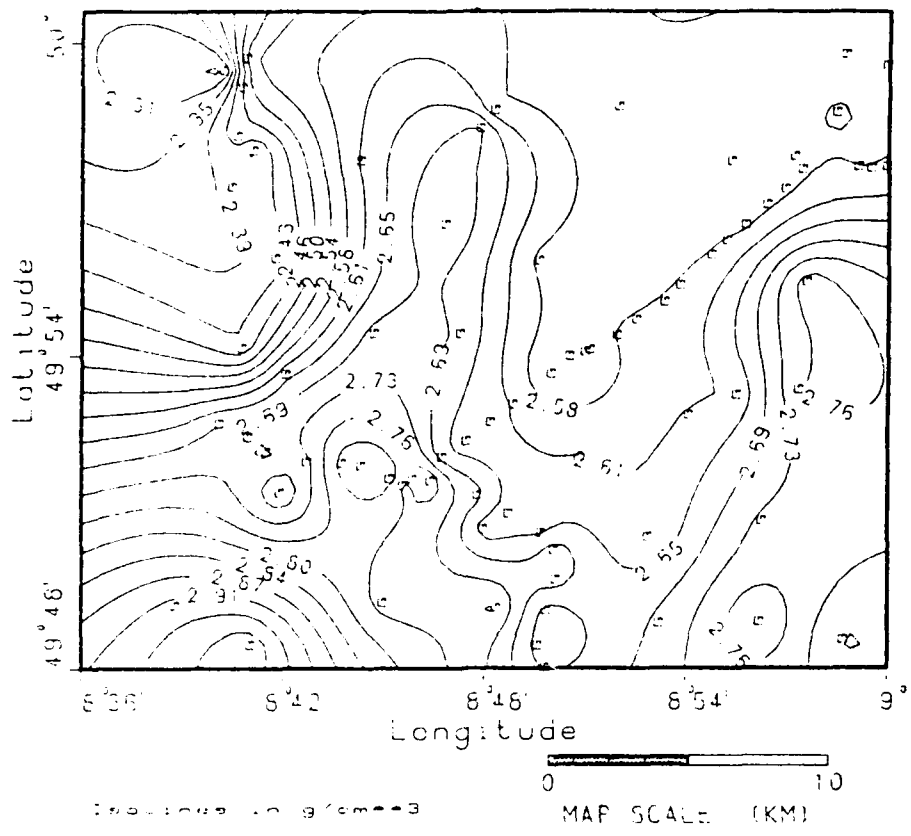


Fig. 8.3. Contour lines of surface point densities.

8.2 Test area "European Alps"

The test area European Alps extends from 45.0° to 48.5° North and from 6.0° to 16.5° East. It comprises Switzerland, most of Austria, southern Germany to the Danube River, northern Italy including the Po plain, and easternmost France excluding the western Alps and the Lake Alps. The following section describes the data that are used in the geophysical modelling (see chap. 3) as well as in the numerical computations with respect to gravity prediction. Part of the data are digitally represented on an equidistant grid of 6' × 10' ($\Delta\varphi \times \Delta\lambda$), corresponding to an area of 11 × 13 km². The grid was chosen because other data sets were already available on it (area means of topography and free-air anomalies). The data values are considered as mean values for the grid compartments. Gridded data used in our investigations are digital models of topography (digital terrain models), equiangularly-spaced mean block values of gravity anomalies, and a model of surface rock densities.

Block mean values of gravity and point values have considerably different spectral properties. There was also a need to use point values of gravity field functionals, especially in the context of least-squares collocation for the determination of a corresponding reasonable covariance function of the gravity anomalies.

8.2.1 Topography

The anomalous gravity field is primarily due to two facts that seem at the first glance quite different: variations in the visible topography and radial as well as lateral inhomogeneities of the sub-surface masses. A major part in local gravity field variations (medium and high frequencies of the spectrum of the gravity field) is a direct consequence of the topography.

So one of the fundamentals of a proper modelling of the gravity field is a *model of the heights* in the area of interest. Heights stored in gridded form together with the assumption of a constant density form a zero-order model of the distribution of masses whose successful use has been demonstrated in various applications (e.g., KEARSLEY *et al* 1985; FORSBERG, TSCHERNING 1981).

For our computations several sets of height data were collected and used:

- The *global* set of block mean values of heights/depths released by the working group of Prof. Sünkel, Technical University of Graz, described in (WIESER 1988). This set,

referred to as TUG87m5, has a resolution of 5' by 5' and is referring to geographical coordinates (φ , λ). It is compiled from two sets of 5' by 5' resolution: ETOPO5 and DB5B5 (previously SYNAPS). Processing of both sets consisted not only of merging the data but primarily included also detection and removal of gross errors.

- The *Austrian* digital terrain model with a resolution of 20" by 20" is based on geographical coordinates and was developed by the Institute of Photogrammetry of the Technical University of Vienna (*HAITZMANN 1983*). This model is referred to as POHEKR, see Fig. 8.4 for a plot of a $1^\circ \times 1^\circ$ block.
- For *Switzerland* a set of approximately 100 m by 100 m point values was available called RIMINI (*De MARCHI 1983*). The model is based on the map 1 : 25 000 of the Federal Office of Topography. It comprises whole Switzerland (a total of 330 maps 1 : 25 000) resulting in 1.15 million height values.

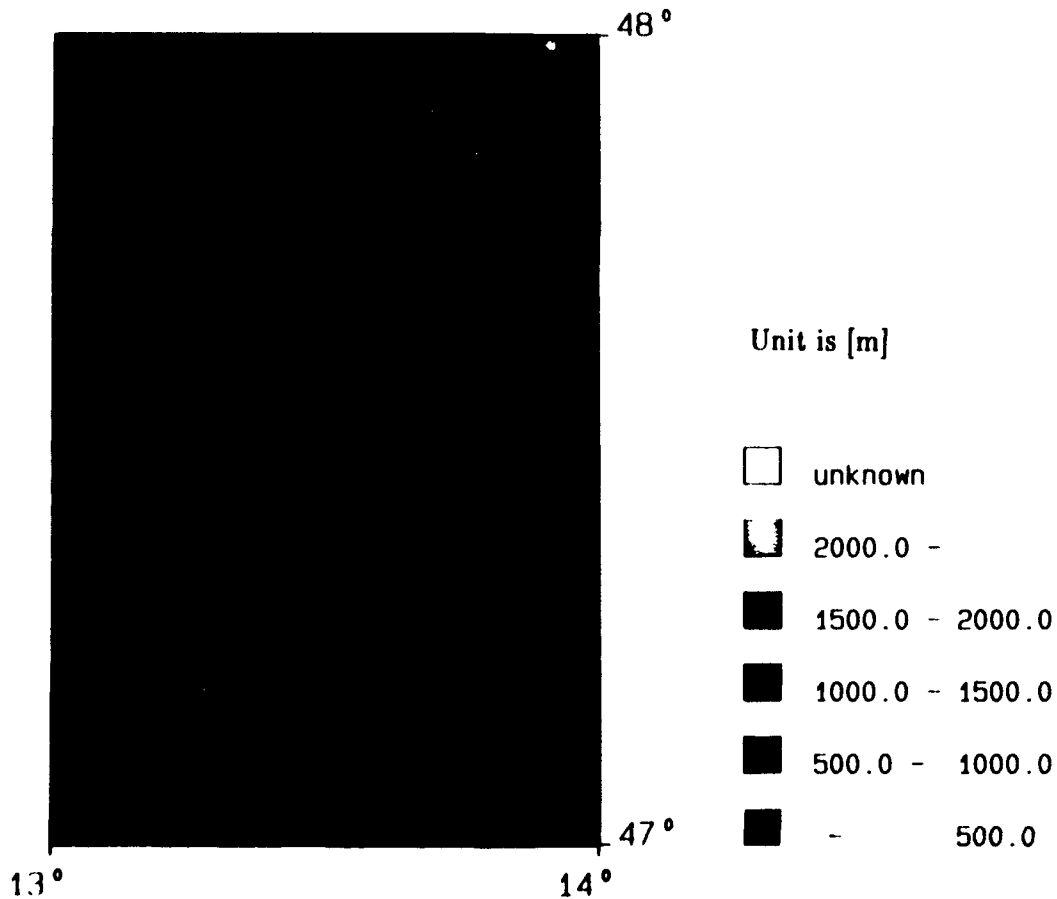


Fig. 8.4. Heights in a $1^\circ \times 1^\circ$ block of the European Alps.

- For the southern part of Germany a set of point values based on UTM-coordinates is available. Its resolution is approximately $100 \times 100 \text{ m}^2$. For a limited area we had also access to a model of resolution $\sim 50 \times 50 \text{ m}^2$.

An overview over all available sets is given in Fig. 8.5.

8.2.2 Gravimetric observations

The largest data set of observations consists of an amount of 41 681 gravity values within our Alpine area. For an overview the data have been thinned to a minimum point separation of 10 km and plotted, see Fig. 8.6.

The gravity values for the eastern part of France as well as for whole Switzerland have been made available by the Bureau Gravimétrique International, Toulouse. The Italian petrol company AGIP provided a data set covering that part of northern Italy which was of interest for our investigations. The Technical University of Graz, Austria, provided the data for the Austrian part of our area.

The computation of the mean Bouguer anomaly values for the $6' \times 10'$ areas is based on the mean free-air anomaly and elevation values for Europe, as supplied by Institut für Angewandte Geodäsie (IFAG). Application of the mean Bouguer reduction to the mean free-air anomalies results in an anomaly which approaches the mean Bouguer anomaly. In the Alps this anomaly is strongly correlated (with negative sign) with the mean elevation. It reflects the fact that the mean elevation is closely correlated with Moho depth. The simple Bouguer reduction applied is defined by:

$$\delta g_B = 2\pi G \rho H \quad (8-1)$$

with H being the mean elevation value of a compartment, $G = 6.673 \cdot 10^{-8} [\text{g}^{-1} \text{cm}^3 \text{s}^{-2}]$, δg_B in mGal. The density ρ was everywhere assumed to be 2.67 g/cm^3 , the value usually taken for the average crust.

For relatively flat areas the approximation of an infinitely extended Bouguer-plate is sufficient but for most of our area the full terrain reduction had to be computed. This was done using the prism integration method which allowed also to simultaneously determine the isostatic effect due to the topographic load. For the isostatic compensation the Airy-

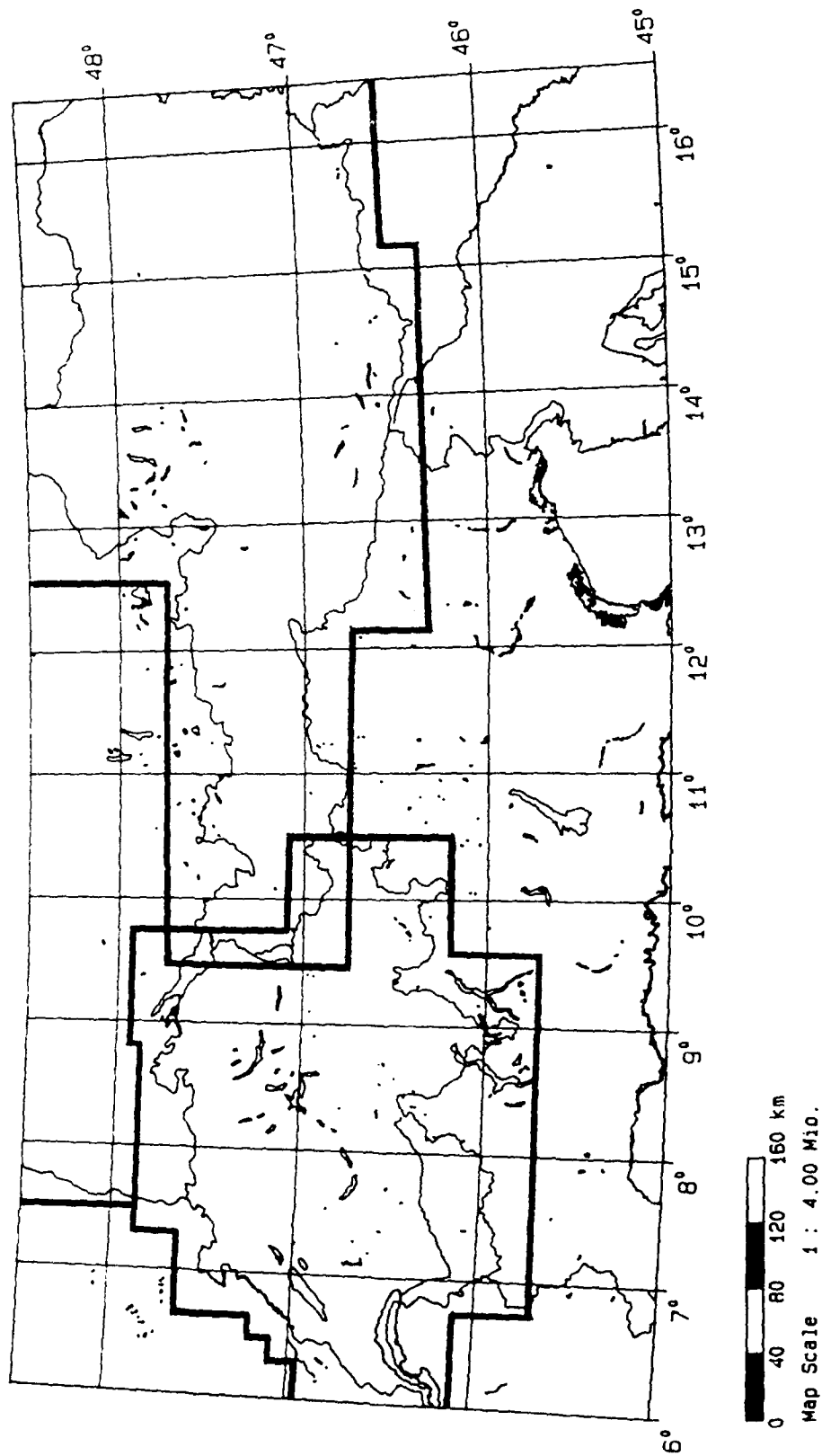


Fig. 8.5. Available digital terrain models over the European Alps.

Number of gravity values plotted: 1725

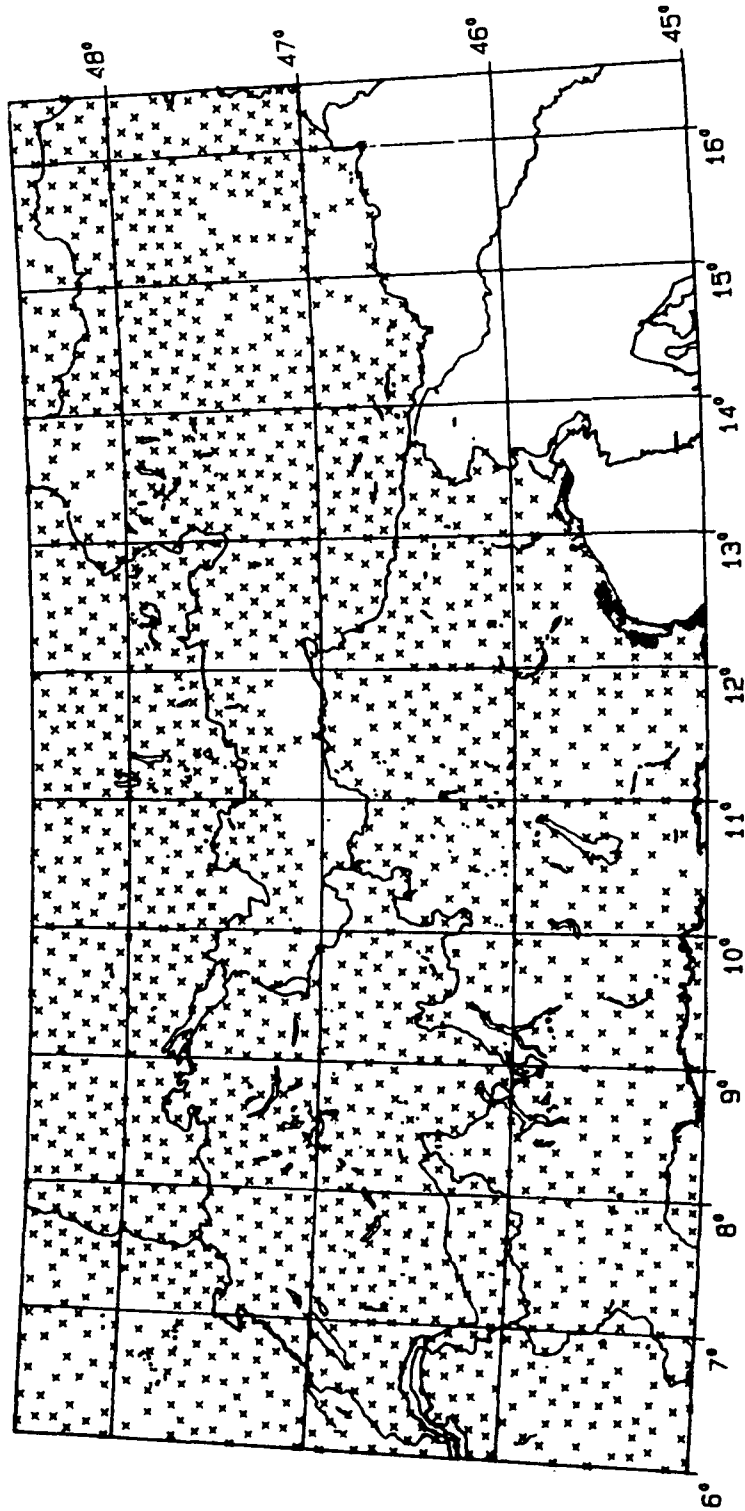


Fig. 8.6. Available point gravity anomalies over the European Alps.

Heiskanen compensation mechanism was used assuming the following parameters: $\rho = 2.67$ g/cm³, $T = 32$ km, $\Delta\rho = 0.4$ g/cm³.

Unfortunately there are gaps in the given data sets resulting in significant gaps of the Bouguer anomaly particularly in the Central Alps. Fig. 8.7 is a crude representation of the distribution of Bouguer anomaly values.

8.2.3 Astronomical observations (deflections of the vertical)

For *Austria* a set of astronomical latitudes and longitudes (deflections of the vertical) with a total of 521 values was available. Field work and accuracies are documented in (*BRAND-STÄTTER 1987*). Parts of the observations were carried out by the Institute of Theoretical Geodesy and Geophysics, Vienna, Austria (Prof. Bretterbauer).

Switzerland (Prof. Kahle, ETH Zürich) provided a set of 240 deflections of the vertical. A good number of them are published in (*GURTNER 1978*).

For the southern part of *Germany* the deflections of the vertical are taken from (*SCHMIDT, EHLERT 1982*).

For a plot of all available deflections of the vertical see Fig. 8.8.

8.2.4 Seismic data

The crustal structure of the Alpine region has been thoroughly investigated mainly by seismic refraction experiments during the last 30 years. The results have been published in a large number of papers and they do not cover the body of the Alps completely. In recent years a number of attempts have been made to collect all the data and to arrive at a unified areal interpretation (e.g., *MOSTAANPOUR 1984; GEISS 1987*). In spite of the doubtless merit of these attempts, we have not simply incorporated the results, partly because we are aiming at greater detail, partly because the uncritical use of other workers' results is easily misleading. For our computations of the gravity and geoidal effects of the seismically inferred crustal structures we have again reviewed and analysed all the original publications available to us.

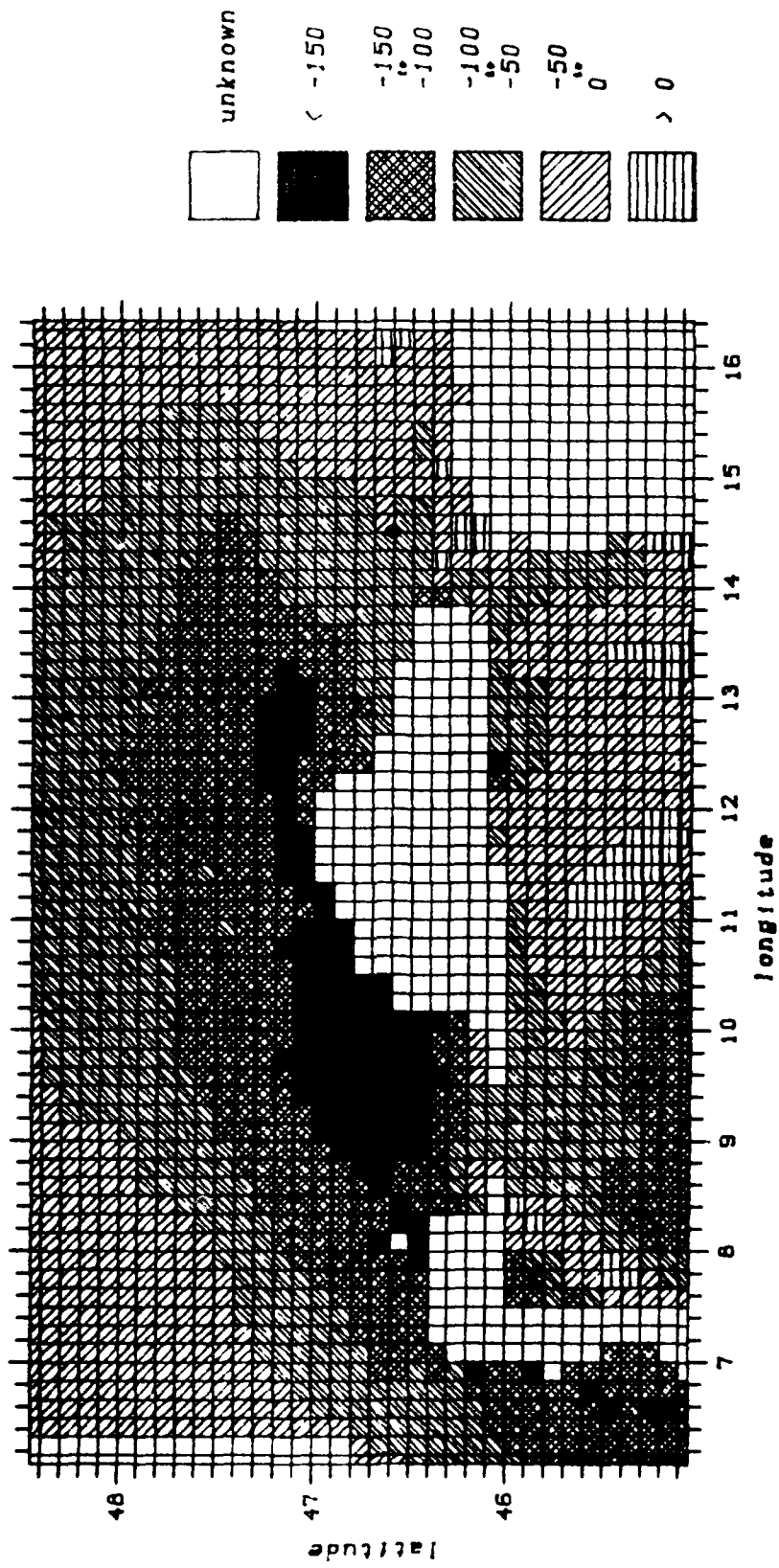


Fig. 8.7. Mean Bouguer anomalies in mGal (6' x 10' blocks) in the Alpine area.

Number of deflections of the vertical: 795

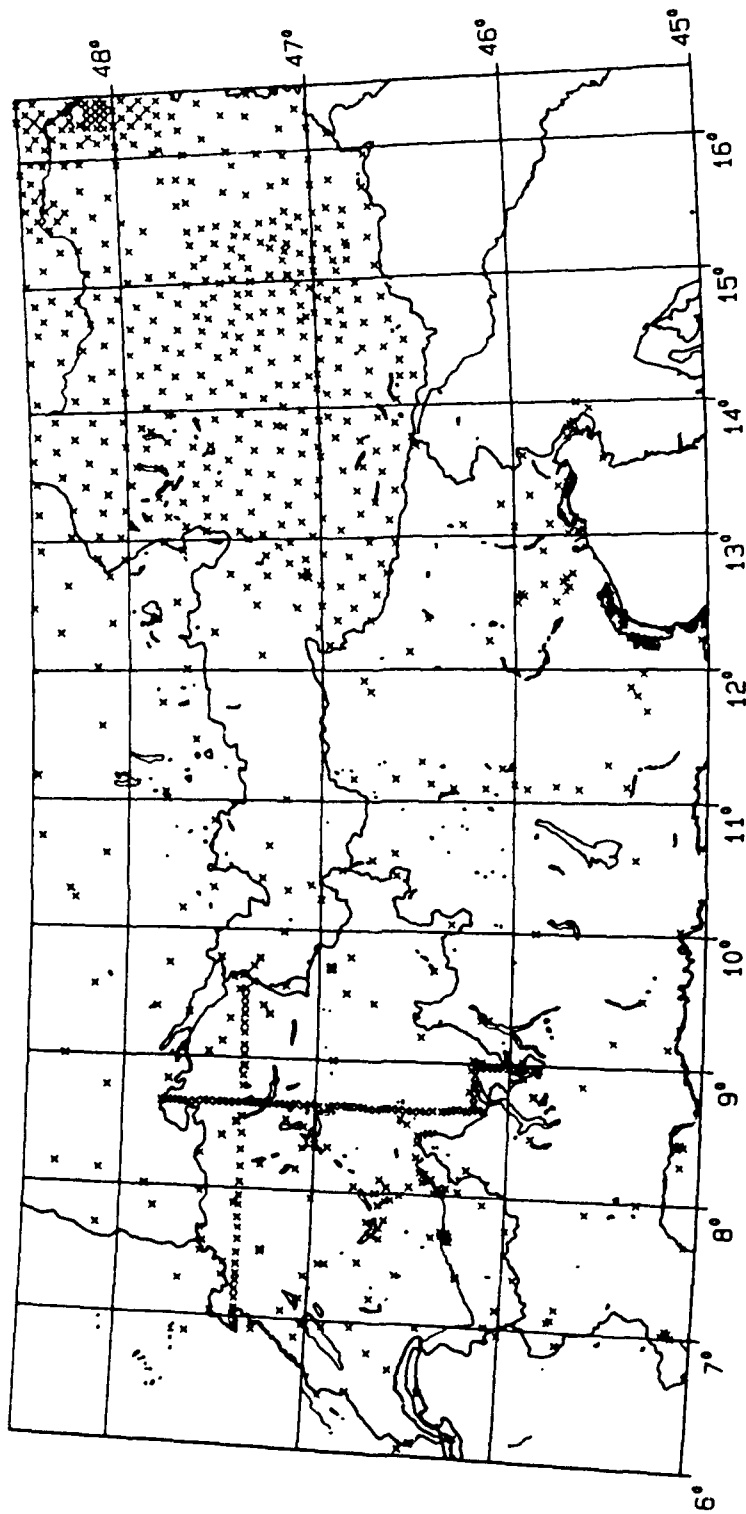


Fig. 8.8. Deflections of the vertical over the European Alps.

The crust and upper mantle have a complicated three-dimensional structure which cannot possibly be represented adequately except on a very fine three-dimensional grid. However, there are elements of order to which the various seismic techniques are sensitive. Refraction experiments (including the methods of data analysis and interpretation) will tend to "see" refractors or layers, while reflection experiments mainly "see" reflectors or surfaces of seismic impedance contrast mostly on a much smaller scale (vertically and horizontally); some may coincide with refractors, but most of them reflect internal structures of the gross layering derived refraction seismology.

For convenience and as a means of data condensation we divided the crust into two layers and the upper mantle similarly into the lithospheric part and the underlying asthenosphere (with no bottom assumed). The most important refractor or large-scale boundary is the Mohorovičić discontinuity dividing crust and upper mantle; its depth, or equivalently the crustal thickness, Z_m , is reasonably well established in the region of study. Another boundary on which we have significant information is the top of the crystalline basement or its depth, Z_b . The depth of the lithosphere-asthenosphere transition (or "boundary"), Z_1 , is known with much less certainty; it is based mainly on the dispersion of (earthquake) surface waves with poor spatial resolution.

To start with, our seismic model can, thus, be represented by three layer boundaries at depths Z_b , Z_m , and Z_1 . However, as argued above, the layers are not homogeneous; in the individual refraction results there is ample evidence for seismic velocity variations within the layers. We attempted to treat these (as far as the data permitted it) as a perturbation of the layered model.

First we constructed the layer boundaries on the basis of published contour maps and, particularly, of seismic sections along observed profiles and a few fans. The sections usually show boundaries and seismic P wave velocities, v_p , mainly at the top of the layers. The refraction results are also often published as velocity-depth functions for refraction profiles or parts of them, pertaining to certain regions. In addition reflection seismic results have been used. As mentioned, the lithosphere bottom was taken from interpretations of surface wave dispersion and partly of teleseismic traveltimes residuals.

All these data were digitized. The irregular points were then interpolated onto the grid described above. Digitizing the input data had to take into account the different cartographic projections, so that it was done mostly manually with the aid of strongly magnified maps. To reduce the errors of locations (of the data points), mostly points of intersection of contours with lines of latitude or longitude were taken. At the beginning,

only those results were accepted that had been considered reliably by the original authors, and extrapolations to the marginal regions (mostly shown by dashed lines) were omitted. Only in larger regions with no data we included such information of less reliability. In regions of data overlap from two or more sources we tried to avoid discrepancies in the first step. In the second step the data set was analysed with respect to significant discrepancies. These were either eliminated altogether or, in regions of broad scatter, the arithmetic mean was taken.

This procedure resulted in a set of irregularly distributed points values. In the third step this data set was interpolated onto a regular grid. Two methods were used: the method due to Hardy (*GÖPFERT 1977*), called "multiquadratic", has been applied if not otherwise stated; alternatively interpolation by triangulation was used (*AKIMA 1978*), where a 5th order polynomial is expanded within triangles. The multiquadratic interpolation renders a smoother set of point values and it is less sensitive to greater data gaps and strong gradients resulting from discrepancies between close-by points; however, computation takes much longer so that we were limited in the numbers of input and output points because of limitations enforced by the reasonable computing time. The resulting grid (75–120 % of the compartment size, depending on the original data density) was further refined to 20 % of the compartment size with the aid of bicubic splines (*PRESS et al 1986*). Subsequently all grid points thus obtained and lying within a 6' × 10' quadrangle were arithmetically averaged and the mean value is then taken for this quadrangle. Averaging naturally results in some smoothing of the data, but methodical weakness of the different kinds of interpolation is partly cancelled. Tests in which both interpolation methods were compared for some regions have demonstrated, that the results after the final averaging are nearly identical. Thus, we believe that the requirement of a uniform data generation has been satisfied.

Lateral variations or perturbations of the seismic velocities within the layers were estimated for parts of the crust in the following manner. We started from published velocity–depth functions $v(z)$ given for certain "points". Assuming a piecewise–linear velocity distribution, we computed mean velocity \bar{v}_i for n layers i of thickness Z_i . The average velocity \bar{v}_i of a crustal section $Z = \Sigma Z_i$ is given by (*MOSTAANPOUR 1984*):

$$V = \frac{\sum_{i=1}^n Z_i}{\sum_{i=1}^n \frac{Z_i}{v_i}} \quad (8-2)$$

Fig. 8.9 shows the location of crustal sections discussed beside the contour maps. In the following the seismic boundaries are presented from top to bottom, followed by the lateral velocity perturbations.

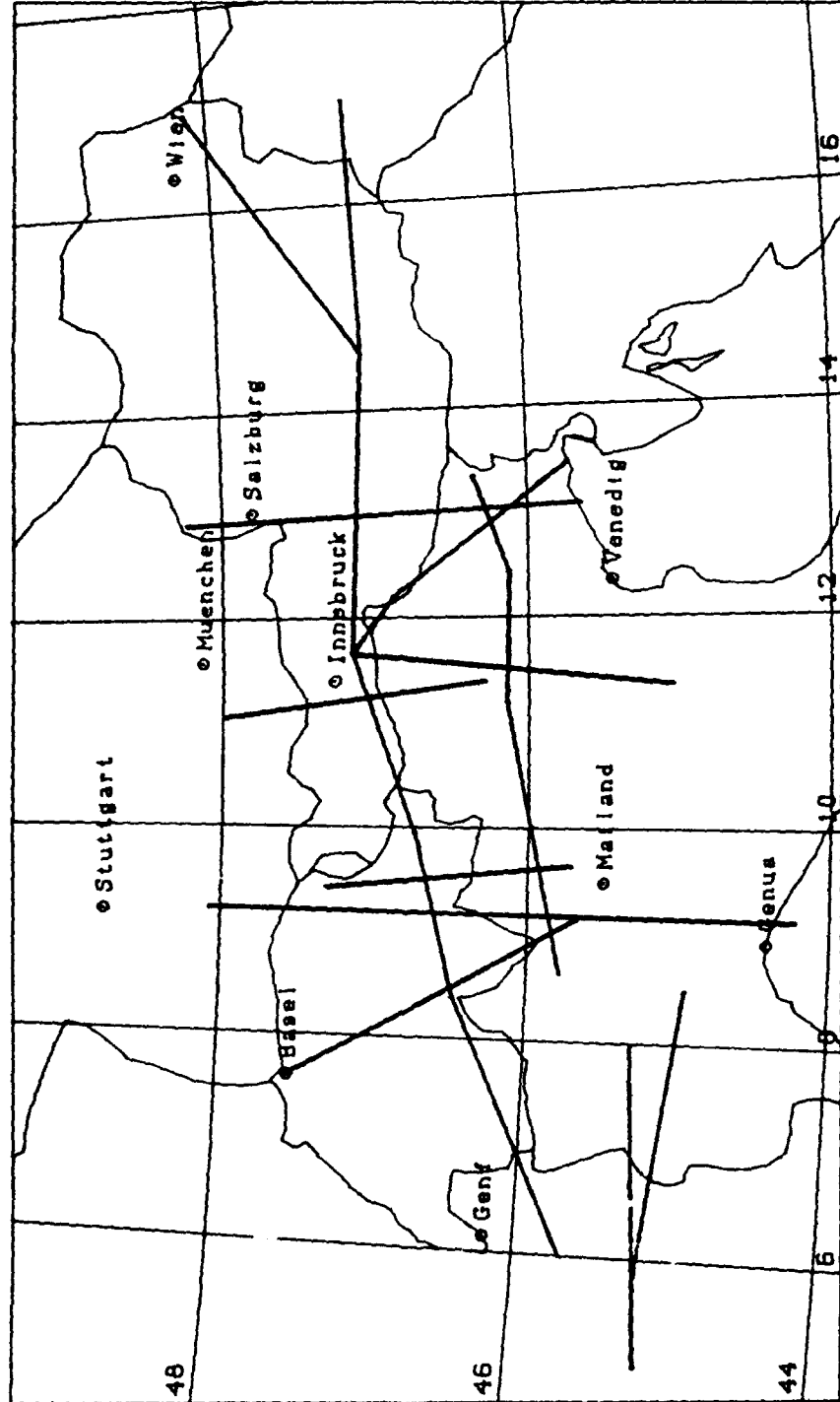


Fig. 8.9. Map of the observation lines used to determine crustal structures.

8.2.5 Depth of the seismic basement

The seismic basement is defined by the depth Z_b , where the P wave velocity v_p first reaches the value 6.0 km/s, not by reflecting horizons as usually done in exploration geophysics. If low-velocity layers exist at greater depth there may be additional 6.0 km/s surfaces which are not included in the "seismic basement". What is the significance of the basement as defined here? In a general way, it will correspond to the top of the crystalline rocks; thus the depth Z_b is equivalent to the thickness of the sedimentary "layers". This, however is not everywhere to be taken literally, particularly not in the Alps. Shallow crystalline rocks, particularly if tectonically deformed usually have v_p -values below 6.0 km/s. This has been demonstrated by *BIRCH (1958)* for normal granite assuming a temperature gradient of 18 °C per km (Fig. 8.10). The relatively low velocities are caused by porosity and particularly by small open joints related to weathering and tectonics; at greater depth pressure generally closes the joints and v_p exceeds 6.0 km/s, usually at depth of about 2 km. There are, however, also sound-hard sediments, e.g., dolomite, with v_p -values greater than 6.0 km/s.

The seismic basement Z_b , as assumed here was essentially based on the interpretation and the contour maps published by *MOSTAANPOUR (1984)*. In addition, we took a number of velocity-depth functions at a few points along the profiles shown in Fig. 8.9; these points were incorporated into the interpolation or were used for checking. The result of our interpolation is presented in Fig. 8.11.

The contours reflect the tectonic gross structures of the study area. The evolution of the Alps that resulted in these structures may be briefly characterized as follows. A number of compressive pulses lead to folding and nappe movement from the central region towards the northern foreland. Today the Alps have an asymmetric structure of the deformed crust. While in the north one crustal nappe after the other separated from its basement and moved north, in the south a suture formed, the Insubric line. It separates the East Alpine Block from the South Alpine block. To the north and south there are two large sedimentary basins, the Molasse and the Po basin, which received the erosional products of the Alpine orogene during repeated uplift phases. In east-west direction the Helveticum and the Penninicum are to be distinguished. Fig. 8.12 shows the tectonic gross structures of the Swiss Alps.

The greatest values of Z_b are formed in the sedimentary basins of the Molasse, the southern Rhine Graben, and the Po region. In the Molasse, the maximum values of 7 to 10 km are reached at the edge of the Alps. In the southern Rhine Graben, values up to 11 km are reached between the much shallower values in Black Forest and Vosges massifs. The Po

basin shows up with values up to 8 km. The shallowest depths of the basement (less than 2 km) are found in the central East Alpine regions and along a narrow arch of the western Alps (the zigzag shape of the contours results from insufficient grid resolution). Somewhat greater Z_b values (3 ... 5 km) correspond to the Helveticum and Penninicum, rising towards the Molasse basin. In the South Alpine region the Z_b values are variable between 2 and 4 km before they drop towards the sedimentary Po basin. The transition is here more gentle.

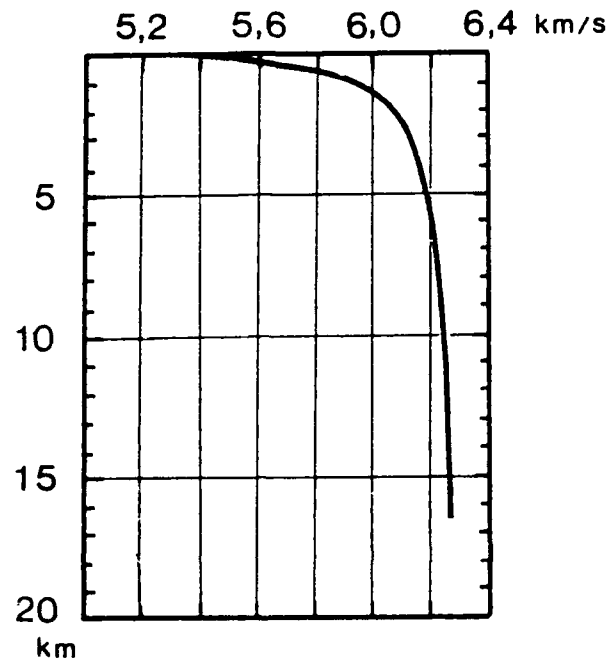


Fig. 8.10. P wave velocity versus depth for a medium granite after *BIRCH (1958)* according to a temperature gradient of 8 °C/km.

8.2.6 Depth of the Mohorovičić discontinuity

The Mohorovičić discontinuity (short: Moho) defines the crust–mantle boundary; it is characteristically a rather abrupt increase of v_p from less than 7 km/s to values around 8.0 km/s (extreme values of 7.5 and 8.5 km/s are rare). The increase is not truly a first order discontinuity although for long wavelengths it may be modelled that way; in reality it will always be a transition zone between crust and mantle of up to several kilometers vertical extent. Therefore it is a matter of definition at which depth exactly the Moho lies and one must pay attention to this if one wishes to accept published results. A number of possible definitions has been discussed by *MEISSNER (1986)*. According to him the most common definition is the top of the transition zone (or layer) of the greatest vertical P wave velocity

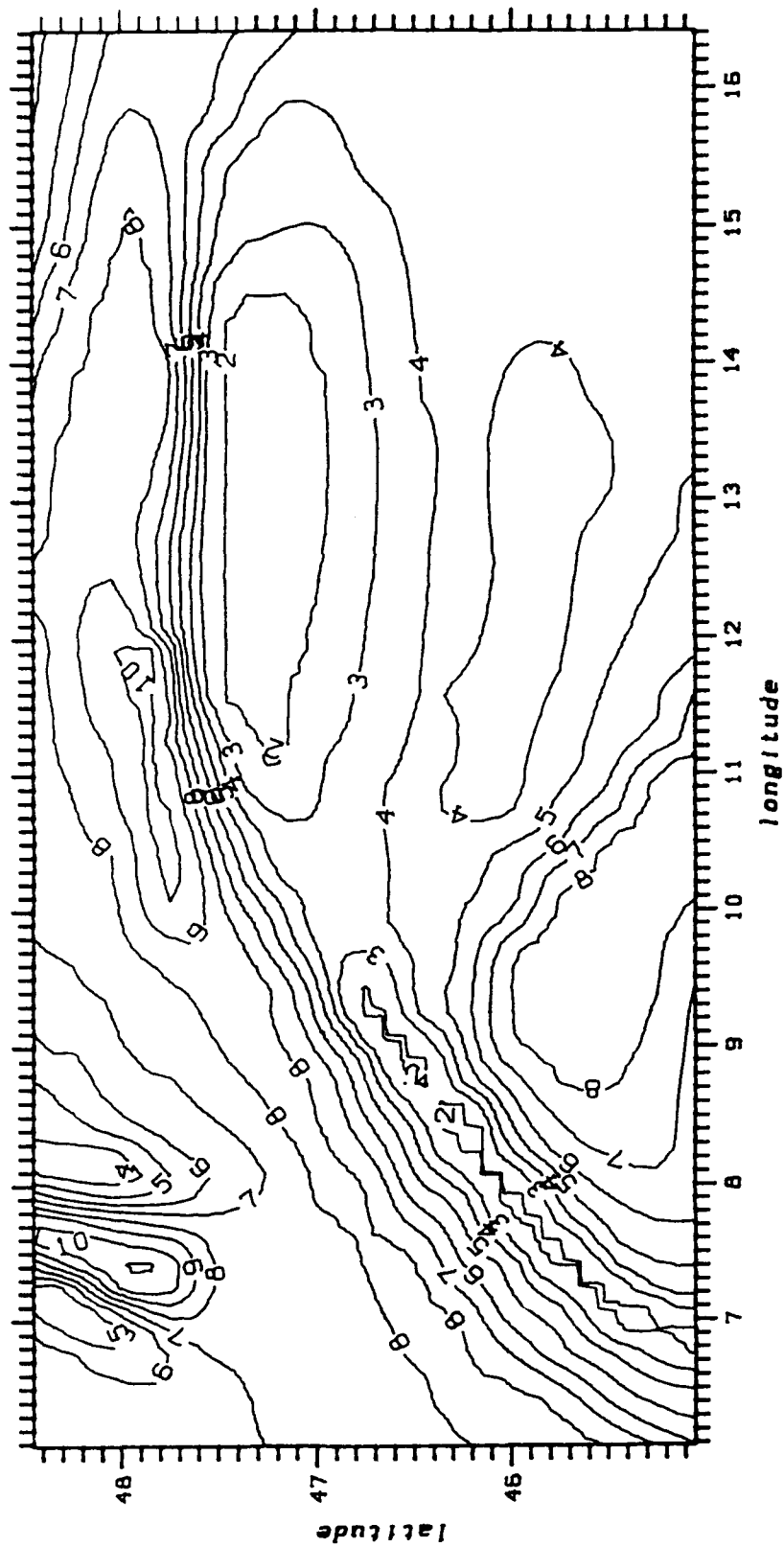


Fig. 8.11. Depth of seismic basement ($v_p = 6.0$ km/s) in the Alps. Contour interval 1.0 km.

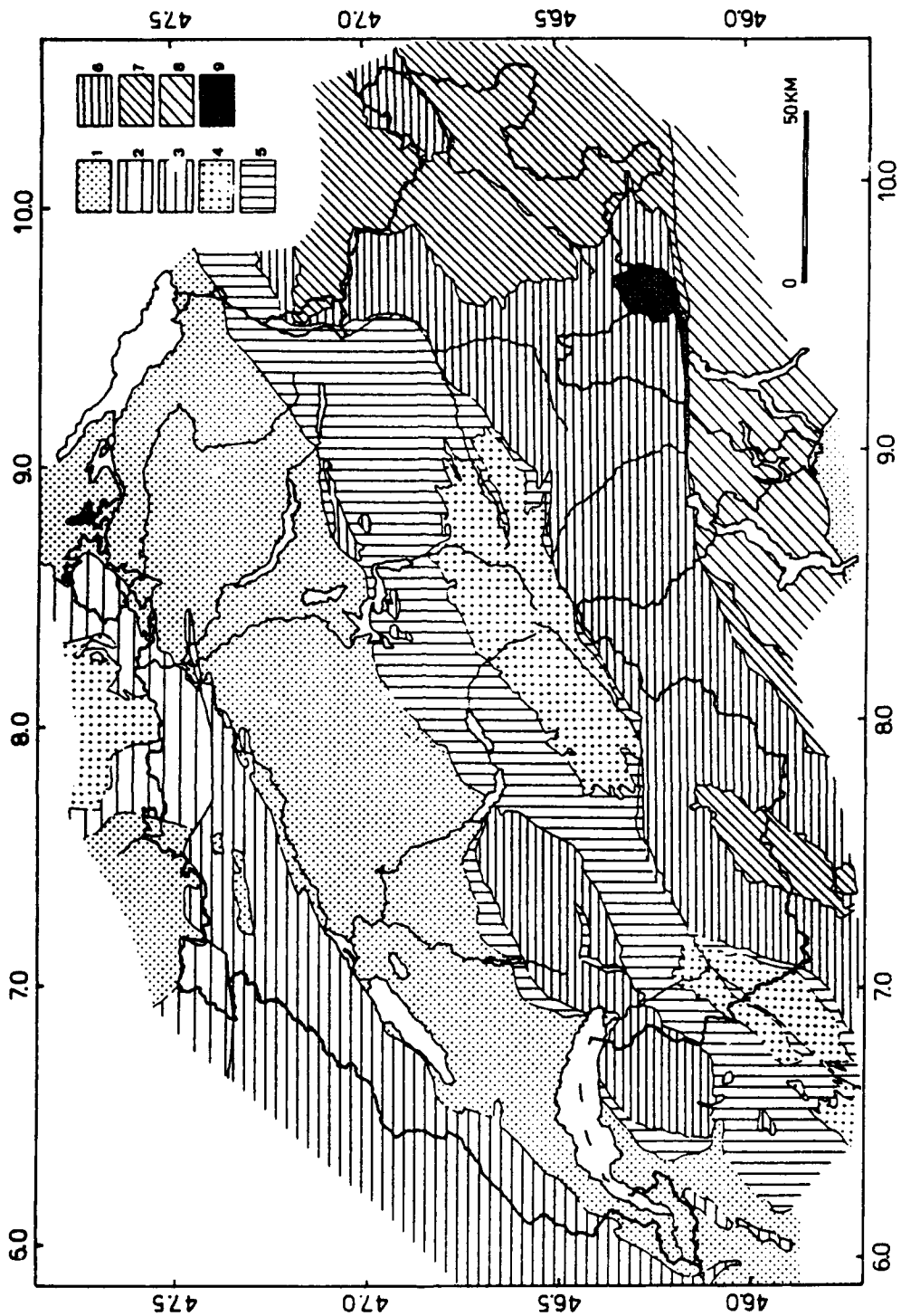


Fig. 8.12. Tectonic sketch map for the Swiss Alps taken from *KLINGELE, KISSLING (1982)*. (1) Molasse sediments, (2) + (3) Swiss jura, (4) + (5) Helveticum, (6) Penninicum, (7) Eastern Alpin, (8) Southern Alpin, (9) Eruptiva.

gradient $\partial v_p / \partial z$ leading to values of 7.5 to 8.5 km/s. This definition is not meant to apply to other high-velocity gradient zones (MOSTAANPOUR 1984). Some authors define the Moho depth at the bottom of the transition zone or at its center. It is also quite common to define the Moho depth Z_m by the exact velocity value of 8.0 km/s. Keeping these uncertainties of definition in mind, the uncertainty of the depth Z_m for the Alps has been estimated by various authors to be ± 2 km (EGLOFF 1979), $\pm 1 \dots 2$ km (PERRIER, RUEGG 1979) and ± 5 km (MOSTAANPOUR 1984).

Since the Moho attracts greatest interest there are more data on it than on any other boundary and the spatial resolution is greatest. In this work a number of more detailed maps and crustal sections have been combined with more regional Moho models (e.g., MOSTAANPOUR 1984; MEISSNER 1987). Because of the numerous data points a routine was used where the interpolating function is a fifth-degree polynomial within each triangle of the x-y surface of the data. In order to avoid edge effects of this method it was necessary to include a 0.75° to 1° strip outside the actual study area. The result is shown in Fig. 8.13.

Multiple coverage of some regions from several publication also allows us to estimate the confidence intervals of Z_m in an empirical manner. The results are not given as usual as a symmetric standard deviation ($\pm \Delta Z$) but asymmetrically for the shallowest and the deepest Moho depth for each $6' \times 10'$ quadrangle. For the best cases the minimum uncertainty was assumed to be ± 1 km. In some regions, however, we found differences of $Z_m \geq 10$ km. If those discrepancies could be traced to the differences of Moho definition in the various publications, the data were excluded from the interpolation, but they were still used to estimate the confidence limits. Discrepancies caused by unknown effects were averaged or treated as described above.

For the arc of the western Alps and for the Swiss Alps there were about 100 discrete data points available (CLOSS, LABROUSTE 1963; KISSLING 1982). In addition there were a few published contour maps for these regions. The data had to be fitted together mainly in southwestern Switzerland. Here also contour maps of the whole Alpine region (GIESE *et al* 1976) were taken into account. The Alpine forelands in the north and south were represented only by contour maps (DRISLER, JACOBY 1983; GIESE *et al* 1976; BARAZANGI, BROWN 1986) which are consistent with other representations. Only in the regions of the Swiss Jura and the southern Rhine Graben we noticed significant discrepancies in the Moho depth. The eastern part of Austria is not well known with only 30 data points along three seismic profiles (ARIC 1987) available. The Yugoslavian part of the study area is not covered by reliable data; we had to revert to extrapolation. The data density is much

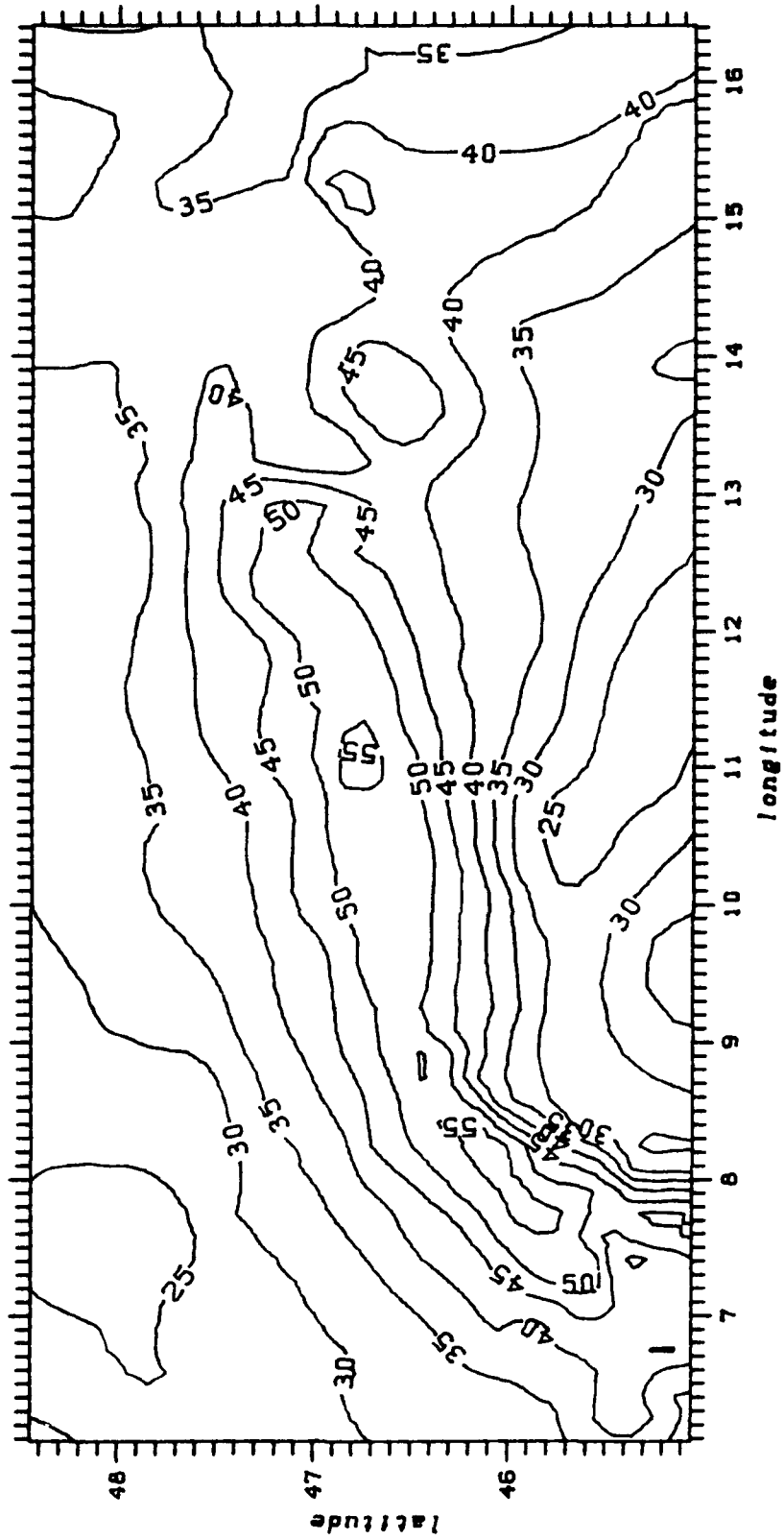


Fig. 8.13. Depth of Mohorovičić discontinuity in the Alps. Contour interval 5.0 km.

greater in the western part of the test area than in the eastern part, and the data sources are also more detailed and reliable in the west.

The upper and lower confidence limits of Z_m are represented as two sets of discrete integer values of length in kilometer. They are shown in Figs. 8.14 and 8.15. A representation in the form of contour lines is of no meaning and no value.

The contour map of the Mohorovičić discontinuity clearly shows the arc structure of the Alps. The Z_m values continuously increase from about 32–38 km in the region of the northern Molasse across the strike direction towards the axis of the Alps to 40–45 km in the Helveticum and Penninicum. In West Alpine maximum Z_m values of nearly 60 km are reached. In contrast, the crust–mantle boundary in the central East Alpine is only 45–50 km deep. In the Po basin the crustal thickness is only 25–35 km, distinctly less than in the Molasse to the north. This is similar to the sedimentary thickness.

Our contour map (Fig. 8.13) differs clearly from other interpretations (e.g., *MOSTAAN-POUR 1984*; *MEISSNER 1987*) in that way that Z_m gradually varies from the center of the Alps to the south. The maps mentioned show a rise of the crust–mantle boundary from the Po basin to the margin of the western Alpine arc to about 10 km from which the boundary abruptly drops to values of about 50 km to the north of the Insubric Line. This behavior is an expression of the Ivrea body, which is also evident in the partial overlap of the contour lines manually constructed. Such a small–scale structure cannot be resolved with the chosen grid, and the interpolation procedures can only produce smooth surfaces with no discontinuities. The Ivrea zone has the effect that the contours are quite dense in this zone.

The Z_m values of the Po plain belong to the "Adriatic plate". Crustal doubling as postulated, e.g., by *WIGGER (1984)* and *GIESE (1985)* cannot be recognized in our model and was not taken into account in our estimate of the confidence limits. There is no evidence for the Eurasian plate to have been pushed a long distance south of the Insubric line below the Adriatic plate. Locally at the contact of the Eurasian and Adriatic plates there is seismic evidence for crustal subduction at the southern margin of the west Alpine arc and the coastal regions of Toscana till the island Elba. A continuous connection between these two regions could, however, not be verified by refraction seismology.

Finally we note the shallow Moho with Z_m values of 22 ... 25 km below the southern Rhine Graben. However, in contrast to seismic basement there is no abrupt change towards the Black Forest and Vosges massifs.

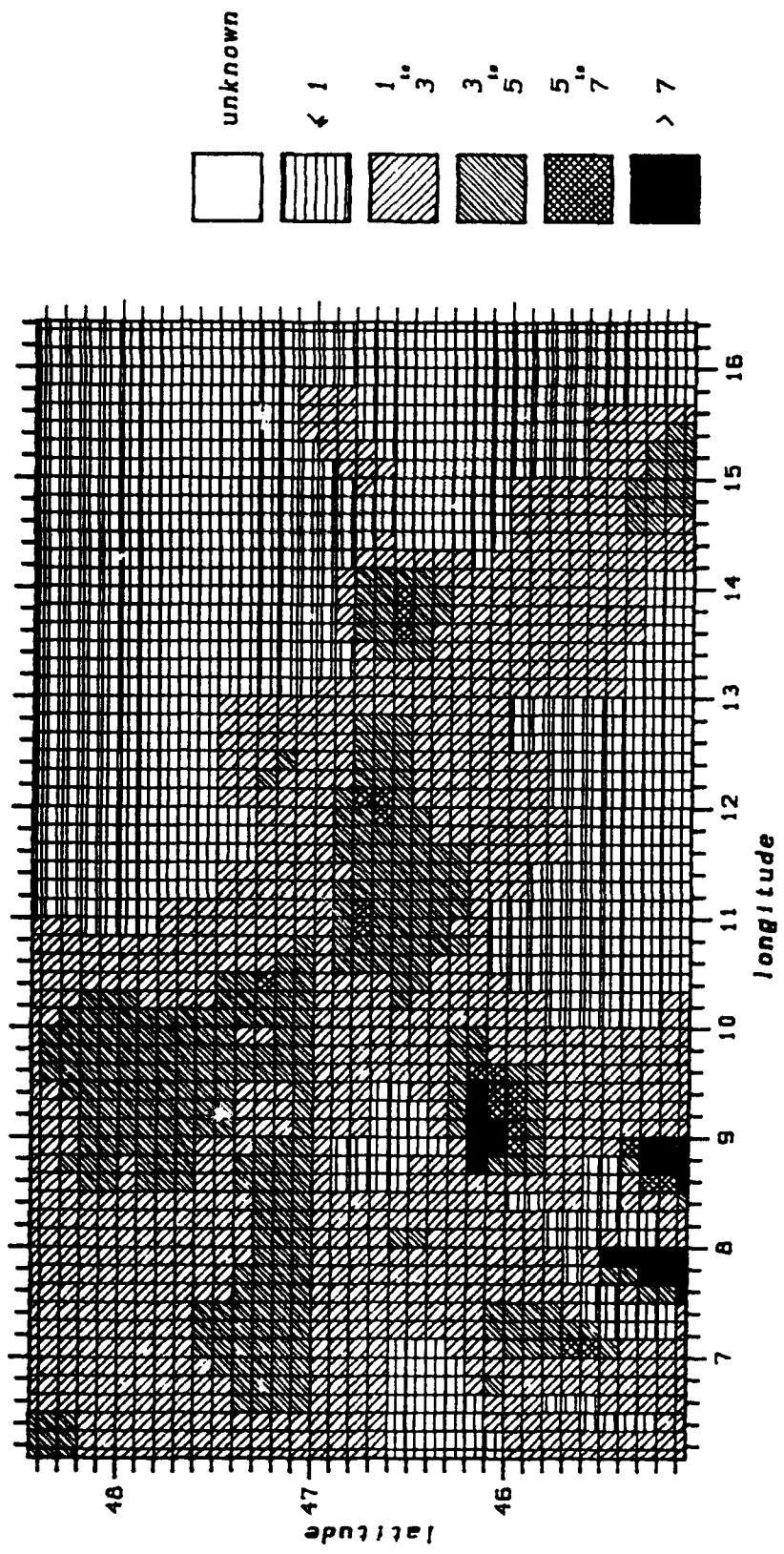


Fig. 8.14. Uncertainty of the depth of the Mohorovičić discontinuity in [km] in case of a possible *lower crust/mantle* boundary.

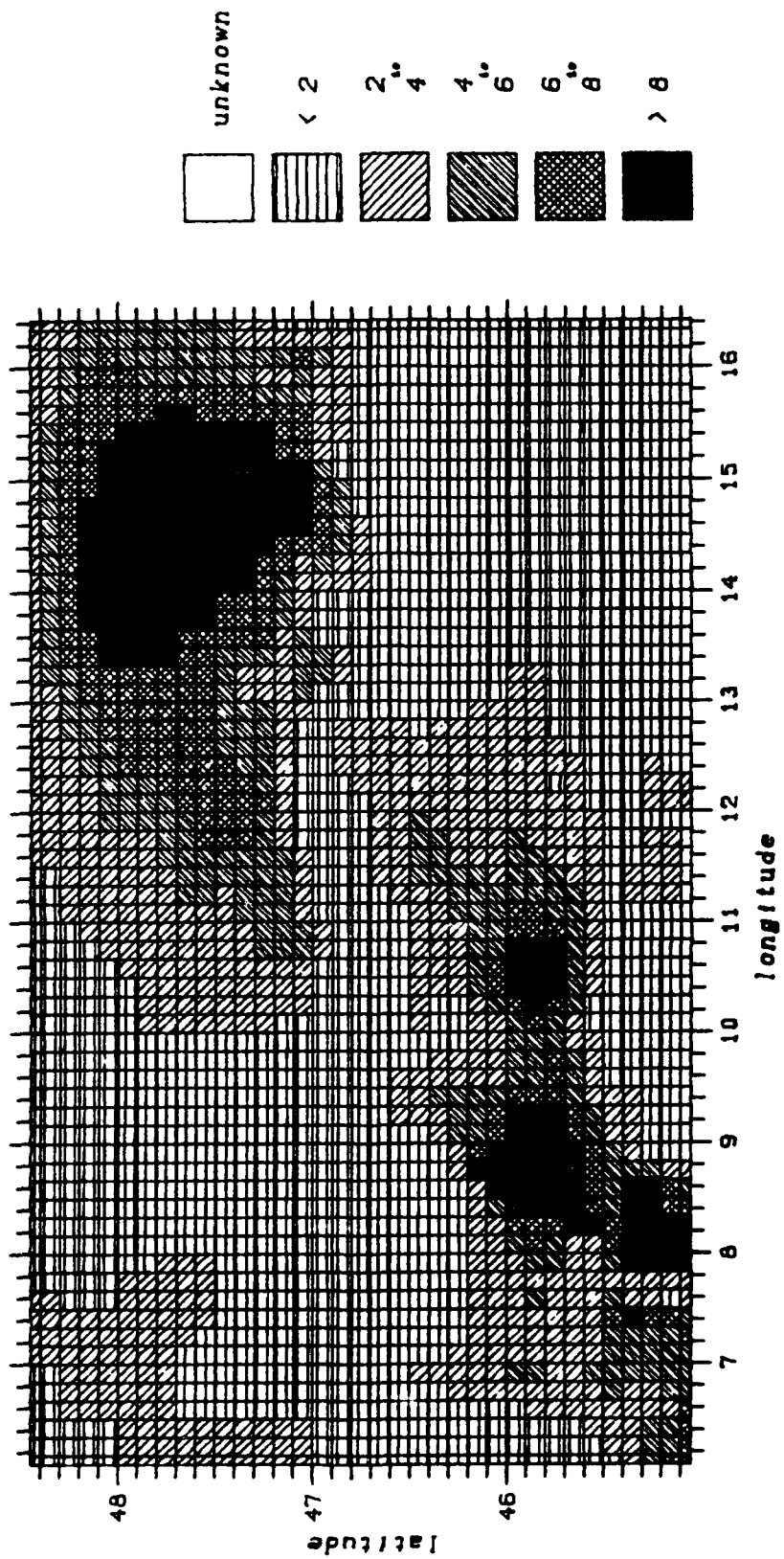


Fig. 8.15: Uncertainty of the depth of the Mohorovičić discontinuity in [km] in case of a possible deeper crust/mantle boundary.

The possible deviations of the Moho depth from the values in Fig. 8.13 are in large areas less than ± 2 km (Figs. 8.14, 8.15). Possibly greater Z_m values may be suspected in two regions: in the Ivrea zone to the southern end of the west Alpine arc and broadly in the eastern Alps. The main reasons are the problems of incorporating a complicated structure as that of the Ivrea zone and considerable discrepancies in different Moho maps for Europe (MEISSNER 1987); here the 50 km contour extends about 100 km further east than in all other maps. Regions with possibly smaller Z_m values are again along the west Alpine arc and especially in the Ivrea Zone, as well as in the central East Alpine. Also the Swiss part of the northern Molasse basin shows uncertainties towards shallower depths by 3 ... 5 km. In Figs. 8.14 and 8.15 it is evident, that generally (with the exception of the Ivrea zone) the reliability and accuracy in the western (Swiss) part of the study area are much better than in the east. The reasons are the higher data density and the better seismic model.

8.2.7 Thickness of the lithosphere

The lithosphere plays an important geodynamic role as the uppermost quasi-rigid moving plate. It consists of the crust and the uppermost part of the mantle. The transition to the subjacent asthenosphere layer is, though gradual, a drastic change in rheology, i.e., a decrease of viscosity by several orders of magnitude. The asthenosphere is also a layer of low seismic velocities which may be explained by partial melt. However, the transition is principally not resolvable as a reflecting or refracting boundary. The depth Z_1 can only be determined with the aid of surface wave dispersion analysis and by teleseismic travel time residuals. Both will never allow the definition of a sharp boundary. Another indirect method to determine the thickness of the lithosphere is by modelling the terrestrial heat flow (ČERMÁK 1982). However, this kind of modelling is ambiguous and depends on many vague assumptions.

The present map (Fig. 8.16) was based on published work by BABUŠKA *et al* (1985), SUHADOLC, PANZA (1988), and PANZA *et al* (1980). PANZA (1981) has estimated the uncertainty to be ± 30 km. Fig. 8.16 differs in parts considerably from other published maps. For example, PANZA, MÜLLER (1980) postulated a lithospheric root below the Alps up to 200 km thickness and thermally induced high seismic velocities on the basis of travel time residuals (particularly in the east and below the west Alpine arc). This root has not been included by GEISS (1987), but he assumes a generally thickened lithosphere (to 130 km) below the Alps. At present, the existence of the lithosphere is being debated altogether, e.g., by VIEL (1987) on the basis of observations of travel time residuals at his Al-

pine stations and of model computations. The residuals were explained by him by crustal thickening.

Fig. 8.16 represents the version most acceptable to us. There are two thickness maxima near the west Alpine arc and below the central eastern Alps. Towards the margins of the Alps the lithospheric thickness decreases strongly to values of 110 ... 130 km. A special feature is the southern Rhine Graben with a thickness of only 90 ... 100 km. But here the uncertainty probably greatly exceeds the value of ± 30 km, particularly in view of the 45 ... 50 km given by *PANZA et al (1980)* for the whole European rift system. The same is true for the transition from the Alps to the Dinarides in the southeastern part of the study area, however, with the opposite sign. *PANZA et al (1980)* give values ≥ 120 km for that area. Generally one has to take into account that surface wave dispersion analysis cannot give much spatial resolution horizontally since dispersion can only become evident along a certain horizontal path length; therefore features of small lateral extent will appear smoothed if recognizable at all.

8.2.8 Perturbations of seismic velocities

The interpretation is based on the same data as the construction of the contour map of Z_b , does. Digitizing the contour maps was difficult, since the manually constructed contour lines of *MOSTAANPOUR (1984)* are incomplete and appear topologically incorrect at places. Therefore we took more of the original seismic profiles into account. In a broad sense, however, the results are comparable to those of *MOSTAANPOUR (1984)*. We determined the lateral variation of the mean P wave velocity in certain regions of the crust, i.e., from the depth range from the surface to the seismic basement: \bar{v}_b (Fig. 8.17), and for the whole crust: \bar{v}_m (Fig. 8.18). From these values one can compute the mean velocity \bar{V}_{lc} of the crust below the sediments, i.e., from Z_b to Z_m (Fig. 8.19); according to *MOSTAANPOUR (1984)*

$$\bar{v}_{lc} = \frac{\Delta Z}{\frac{Z_m}{\bar{v}_m} - \frac{Z_b}{\bar{v}_b}} \quad \text{with} \quad \Delta Z = Z_m - Z_b. \quad (8-3)$$

Finally the P_n velocity v_{cm} at the crust mantle boundary has been digitized. It is the velocity immediately below the Mohorovičić discontinuity (Fig. 8.20).

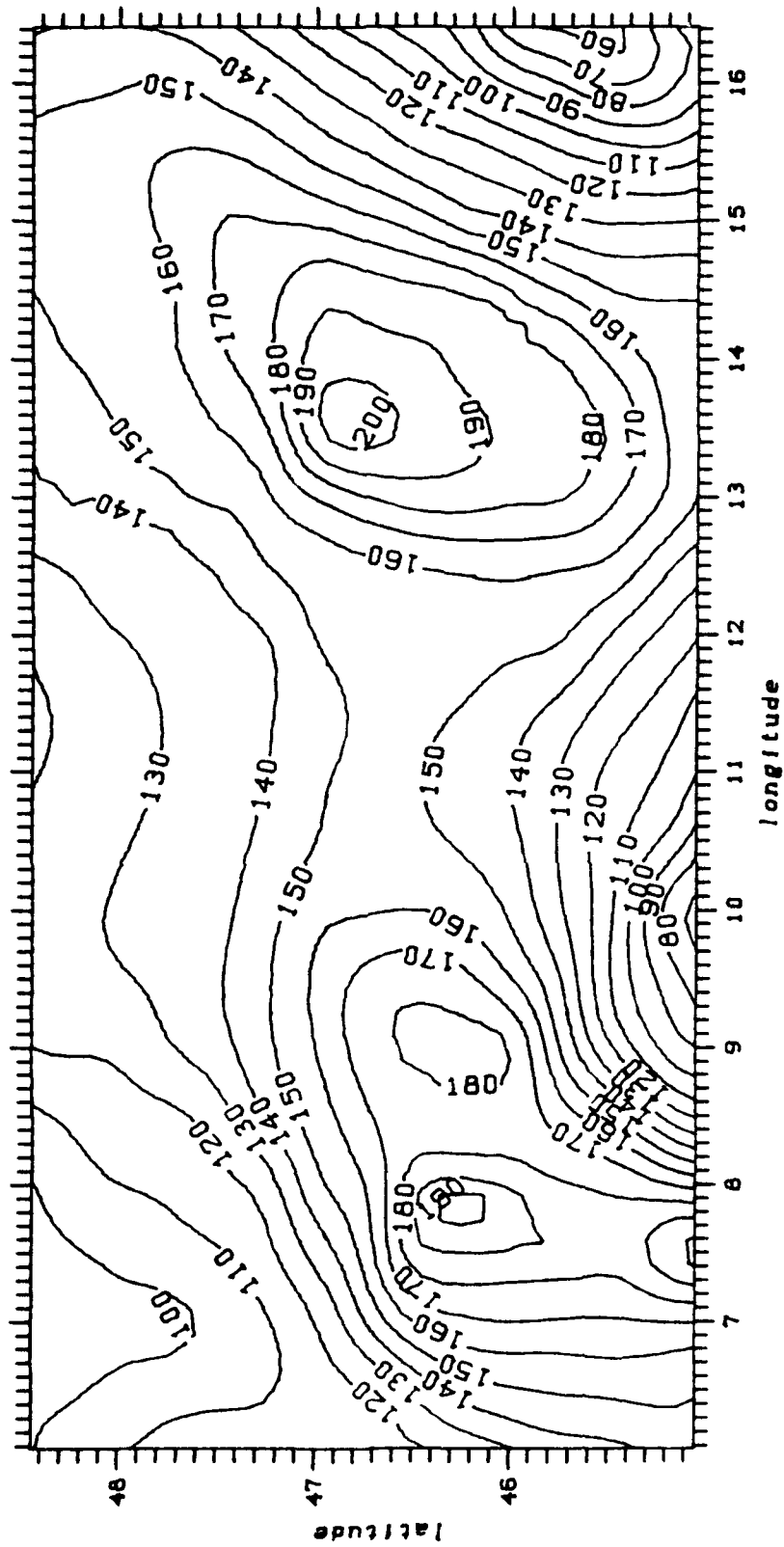


Fig. 8.16. Thickness of lithosphere derived from seismological observations in the Alps. Contour interval 10 km.

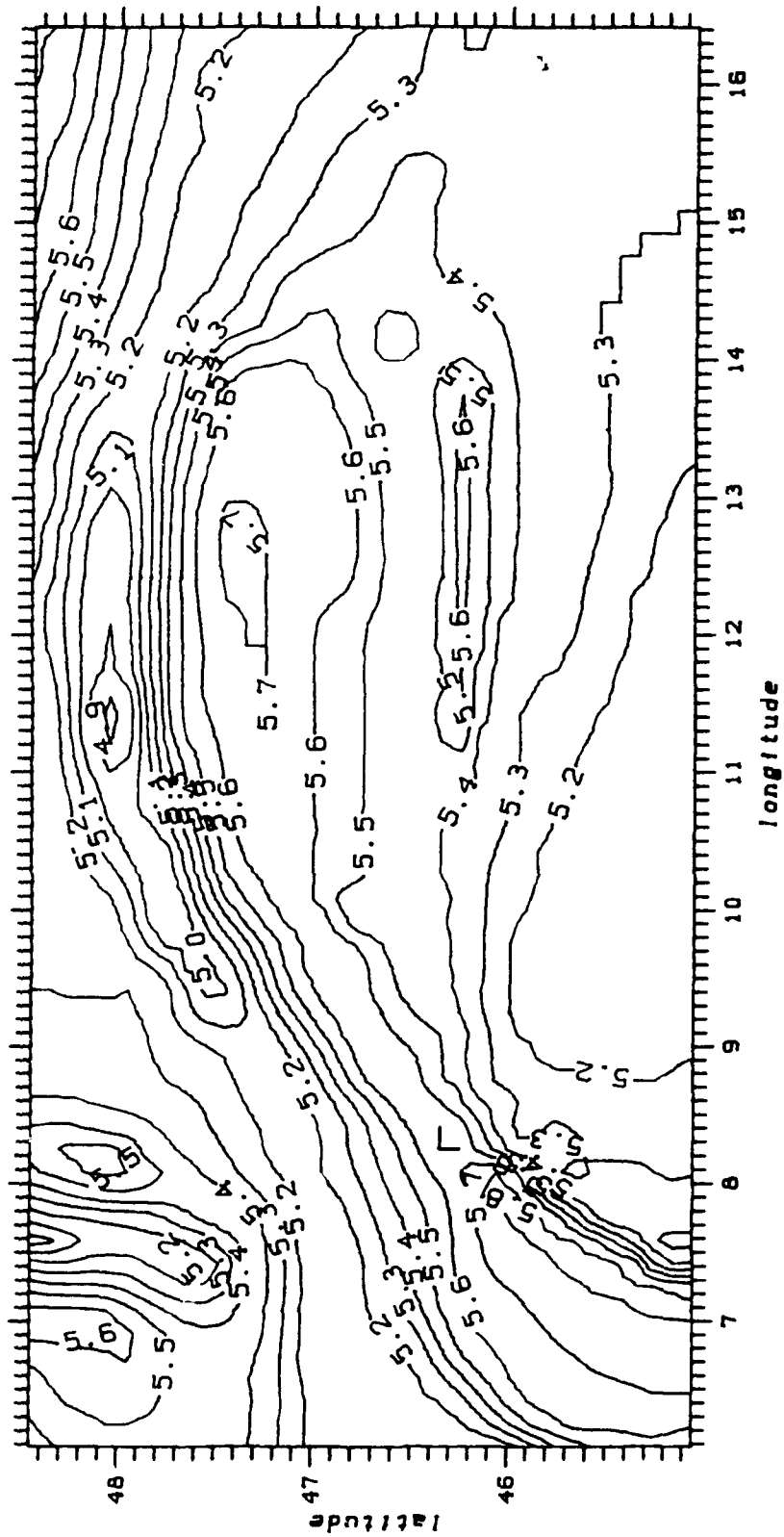


Fig. 8.17. Mean seismic P wave velocity in the upper crust \bar{v}_b (layer from surface down to seismic basement). Contour interval 0.1 km/s.

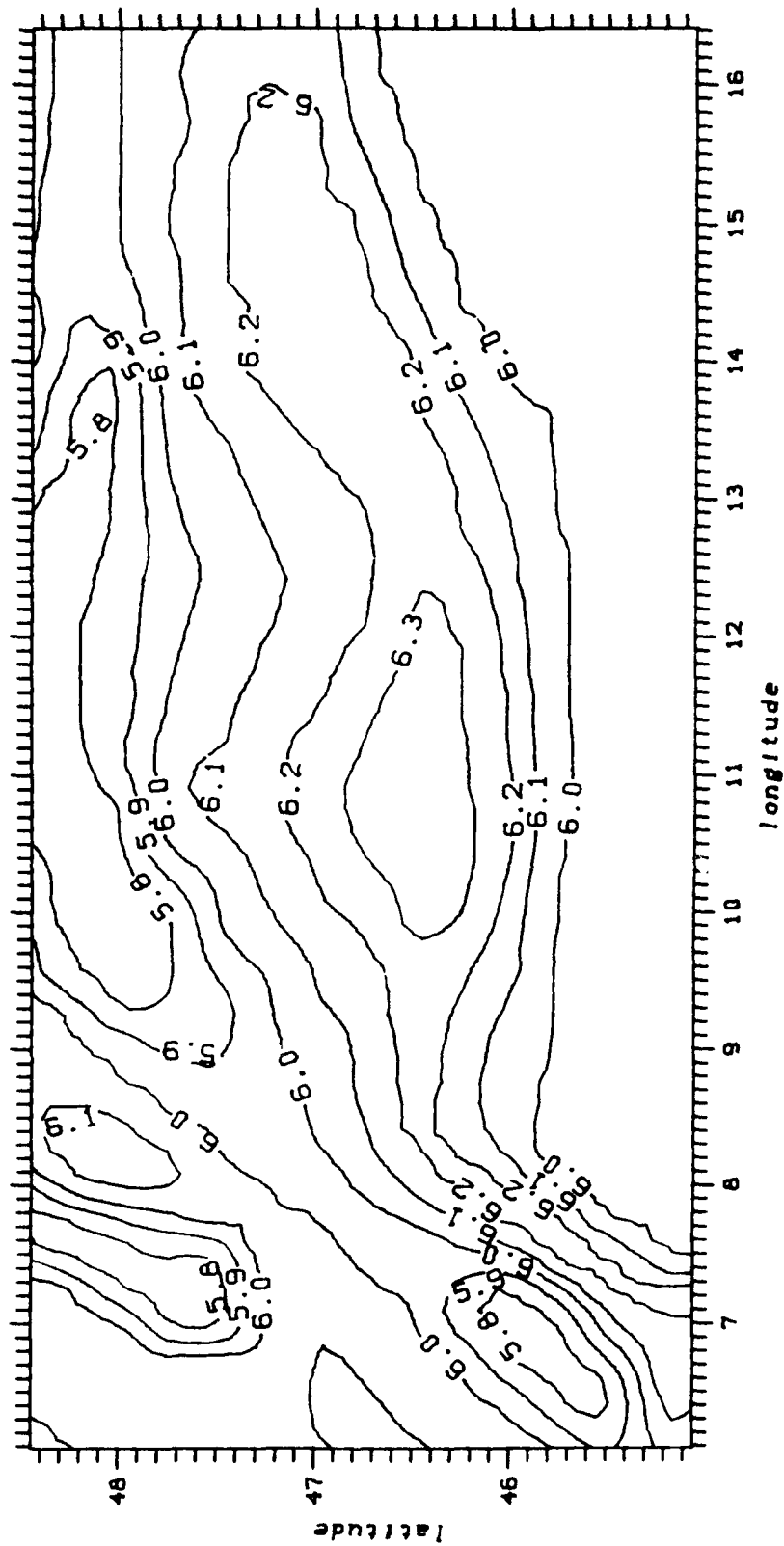


Fig. 8.18. Mean crustal seismic P wave velocity \bar{v}_m , (layer from surface down to Moho). Contour interval 0.1 km/s.

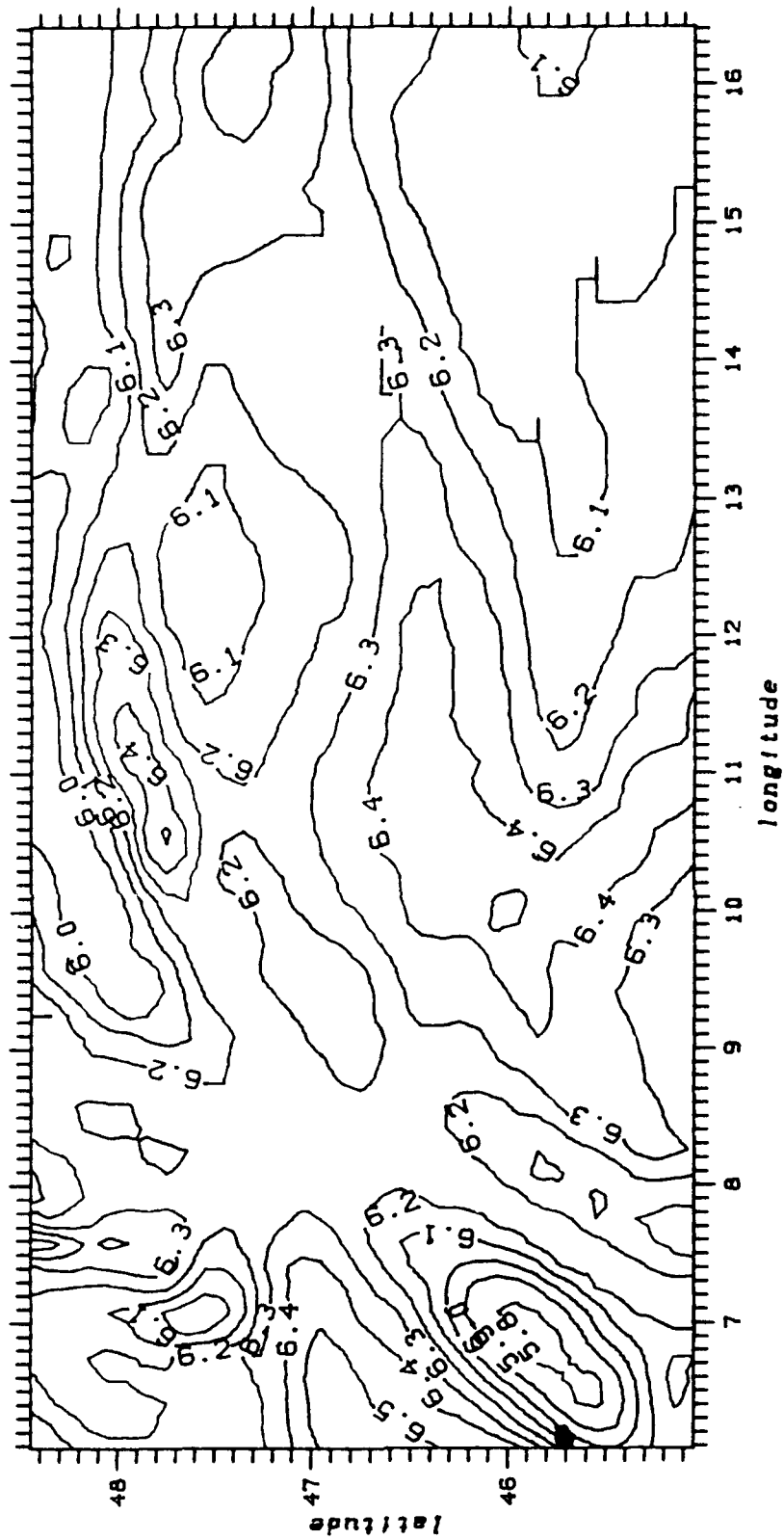


Fig. 8.19. Mean seismic P wave velocity \bar{v}_{lc} in the middle and lower crust calculated for each $6' \times 10'$ block from formula (8-3). Contour interval 0.1 km/s.

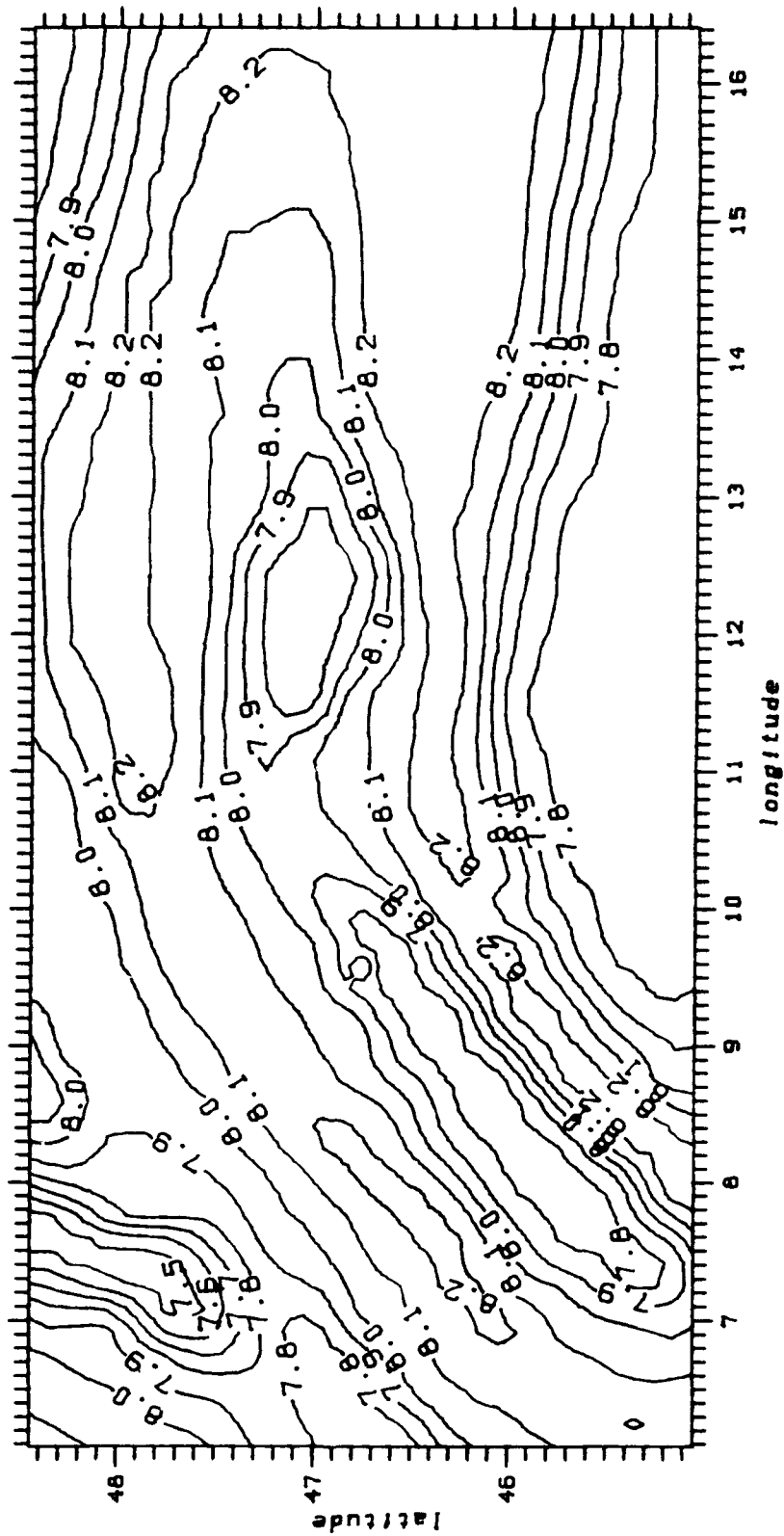


Fig. 8.20. Seismic velocity v_{cm} at the crust/mantle boundary (uppermost part of the mantle). Contour interval 0.1 km/s.

The contours of \bar{v}_b again show the typical structure of the Alps. The Molasse basins and the southern Rhine Graben filled with sediments are characterized by low seismic velocity as theoretically expected. In the central East Alpine and the western Alpine arc \bar{v}_b reaches relatively high values of 5.6 ... 5.8 km/s. It may be suspected that the definition of the seismic basement (see section 8.2.5) is not valid there. The variation of the mean P wave velocity \bar{v}_m for the whole crust is much smaller (about 5.8 ... 6.3 km/s) than that within the upper crust. The variation correlates well with the locations of the sedimentary basins. We note, however, the anomalously low average velocity in the western Alps (5.8 km/s). Here the mean P wave velocity is the same in the upper and lower crustal layers. This is also noticeable in the mean velocities \bar{v}_{lc} in the sediment-stripped crust (Fig. 8.19). Otherwise the mean velocities in the lower crustal regions range between 6.0 and 6.5 km/s. The maximum values are found below the sedimentary basins. This agrees with results of *BIRCH (1958)*.

Note that Fig. 8.19 clearly differs from the picture presented by *MOSTAANPOUR (1984)*. The reason for this is partly that we computed the average velocity \bar{v}_{lc} for each $6' \times 10'$ quadrangle, while *MOSTAANPOUR (1984)* had computed \bar{v}_{lc} only for a few points and constructed the contour lines manually.

The P_n velocity v_{cm} just below the crust-mantle boundary shows relatively low values (7.8 km/s) in the region of the deepest Moho. These regions are surrounded by zones of relatively high P_n velocity (8.2 km/s). There is some north-south asymmetry in the sedimentary basins; the Molasse is underlain by high velocities (8.0 ... 8.2 km/s) while the Po plain is underlain by relatively low velocities (7.8 km/s). The anomalously low velocities in the lower crust of the western Alps has no counterpart below the crust mantle boundary, but there are anomalously low P_n velocities below the southern Rhine Graben (7.5 ... 7.6 km/s).

8.2.9 Digital density model

In order to compute topographic (terrain) reduction of gravity measurements, one should know the density distribution near the earth's surface above the reference level. For computer-adequate procedures one needs a digital density model besides the digital elevations. The density surface rocks range between 2.0 (unconsolidated sediments) and 3.0 g/cm³ (ultrabasic magmatic rocks). The usual assumption of an average density of 2.67 g/cm³ for the surficial crustal rocks leads to uncertainties or errors in the determination of the topographic reductions. For Austria a digital density model is now available (see Fig. 8.21). It grew

Distribution of Surface Density

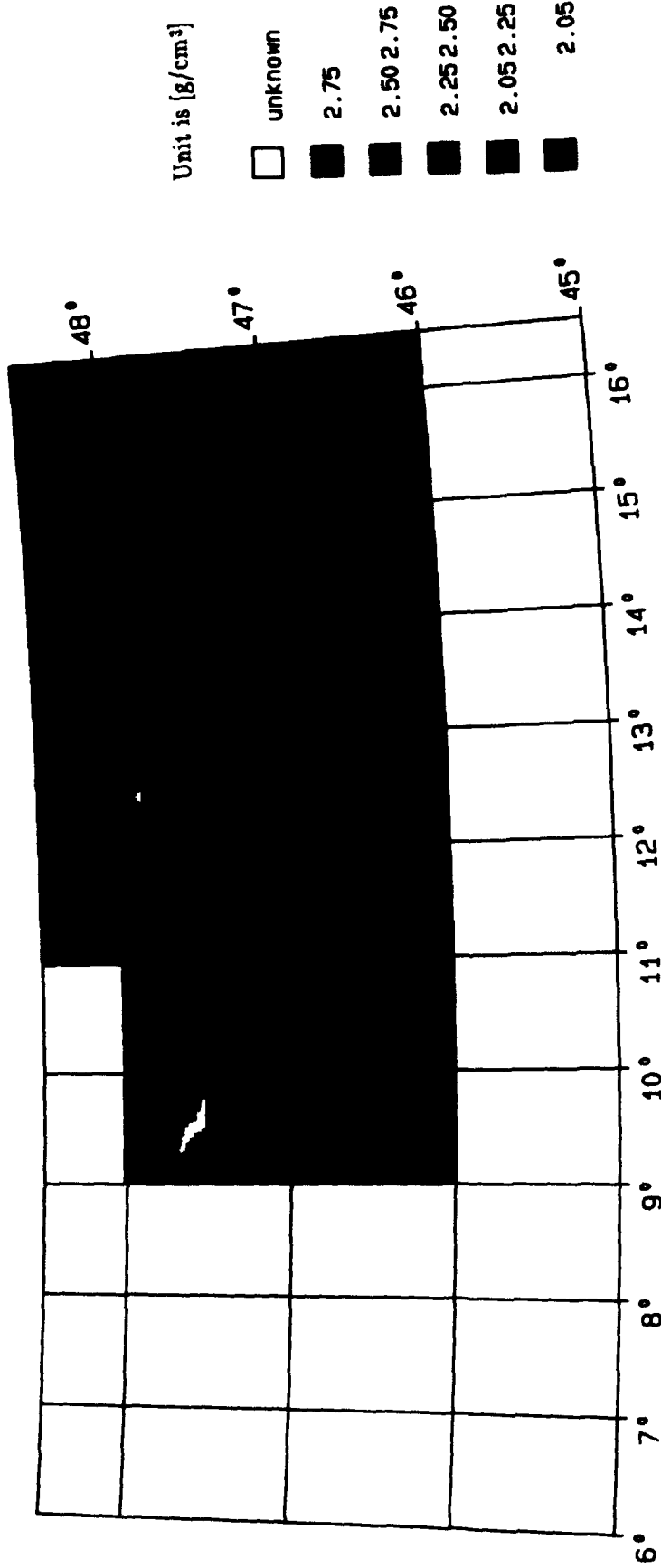


Fig 8.21. Surface density data over the European Alps.

9. NUMERICAL INVESTIGATIONS

9.1 Prediction of gravity anomalies in test area "Rossdorf"

The purpose of the computations was to investigate to what extent (surface) density data can improve the prediction accuracy of gravity anomalies. This includes also the case where gaps without gravity observations can be overbridged via density observations. For the numerical realization methods were preferred fitting into the general integrated geodesy adjustment scheme.

From the various models discussed in chap. 4 two were implemented in FORTRAN77 programs: The method of *quasi-harmonic inversion* and the *attenuated white noise gravity covariance model* of JORDAN, HELLER (1978).

For the investigations the stochastic properties of the gravity anomalies as well as those of the density data had to be evaluated. For the fulfillment of the condition $E\{\cdot\} = 0$ mean values as simple trend were subtracted. Topographic-isostatic reduction of gravity anomalies was done using the prism integration method (FORSBERG 1984), the digital terrain model ($100 \times 100 \text{ m}^2$) and the compensation model of Airy-Heiskanen type (HEISKANEN, MORITZ 1967, p. 195), however, with the mean surface density of $\rho = 2.63 \text{ g/cm}^3$ of all 78 stations. For the determination of the Bouguer anomalies the corresponding *discrete* density data of the stations were applied. The resulting characteristics of the covariance functions are summarized in Tab. 9.1.

Table 9.1. Characteristic parameters of empirical covariance functions in test area "Rossdorf"

Parameters of covariance functions	Free-air gravity anomalies Δg_F	Bouguer gravity anomalies Δg_B	Topographic-isostatic anomalies Δg_{TI}	Surface density data $\delta\rho$
Variance	144 mGal ²	93 mGal ²	103 mGal ²	0.014(g/cm ³) ²
Correlation length ψ	5.9 km	5.8 km	5.7 km	2.3 km
Variance of horizontal gradient	570 E ²	736 E ²	780 E ²	0.1(g/cm ³)/km

As a second step an iterative fit to the analytical covariance model of *TSCHERNING, RAPP (1974)* to the empirically determined covariance functions was carried out (for use in the quasi-harmonic inversion method). The results can be found in Tab. 9.2.

Table 9.2. Parameters of the *TSCHERNING, RAPP (1974)* covariance model for the test area "Rossdorf" using Δg_{TI} .

Order of local covariance function n	619
$(R_B/R_E)^2$	0.999615
AVAR	96.91

In Tab. 9.2 $(R_B/R_E)^2$ is the square of the ratio of the radius R_B of the so-called Bjerhammar sphere to the earth's radius R_E , and AVAR is a scale factor of the model. Comparison of the model crosscovariances $\text{cov}(\Delta g, \delta\rho)$ with the corresponding empirical values, however, showed a significant disagreement (Figs. 9.1 to 9.3)

The third step was the prediction of gravity anomalies. The method applied was the following: We assumed for each point P_i no observation being available and predicted for P_i the gravity anomaly from its 77 ($= 78 - 1$) neighbours. The difference between the available "observation" Δg and the predicted value Δg_{pred} can be considered as the contribution of point P_i to a "true" prediction error defined by

$$\sigma = \sqrt{\sum_{i=1}^n (\Delta g - \Delta g_{\text{pred}})_i^2 / n}. \quad (9-1)$$

The predictions were done using gravity anomalies Δg alone, a combination of gravity anomalies and surface densities, and also using density values alone.

Prediction results using the quasi-harmonic inversion method

Results of the test runs are given in Tab. 9.3.

Table 9.3. Results of gravity anomaly prediction in the test area "Rossdorf" using the quasi-harmonic inversion method. "True" prediction errors in [mGal].

Data	Δg_F	Δg_B	Δg_{TI}
Gravity anomalies alone	4.0	2.9	2.8
Gravity anomalies and density data	5.9	4.4	4.4
Density data alone	5.4	4.3	4.4

The prediction of gravity anomalies using only gravity anomalies was more or less carried out in order to get some kind of reference. As expected the consideration of a simple Bouguer plate as height model ($\rightarrow \Delta g_B$) resulted already in a significant improvement in the gravity prediction. Whereas the use of a detailed elevation grid assuming in addition an isostatic compensation could not show any further reduction in the "true" prediction error. This could possibly be explained that for the determination of the Bouguer plate effect observed (point) density values were used and secondly, that it might be questioned whether in that area the consideration of an isostatic compensation mechanism is justified. It is surprising that the free-air gravity anomaly prediction from density data alone was only slightly worse (± 5.4 mGal) than the one from gravity anomalies (± 4.0 mGal).

What at the moment cannot reasonably be explained is the fact that no improvement in gravity prediction was achieved when using a combined set of gravity anomalies *and* density data.

Gravity prediction using the attenuated white noise gravity covariance model

For numerical investigations the spherical (6-19) as well as the flat-earth form (6-21) of the attenuated white noise gravity covariance model (see chap. 6.2) were programmed. The expressions for the necessary covariance and crosscovariance functions can be found in Appendix A.

By varying the parameters D (characteristic depth) and C_{0T} (variance of the disturbing potential) of the attenuated white noise gravity covariance model the following empirical relations between D , C_{0T} and $C_{0\Delta g}$, ψ (variance and correlation length of the autocovariance function of gravity anomalies) were found:

$$D = \frac{4}{3} \psi, \quad (9-2)$$

$$C_{0T} = \frac{C_0 \Delta g}{15\,000} D^2 \left[1 + \frac{D}{R} \right]^3 \quad (9-3)$$

or, when using the asymptotic forms (flat-earth model),

$$C_{0T} = \frac{C_0 \Delta g}{15\,000} D^2. \quad (9-4)$$

The used units are:

$$\begin{aligned} D, \psi, R & \quad [\text{km}], \\ C_{0T} & \quad [(\text{m/s})^4], \\ C_0 \Delta g & \quad [\text{mgal}^2]. \end{aligned}$$

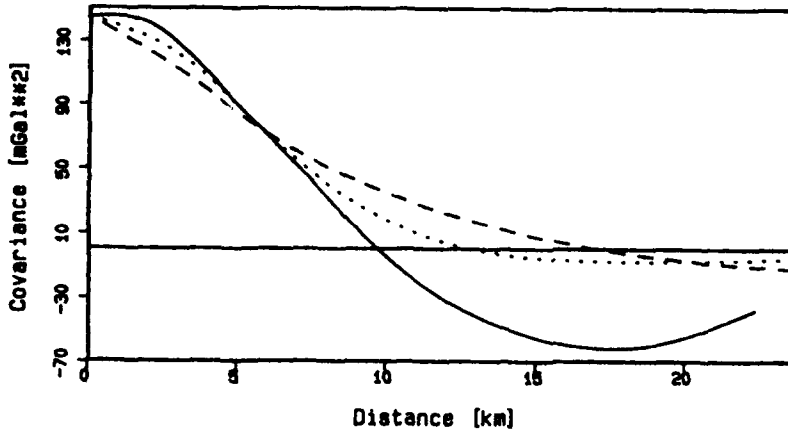
For the "Rossdorf" test area the free parameters are determined as function of the variance and the correlation length of the autocovariance function of the corresponding gravity anomalies (free-air, Bouguer, topographic-isostatic).

Table 9.4. Characteristic depth D and variance of the disturbing potential C_{0T} as function of the correlation length ψ and the variance $C_0 \Delta g$ of the corresponding gravity anomaly covariance function.

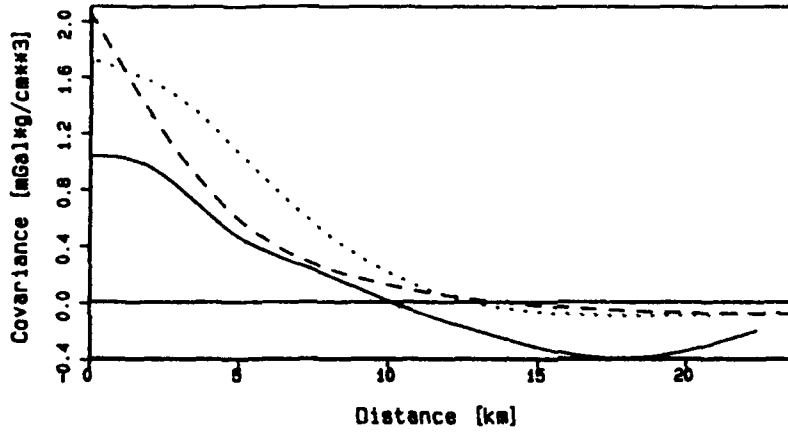
	Free-air gravity anomalies Δg_F	Bouguer gravity anomalies Δg_B	Topographic- isostatic anomalies Δg_{TI}
Variance $C_0 \Delta g$	144 mGal ²	93 mGal ²	103 mGal ²
Correlation length ψ	5.9 km	5.8 km	5.7 km
Characteristic depth D	7.9 km	7.8 km	7.7 km
Model variance C_{0T}	0.60 $(\frac{\text{m}}{\text{s}})^4$	0.38 $(\frac{\text{m}}{\text{s}})^4$	0.40 $(\frac{\text{m}}{\text{s}})^4$

Plots of the empirical as well as of the model covariance functions of the Tscherning/ Rapp and the attenuated white noise gravity covariance model of Jordan/Heller are shown for comparison in Figs. 9.1 to 9.3. The graphs indicate that the attenuated white noise

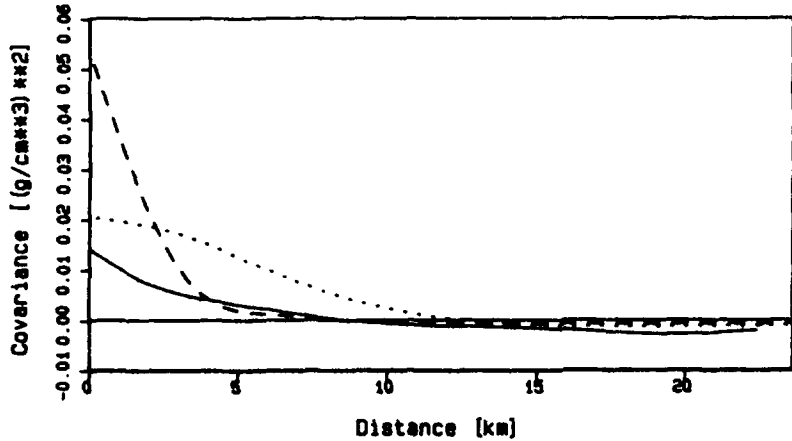
Autocovariance function of free-air gravity anomalies



Crosscovariance function between densities and free-air anomalies



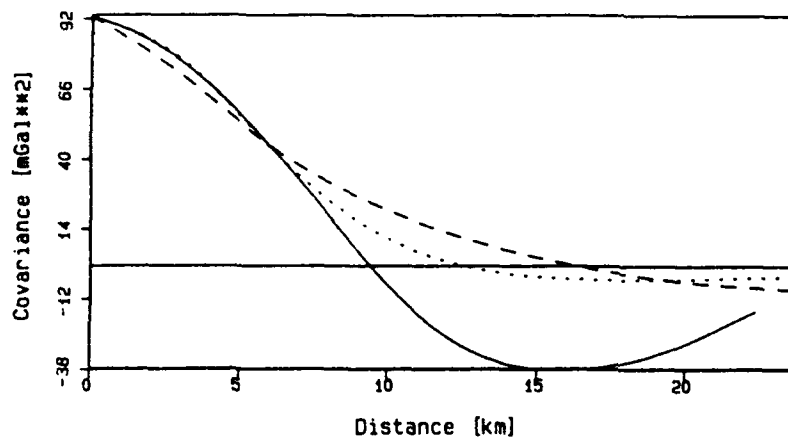
Autocovariance function of surface density values



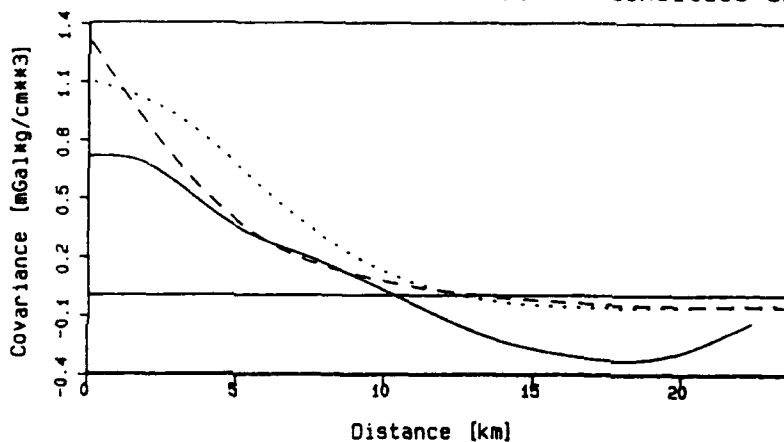
— Empirical
 - - - Tscherning/Rapp
 Jordan/Heller

Fig. 9.1. Covariance functions for the test area "Rossdorf" (Free-air gravity anomaly fit).

Autocovariance function of Bouguer gravity anomalies



Crosscovariance function between densities and Bouguer anomalies



Autocovariance function of surface density values

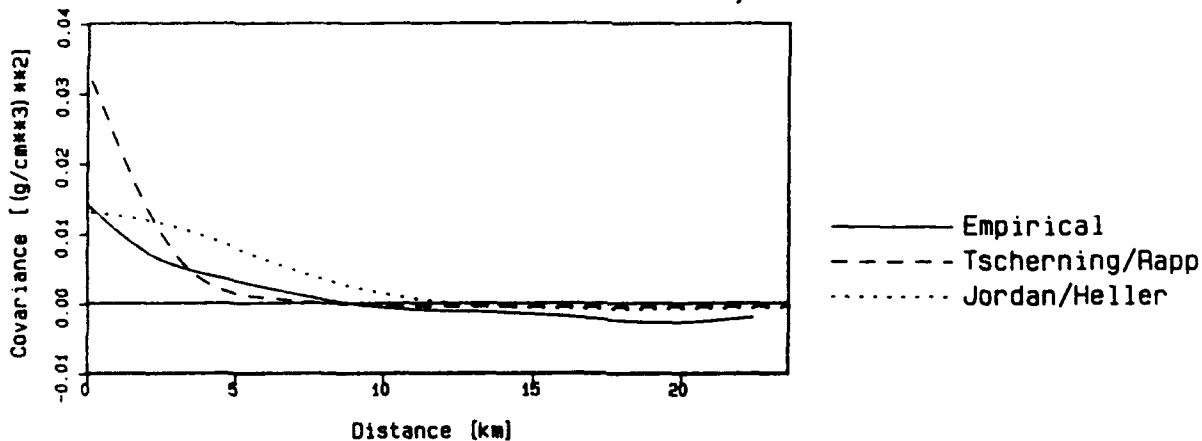


Fig. 9.2. Covariance functions for the test area "Rossdorf" (Bouguer gravity anomaly fit).

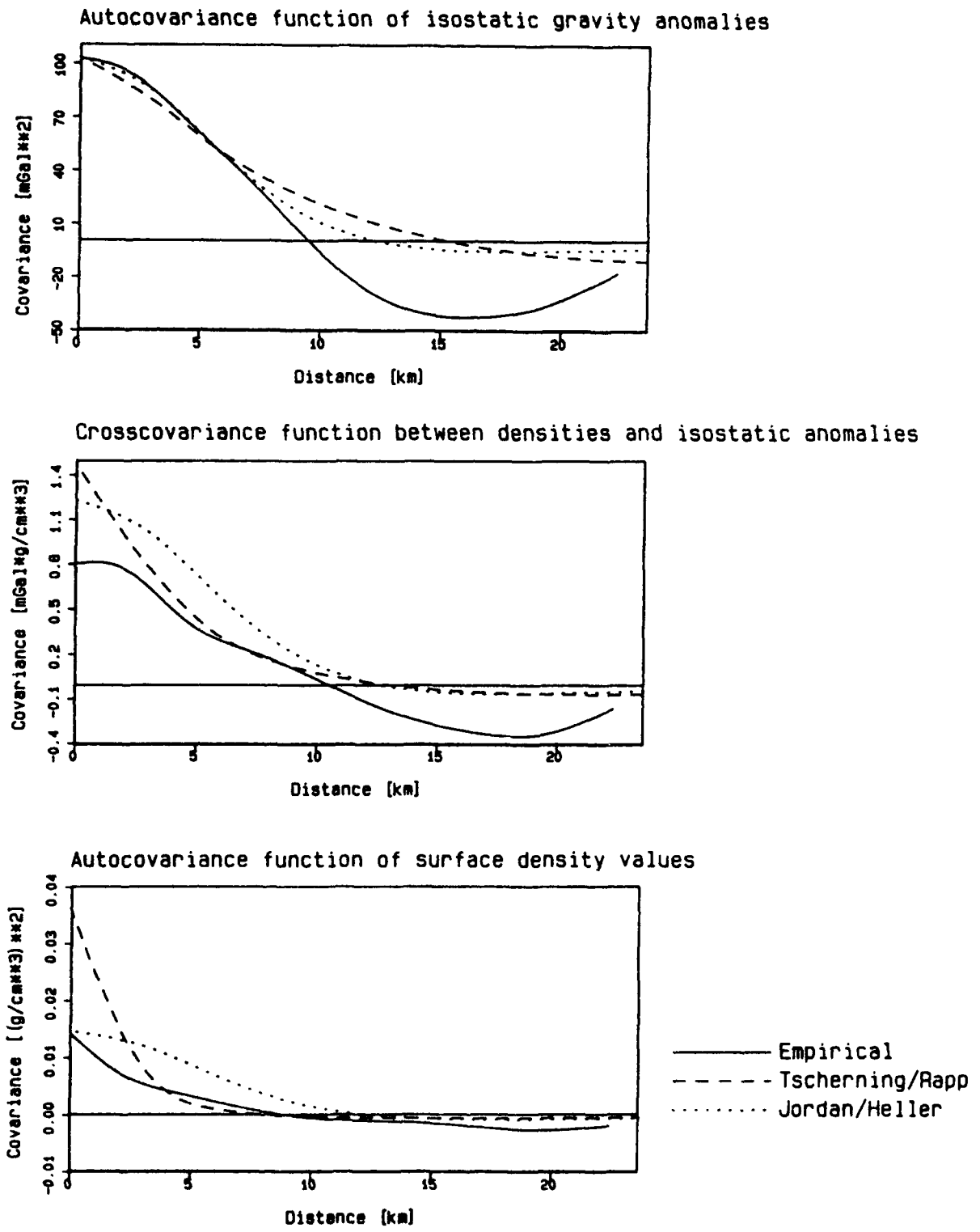


Fig. 9.3. Covariance functions for the test area "Rossdorf" (Topographic-isostatic gravity anomaly fit).

gravity covariance model fits better to the empirical autocovariance functions $C_{\Delta g \Delta g}$, $C_{\delta \rho \delta \rho}$, although its variance $C_{\rho}(\delta \rho, \delta \rho)$ is still too high. Both, crosscovariances $C_{\delta \rho \Delta g}$ and autocovariances $C_{\delta \rho \delta \rho}$ are decreasing too slowly with respect to small distances.

The numerical prediction trials were carried out in the same way as outlined before with regard to the use of the quasi-harmonic inversion method. Only observations within a radius of approx. 6 km (corresponding to a little bit more than the correlation length of the empirical gravity covariance functions, see Tab. 9.1) were considered in the pointwise gravity prediction algorithm. The results are given in Tab. 9.5.

Table 9.5. Results of gravity anomaly prediction in the test area "Rossdorf" using the attenuated white noise gravity covariance model of Jordan/Heller. "True" prediction errors in [mGal].

Data	Δg_F	Δg_B	Δg_{TI}
Gravity anomalies alone	4.3	2.9	2.8
Gravity anomalies and density data	-	-	-
Density data alone	5.8	5.6	5.4

If the reader compares the results in Tab. 9.5 with the ones in Tab. 9.3 no principal differences can be found except that when using the Jordan/Heller covariance model in the form like here - one-layer crust - it is not possible to consider gravity *and* density data in a combined observation set due to ill-conditioning and singularities, resp., in the flat earth one-layer-crust covariance model (see the comments after eq. (6-28)).

Nevertheless, for further studies in gravity prediction using density data the application of a Jordan/Heller multiple-layer crust model considering regional isostatic compensation (for example in the form of eqs. (6-29) to (6-29d)) seems to be promising, since it contains no singularities or ill-conditioning and can be widely adapted to the physical reality (in contrast to the quasi-harmonic method).

An interesting by-product of the developed gravity prediction algorithms is their use for the determination of density from gravity anomalies (inverse problem). The results of these computations can be found in Tab. 9.6.

Table 9.6. True errors of density prediction in [g cm⁻³] in the test area "Rossdorf"

Data	Quasi-harmonic inversion Tscherning/Rapp model	Jordan/Heller covariance model
Gravity anomalies alone	0.10	0.08
Gravity anomalies and density data	0.16	—
Density data alone	0.07	0.08

Although the results here are not representative, the accuracy of estimated density in the range of ± 0.1 g cm⁻³ is remarkable.

9.2 Prediction of gravity anomalies in the European Alps

Whereas in chapter 9.1 test computations were carried out in a very local area, the intention here was to repeat those ones on a more regional scale. For that reason the data collected over the European Alps – described in chap. 8.2 – were used.

Empirical covariance functions over the European Alps ($6^{\circ} \leq \lambda \leq 16^{\circ}5$; $45^{\circ} \leq \varphi \leq 48^{\circ}5$)

For the topographic-isostatic gravity anomalies (see chap. 8.2.2) the empirical covariance function was determined using some kind of homogeneous thinning procedure for the data, similar to the one described by LANDAU *et al* (1988). The residual trend was removed using a simple linear regression of type

$$\Delta g_{TI} = a + b H \quad (9-2)$$

where H denotes the height and a,b are the parameters which were determined to be

$$a = 46.7 \text{ mGal}$$

$$b = -0.029 \text{ mGal/m}$$

For the determination of the corresponding empirical surface density covariance function a simple constant (mean value) as trend was considered to be sufficient, $\bar{\rho} = 2.41 \text{ g/cm}^3$. The results of the computations are summarized in Tab. 9.7.

Table 9.7. Characteristics of empirical covariance functions over the European Alps ($6^\circ \leq \lambda \leq 16^\circ 5'$; $45^\circ \leq \varphi \leq 48^\circ 5'$).

Parameters of covariance functions	Topographic-isostatic gravity anomalies Δg_{TI}	Surface density data ($3' \times 5'$) $\delta\rho$
Variance	660 mGal ²	0.15 (g/cm ³) ²
Correlation length ψ	24.3 km	46.8 km
Variance of horizontal gradient	208 E ²	

Plots of the empirical covariance functions are found in Figs. 9.4 and 9.5.

Comparing parameters for the gravity anomaly covariance function with the results of (SÜNKEL *et al* 1983) shows a difference in the variance. This, however, can be easily explained by the fact that they restricted themselves to data covering Austria only whereas we also included gravity anomalies for the rest of the European Alps. Especially the gravity field in Switzerland and northern Italy shows large variations in the gravity anomalies, compare Tab. 9.8.

Table 9.8. Variations in gravity anomalies in [mGal].

	Austria	F.R. Germany	Italy	Switzerland
Minimum	- 48	- 60	- 108	- 60
Maximum	+ 121	+ 3	+ 160	+ 134

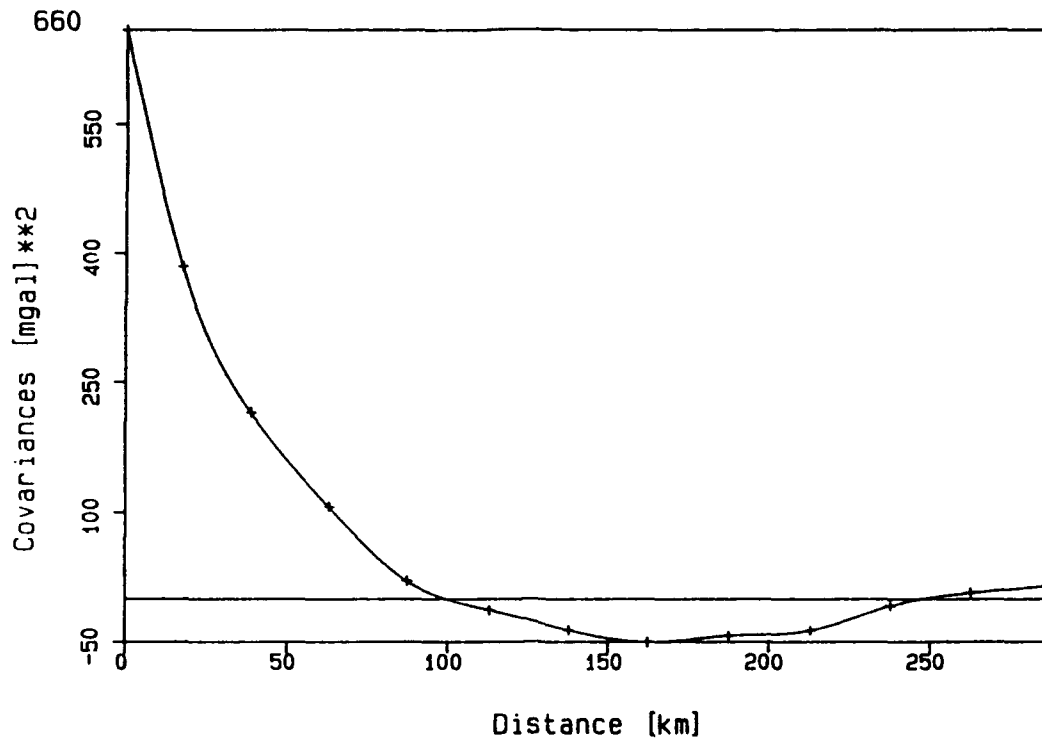


Fig. 9.4. Empirical covariance function of point gravity anomalies using data over the whole European Alps.

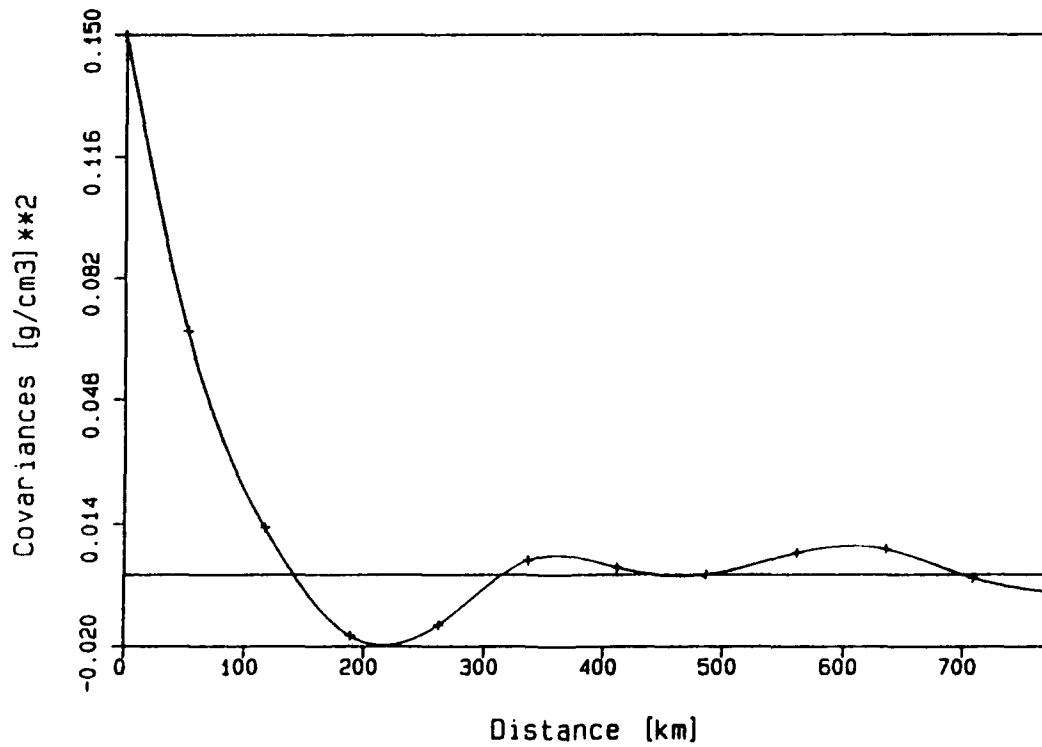


Fig. 9.5. Empirical covariance function of block mean surface density $6' \times 10'$ using data over the whole European Alps.

Empirical covariance functions over the $1^{\circ} \times 1^{\circ}$ block ($13^{\circ} \leq \lambda \leq 14^{\circ}$ and $47^{\circ} \leq \varphi \leq 48^{\circ}$)

In order to save computer time it was decided to test the quasi-harmonic inversion in the $1^{\circ} \times 1^{\circ}$ block mentioned above. There the topography varies from 500 m up to 2000 m (Fig. 8.4). Within this area an amount of 3396 gravity values was found in the data base.

Table 9.9. Characteristics of empirical covariance functions over the $1^{\circ} \times 1^{\circ}$ block ($13^{\circ} \leq \lambda \leq 14^{\circ}$ and $47^{\circ} \leq \varphi \leq 48^{\circ}$) of the European Alps.

Parameters of covariance functions	Topographic-isostatic gravity anomalies Δg_{TI}	Surface density data ($3' \times 5'$) $\delta\rho$
Variance	472 mGal ²	0.013 (g/cm ³) ²
Correlation length ψ	18.5 km	20.3 km
Variance of horizontal gradient	313 E ²	

Similarly to the computations in the "Rossdorf" test area an iterative fit of the analytical covariance model of *TSCHERNING, RAPP (1974)* was carried out which resulted in the parameters outlined in Tab. 9.10.

Table 9.10 Parameters of the *TSCHERNING, RAPP (1974)* covariance model for the $1^{\circ} \times 1^{\circ}$ block of the European Alps.

Order of local covariance function n	200
$(R_D/R_E)^2$	0.998615
AVAR	517.28

Test computations in gravity interpolation were again done in the same manner as in the "Rossdorf" area using the quasi-harmonic inversion method. The results are found in Tab. 9.11.

Table 9.11 Results of gravity anomaly prediction in the European Alps ($1^{\circ} \times 1^{\circ}$ block) using the quasi-harmonic inversion method.

Data	True prediction error
Topographic-isostatic gravity anomalies	5.2 mGal
Topographic-isostatic gravity anomalies and density data	7.0 mGal
Density data alone	failed

The results have to be interpreted as "failed with respect to the assumption of quasi-harmonicity for density". This is also in agreement with results published by *HEIN et al (1988)* and experiences of *STRYKOWSKI, TSCHERNING (1989, pers. comm.)* who also got from numerical investigations the impression that the "quasi-harmonicity" is a too strong condition when using it to solve the inverse gravitational problem. There might be, however, cases where the method gives reasonable results with respect to gravity prediction.

10. CONCLUSIONS

The study presents some first trials to use density and seismic data in a *direct* way in gravity field approximation, in particular gravity prediction. Although the geodesists are primarily not interested in the inverse problem, it is necessary to deal with it to some extent. The geophysicist's view on the structure of the earth's crust and its knowledge through seismics can help to improve the geodetic gravity prediction algorithms. In particular, empirical relationship between seismic velocity and density might be a valuable replacement of complex wave propagation formulas (see chapter 3).

In the theoretical part a few new approaches are presented which seem to be very promising. Since methods developed up till now use rather mathematical than (realistic) physical constraints for the covariance propagation needed in prediction algorithms of collocation type, special emphasis was put to take advantage of Newton's attraction integral for that purpose. The generalized isostatic response theory of *DORMAN, LEWIS (1970)* seems to be a promising candidate in the gravity prediction applications.

Although the quasi-harmonic inversion is based on physically not realistic constraints, it may offer in some cases reasonable prediction results. *HELLER's* 1976 developed attenuated white noise statistical gravity model seems to be more realistic when introducing multiple layers of the earth's crust. In particular, the proposal of *JORDAN (1978)* to extend this covariance theory to regional isostatic compensation might result in an even more realistic model for the terrain and crust-mantle contrasts.

In the consideration of seismic data for gravity prediction (chapter 7) the work of the geophysicist *CHERNOV (1960)* is appreciated. His statements about density and the elastic Lamé parameters at being randomly distributed in space forming a stochastic process allowed the incorporation of density and seismic data in the integrated geodesy adjustment model and the formulation of covariance functions according to seismic wave motion in an inhomogeneous medium.

The detailed numerical investigations in chapter 8 in a local as well as in the European alps brought more insight in the statistical behaviour of density and present various characteristics of covariance functions. Some first gravity predictions using density and the quasi-harmonic inversion method as well as the attenuated white noise statistical gravity covariance model show reasonable results.

Since this report can represent only some initial work in this field, it is recommended to continue this study, in particular, by realizing numerically (i) the proposed covariance model in chapter 6.3 in connection with the generalized isostatic response theory, (ii) the extension of *HELLER's* covariance model to regional compensation as proposed by *JORDAN (1978)*, and (iii) the inclusion of seismic data based on the statistical assumptions found by *CHERNOV (1960)*.

There is no doubt that density and seismic information will strengthen and improve gravity prediction, in particular in areas where gravity gaps are. However, the best method still has to be found in the future. It is hoped that this report provides a platform for further work.

APPENDIX A

Auto- and crosscovariances of the gravity field functionals based on the attenuated white noise statistical gravity model

By HELLER and JORDAN (1979) the autocovariance function of the disturbing potential T is given in the form

$$\text{Cov}(T,T)(r_1,r_2,\text{Psi}) = \frac{D^2 (2R-D)^2 [r_1^2 r_2^2 - (R-D)^4] \text{Co}(T)}{(2R^2 - 2DR + D^2) [(R-D)^4 + r_1^2 r_2^2 - 2r_1 r_2 (R-D) \cos(\text{Psi})]^{3/2}}$$

Substituting in (6-19) D/2 by D and introducing the abbreviations

$$\begin{aligned} A &= D^3 (2R-D)^3 / [R^4 - (R-D)^4] \\ &= D^2 (2R-D)^2 / [R^2 + (R-D)^2] \\ &= [R^2 - (R-D)^2] / [R^2 + (R-D)^2] \\ B &= r_1^2 r_2^2 - (R-D)^4 \\ C &= r_1^2 r_2^2 + (R-D)^4 - 2r_1 r_2 (R-D) \cos(\text{Psi}) \end{aligned}$$

leads to

$$\text{Cov}(T,T)(r_1,r_2,\text{Psi}) = A \frac{B}{C^{3/2}} \text{Co}(T)$$

The auto- and crosscovariances between the functionals of the gravity field were computed with the help of the Algebraic Computation Software REDUCE (RAYNA,1987). So the derivatives of T and Cov(T,T) with respect to r1, r2, ... are written in the form

$$\begin{aligned} &DF(T,r_1), DF(T,r_2), \dots \\ &DF(\text{Cov}(T,T),r_1), \dots \end{aligned}$$

To get higher derivatives you have to add further arguments, e.g.

$$DF(\text{Cov}(T,T),r_1,2,r_2)$$

means the second derivative with respect to r1, first with respect to r2.

The functionals of the gravity field in P are introduced by the following expressions:

- | | |
|--|--|
| 1) geoidal height | $N_1 = T_1/G$ |
| 2) gravity disturbance | $d g_1 = - DF(T_1, r_1)$ |
| 3) gravity anomaly | $D g_1 = - DF(T_1, r_1) - 2*T_1/r_1$ |
| 4) radial gravity gradient | $= - DF(T_1, r_1, 2) - 2*DF(T_1, r_1)/r_1$ |
| 5) second radial derivative of T | $= + DF(T_1, r_1, 2)$ |
| 6) N-S-component of the deflection of the vertical | $X_{11} = - DF(T_1, p_1)/(G*R)$ |
| 7) E-W-component of the deflection of the vertical | $E_{11} = - DF(T_1, l_1)/(G*R*cos(p_1))$ |
| 8) density contrast | $d \rho = - DF(T_1, r_1)*DIRAC(r_1 - R')/(4*Pi*k)$ |

In the formulas above G is the normal gravity value, k the Newtonian gravity constant, R the earth's mean radius, R' the radius of the density contrast, p1 the geographical latitude and l1 the geographical longitude of P.

To get the functionals in Q substitute T1, r1, p1, l1 by T2, r2, p2, l2.

The covariances between the functionals are computed as matrix elements Cov(i, j), where i and j are the numbers of the functionals in P and Q, e.g. Cov(3, 8) is the crosscovariance between the gravity anomaly in P and the density contrast in Q.

$$Cov(1, 1) = Cov(T, T)/G^2$$

$$Cov(1, 2) = - DF(Cov(T, T), r_2)/G$$

$$Cov(1, 3) = (- DF(Cov(T, T), r_2) - 2*Cov(T, T)/r_2)/G$$

$$Cov(1, 4) = (- DF(Cov(T, T), r_2, 2) - 2*DF(Cov(T, T), r_2)/r_2)/G$$

$$Cov(1, 5) = DF(Cov(T, T), r_2, 2)/G$$

$$Cov(1, 6) = - DF(Cov(T, T), p_2)/(G * R)^2$$

$$Cov(1, 7) = - DF(Cov(T, T), l_2)/(G * R*cos(p_2))^2$$

$$Cov(1, 8) = - DF(Cov(T, T), r_2)*DIRAC(r_2 - R'), (4*Pi*k*G)$$

$$Cov(2, 1) = - DF(Cov(T, T), r_1)/G$$

$$\begin{aligned}
\text{Cov}(2,2) &= \text{DF}(\text{Cov}(T,T), r1, r2) \\
\text{Cov}(2,3) &= \text{DF}(\text{Cov}(T,T), r1, r2) + 2*\text{DF}(\text{Cov}(T,T), r1)/r2 \\
\text{Cov}(2,4) &= \text{DF}(\text{Cov}(T,T), r1, r2, 2) + 2*\text{DF}(\text{Cov}(T,T), r1, r2)/r2 \\
\text{Cov}(2,5) &= - \text{DF}(\text{Cov}(T,T), r1, r2, 2) \\
\text{Cov}(2,6) &= \text{DF}(\text{Cov}(T,T), r1, p2)/(G*R) \\
\text{Cov}(2,7) &= \text{DF}(\text{Cov}(T,T), r1, l2)/(G*R*\cos(p2)) \\
\text{Cov}(2,8) &= \text{DF}(\text{Cov}(T,T), r1, r2)*\text{DIRAC}(r2 - R')/(4*Pi*k) \\
\\
\text{Cov}(3,1) &= (- \text{DF}(\text{Cov}(T,T), r1) - 2*\text{Cov}(T,T)/r1)/G \\
\text{Cov}(3,2) &= \text{DF}(\text{Cov}(T,T), r1, r2) + 2*\text{DF}(\text{Cov}(T,T), r2)/r1 \\
\text{Cov}(3,3) &= \text{DF}(\text{Cov}(T,T), r1, r2) + 2*\text{DF}(\text{Cov}(T,T), r1)/r2 \\
&\quad + 2*\text{DF}(\text{Cov}(T,T), r2)/r1 + 4*\text{Cov}(T,T)/(r1*r2) \\
\text{Cov}(3,4) &= \text{DF}(\text{Cov}(T,T), r1, r2, 2) + 2*\text{DF}(\text{Cov}(T,T), r1, r2)/r2 \\
&\quad + 2*\text{DF}(\text{Cov}(T,T), r2, 2)/r1 + 4*\text{DF}(\text{Cov}(T,T), r2)/(r1*r2) \\
\text{Cov}(3,5) &= - \text{DF}(\text{Cov}(T,T), r1, r2, 2) - 2*\text{DF}(\text{Cov}(T,T), r2, 2)/r1 \\
\text{Cov}(3,6) &= (\text{DF}(\text{Cov}(T,T), r1, p2) + 2*\text{DF}(\text{Cov}(T,T), p2)/r1)/(G*R) \\
\text{Cov}(3,7) &= (\text{DF}(\text{Cov}(T,T), r1, l2) + 2*\text{DF}(\text{Cov}(T,T), l2)/r1)/(G*R*\cos(p2)) \\
\text{Cov}(3,8) &= \text{DIRAC}(r2 - R')*(\text{DF}(\text{Cov}(T,T), r1, r2) + 2*\text{DF}(\text{Cov}(T,T), r2)/r1)/(4*Pi*k) \\
\\
\text{Cov}(4,1) &= (- \text{DF}(\text{Cov}(T,T), r1, 2) - 2*\text{DF}(\text{Cov}(T,T), r1)/r1)/G \\
\text{Cov}(4,2) &= \text{DF}(\text{Cov}(T,T), r1, 2, r2) + 2*\text{DF}(\text{Cov}(T,T), r1, r2)/r1 \\
\text{Cov}(4,3) &= \text{DF}(\text{Cov}(T,T), r1, 2, r2) + 2*\text{DF}(\text{Cov}(T,T), r1, r2)/r1 \\
&\quad + 2*\text{DF}(\text{Cov}(T,T), r1, 2)/r2 + 4*\text{DF}(\text{Cov}(T,T), r1)/(r1*r2) \\
\text{Cov}(4,4) &= \text{DF}(\text{Cov}(T,T), r1, 2, r2, 2) + 2*\text{DF}(\text{Cov}(T,T), r1, r2, 2)/r1 \\
&\quad + 2*\text{DF}(\text{Cov}(T,T), r1, 2, r2)/r2 + 4*\text{DF}(\text{Cov}(T,T), r1, r2)/(r1*r2) \\
\text{Cov}(4,5) &= - \text{DF}(\text{Cov}(T,T), r1, 2, r2, 2) - 2*\text{DF}(\text{Cov}(T,T), r1, r2, 2)/r1 \\
\text{Cov}(4,6) &= (\text{DF}(\text{Cov}(T,T), r1, 2, p2) + 2*\text{DF}(\text{Cov}(T,T), r1, p2)/r1)/(G*R) \\
\text{Cov}(4,7) &= (\text{DF}(\text{Cov}(T,T), r1, 2, l2) + 2*\text{DF}(\text{Cov}(T,T), r1, l2)/r1)/(G*R*\cos(p2)) \\
\text{Cov}(4,8) &= (\text{DIRAC}(r2 - R')*(\text{DF}(\text{Cov}(T,T), r1, 2, r2) + 2*\text{DF}(\text{Cov}(T,T), r1, r2)/r1)/ \\
&\quad (4*Pi*k)
\end{aligned}$$

$$\begin{aligned}
\text{Cov}(5,1) &= + \text{DF}(\text{Cov}(T,T), r1, 2)/G \\
\text{Cov}(5,2) &= - \text{DF}(\text{Cov}(T,T), r1, 2, r2) \\
\text{Cov}(5,3) &= - \text{DF}(\text{Cov}(T,T), r1, 2, r2) - 2*\text{DF}(\text{Cov}(T,T), r1, 2)/r2 \\
\text{Cov}(5,4) &= - \text{DF}(\text{Cov}(T,T), r1, 2, r2, 2) - 2*\text{DF}(\text{Cov}(T,T), r1, 2, r2)/r2 \\
\text{Cov}(5,5) &= + \text{DF}(\text{Cov}(T,T), r1, 2, r2, 2) \\
\text{Cov}(5,6) &= - \text{DF}(\text{Cov}(T,T), r1, 2, p2)/(G*R) \\
\text{Cov}(5,7) &= - \text{DF}(\text{Cov}(T,T), r1, 2, l2)/(G*R*\cos(p2)) \\
\text{Cov}(5,8) &= - \text{DF}(\text{Cov}(T,T), r1, 2, r2)*\text{DIRAC}(r2 - R')/(4*Pi*k)
\end{aligned}$$

$$\begin{aligned}
\text{Cov}(6,1) &= - \text{DF}(\text{Cov}(T,T), p1)/(G^2 *R) \\
\text{Cov}(6,2) &= \text{DF}(\text{Cov}(T,T), p1, r2)/(G*R) \\
\text{Cov}(6,3) &= (\text{DF}(\text{Cov}(T,T), p1, r2) + 2*\text{DF}(\text{Cov}(T,T), p1)/r2)/(G*R) \\
\text{Cov}(6,4) &= (\text{DF}(\text{Cov}(T,T), p1, r2, 2) + 2*\text{DF}(\text{Cov}(T,T), p1, r2)/r2)/(G*R) \\
\text{Cov}(6,5) &= - \text{DF}(\text{Cov}(T,T), p1, r2, 2)/(G*R) \\
\text{Cov}(6,6) &= \text{DF}(\text{Cov}(T,T), p1, p2)/(G^2 *R^2) \\
\text{Cov}(6,7) &= \text{DF}(\text{Cov}(T,T), p1, l2)/(G^2 *R^2 *\cos(p2)) \\
\text{Cov}(6,8) &= \text{DF}(\text{Cov}(T,T), p1, r2)*\text{DIRAC}(r2 - R')/(4*Pi*k*G*R)
\end{aligned}$$

$$\begin{aligned}
\text{Cov}(7,1) &= - \text{DF}(\text{Cov}(T,T), l1)/(G^2 *R*\cos(p1)) \\
\text{Cov}(7,2) &= \text{DF}(\text{Cov}(T,T), l1, r2)/(G*R*\cos(p1)) \\
\text{Cov}(7,3) &= (\text{DF}(\text{Cov}(T,T), l1, r2) + 2*\text{DF}(\text{Cov}(T,T), l1)/r2)/(G*R*\cos(p1)) \\
\text{Cov}(7,4) &= (\text{DF}(\text{Cov}(T,T), l1, r2, 2) + 2*\text{DF}(\text{Cov}(T,T), l1, r2)/r2)/(G*R*\cos(p1)) \\
\text{Cov}(7,5) &= - \text{DF}(\text{Cov}(T,T), l1, r2, 2)/(G*R*\cos(p1)) \\
\text{Cov}(7,6) &= \text{DF}(\text{Cov}(T,T), l1, p2)/(G^2 *R^2 *\cos(p1)) \\
\text{Cov}(7,7) &= \text{DF}(\text{Cov}(T,T), l1, l2)/(G^2 *R^2 *\cos(p1)*\cos(p2)) \\
\text{Cov}(7,8) &= \text{DF}(\text{Cov}(T,T), l1, r2)*\text{DIRAC}(r2 - R')/(4*Pi*k*G*R*\cos(p1))
\end{aligned}$$

$$\begin{aligned}
\text{Cov}(8,1) &= - \text{DF}(\text{Cov}(T,T),r1) * \text{DIRAC}(r1 - R') / (4 * \text{Pi} * k * G) \\
\text{Cov}(8,2) &= \text{DF}(\text{Cov}(T,T),r1,r2) * \text{DIRAC}(r1 - R') / (4 * \text{Pi} * k) \\
\text{Cov}(8,3) &= \text{DIRAC}(r1 - R') * (\text{DF}(\text{Cov}(T,T),r1,r2) + 2 * \text{DF}(\text{Cov}(T,T),r1) / r2) / (4 * \text{Pi} * k) \\
\text{Cov}(8,4) &= \text{DIRAC}(r1 - R') * (\text{DF}(\text{Cov}(T,T),r1,r2,2) + 2 * \text{DF}(\text{Cov}(T,T),r1,r2) / r2) / \\
&\quad (4 * \text{Pi} * k) \\
\text{Cov}(8,5) &= - \text{DF}(\text{Cov}(T,T),r1,r2,2) * \text{DIRAC}(r1 - R') / (4 * \text{Pi} * k) \\
\text{Cov}(8,6) &= \text{DF}(\text{Cov}(T,T),r1,p2) * \text{DIRAC}(r1 - R') / (4 * \text{Pi} * k * G * R) \\
\text{Cov}(8,7) &= \text{DF}(\text{Cov}(T,T),r1,l2) * \text{DIRAC}(r1 - R') / (4 * \text{Pi} * k * G * R * \cos(p2)) \\
\text{Cov}(8,8) &= \text{DF}(\text{Cov}(T,T),r1,r2) * \text{DIRAC}(r1 - R') * \text{DIRAC}(r2 - R') / (16 * \text{Pi} * k^2)
\end{aligned}$$

To get the derivatives of the autocovariance function $\text{Cov}(T,T)$ of the disturbing potential, first the derivatives of the expressions B, C and Psi have to be computed. This was also done by means of REDUCE:

Derivatives of $B = r1^2 * r2^2 - (R-D)^4$:

$$\text{DF}(B,r2) = 2 * r1^2 * r2$$

$$\text{DF}(B,r2,2) = 2 * r1^2$$

$$\text{DF}(B,r1) = 2 * r1 * r2^2$$

$$\text{DF}(B,r1,r2) = 4 * r1 * r2$$

$$\text{DF}(B,r1,r2,2) = 4 * r1$$

$$\text{DF}(B,r1,2) = 2 * r2^2$$

$$\text{DF}(B,r1,2,r2) = 4 * r2$$

$$\text{DF}(B,r1,2,r2,2) = 4$$

Derivatives of Psi :

$$\cos(\Psi) = \sin(p_1) * \sin(p_2) + \cos(p_1) * \cos(p_2) * \cos(l_2 - l_1)$$

$$DF(\Psi, p_2) = (- \sin(p_1) * \cos(p_2) + \sin(p_2) * \cos(l_1 - l_2) * \cos(p_1)) / \sin(\Psi)$$

$$DF(\Psi, l_2) = - \sin(l_1 - l_2) * \cos(p_1) * \cos(p_2) / \sin(\Psi)$$

$$DF(\Psi, p_1) = (\sin(p_1) * \cos(l_1 - l_2) * \cos(p_2) - \sin(p_2) * \cos(p_1)) / \sin(\Psi)$$

$$DF(\Psi, p_1, p_2) = (\cos(\Psi) * (\sin(p_1)^2 * \cos(l_1 - l_2) * \cos(p_2)^2 - \sin(p_1) * \sin(p_2) * \cos(l_1 - l_2) * \cos(p_1) * \cos(p_2)^2 - \sin(p_1) * \sin(p_2) * \cos(p_1) * \cos(p_2) + \sin(p_2)^2 * \cos(l_1 - l_2) * \cos(p_1)^2) - \sin(\Psi)^2 * (\sin(p_1) * \sin(p_2) * \cos(l_1 - l_2) + \cos(p_1) * \cos(p_2))) / \sin(\Psi)^3$$

$$DF(\Psi, p_1, l_2) = (\cos(\Psi) * \sin(l_1 - l_2) * \cos(p_1) * \cos(p_2) * (\sin(p_1) * \cos(l_1 - l_2) * \cos(p_2) - \sin(p_2) * \cos(p_1)) + \sin(\Psi)^2 * \sin(l_1 - l_2) * \sin(p_1) * \cos(p_2)) / \sin(\Psi)^3$$

$$DF(\Psi, l_1) = \sin(l_1 - l_2) * \cos(p_1) * \cos(p_2) / \sin(\Psi)$$

$$DF(\Psi, l_1, p_2) = (\cos(\Psi) * \sin(l_1 - l_2) * \cos(p_1) * \cos(p_2) * (\sin(p_1) * \cos(p_2) - \sin(p_2) * \cos(l_1 - l_2) * \cos(p_1)) - \sin(\Psi)^2 * \sin(l_1 - l_2) * \sin(p_2) * \cos(p_1)) / \sin(\Psi)^3$$

$$DF(\Psi, l_1, l_2) = (\cos(\Psi) * \sin(l_1 - l_2) * \cos(p_1)^2 * \cos(p_2)^2 - \sin(\Psi)^2 * \cos(l_1 - l_2) * \cos(p_1) * \cos(p_2)) / \sin(\Psi)^3$$

Derivatives of $C = r_1^2 * r_2^2 + (R-D)^4 - 2*r_1*r_2*(R-D)^2 * \cos(\Psi) :$

$$DF(C, p2) = 2*DF(\Psi, p2)*\sin(\Psi)*r_1*r_2*(R-D)^2$$

$$DF(C, l2) = 2*DF(\Psi, l2)*\sin(\Psi)*r_1*r_2*(R-D)^2$$

$$DF(C, r2) = - 2*\cos(\Psi)*r_1*(R-D)^2 + 2*r_1^2 * r_2^2$$

$$DF(C, r2, 2) = 2*r_1^2$$

$$DF(C, p1) = 2*DF(\Psi, p1)*\sin(\Psi)*r_1*r_2*(R-D)^2$$

$$DF(C, p1, p2) = 2*\cos(\Psi)*DF(\Psi, p1)*DF(\Psi, p2)*r_1*r_2*(R-D)^2$$

$$+ 2*DF(\Psi, p1, p2)*\sin(\Psi)*r_1*r_2*(R-D)^2$$

$$DF(C, p1, l2) = 2*\cos(\Psi)*DF(\Psi, p1)*DF(\Psi, l2)*r_1*r_2*(R-D)^2$$

$$+ 2*DF(\Psi, p1, l2)*\sin(\Psi)*r_1*r_2*(R-D)^2$$

$$DF(C, p1, r2) = 2*DF(\Psi, p1)*\sin(\Psi)*r_1*(R-D)^2$$

$$DF(C, p1, r2, 2) = 0$$

$$DF(C, l1) = 2*DF(\Psi, l1)*\sin(\Psi)*r_1*r_2*(R-D)^2$$

$$DF(C, l1, p2) = 2*\cos(\Psi)*DF(\Psi, l1)*DF(\Psi, p2)*r_1*r_2*(R-D)^2$$

$$+ 2*DF(\Psi, l1, p2)*\sin(\Psi)*r_1*r_2*(R-D)^2$$

$$DF(C, l1, l2) = 2*\cos(\Psi)*DF(\Psi, l1)*DF(\Psi, l2)*r_1*r_2*(R-D)^2$$

$$+ 2*DF(\Psi, l1, l2)*\sin(\Psi)*r_1*r_2*(R-D)^2$$

$$DF(C, l1, r2) = 2*DF(Psi, l1)*sin(Psi)*r1*(R-D)^2$$

$$DF(C, l1, r2, 2) = 0$$

$$DF(C, r1) = - 2*cos(Psi)*r2*(R-D)^2 + 2*r1*r2^2$$

$$DF(C, r1, p2) = 2*DF(Psi, p2)*sin(Psi)*r2*(R-D)^2$$

$$DF(C, r1, l2) = 2*DF(Psi, l2)*sin(Psi)*r2*(R-D)^2$$

$$DF(C, r1, r2) = - 2*cos(Psi)*(R-D)^2 + 4*r1*r2$$

$$DF(C, r1, r2, 2) = 4*r1$$

$$DF(C, r1, 2) = 2*r2^2$$

$$DF(C, r1, 2, p2) = 0$$

$$DF(C, r1, 2, l2) = 0$$

$$DF(C, r1, 2, r2) = 4*r2$$

$$DF(C, r1, 2, r2, 2) = 4$$

Derivatives of Cov(T,T) :

$$DF(Cov(T,T), p2) = - 3*DF(C, p2)*A*B*Co(T)/(2*C^{5/2})$$

$$DF(Cov(T,T), l2) = - 3*DF(C, l2)*A*B*Co(T)/(2*C^{5/2})$$

$$DF(Cov(T,T), r2) = A*Co(T)*(2*DF(B, r2)*C - 3*DF(C, r2)*B)/(2*C^{5/2})$$

$$DF(Cov(T,T), r2, 2) = A*Co(T)*(4*DF(B, r2, 2)*C^2 - 12*DF(B, r2)*DF(C, r2)*C - 6*DF(C, r2, 2)*B*C + 15*DF(C, r2)^2*B)/(4*C^{7/2})$$

$$\begin{aligned}
DF(\text{Cov}(T,T),p1) &= - 3*DF(C,p1)*A*B*Co(T)/(2*C^{5/2}) \\
DF(\text{Cov}(T,T),p1,p2) &= 3*A*B*Co(T)*(- 2*DF(C,p1,p2)*C + 5*DF(C,p1)*DF(C,p2))/(4*C^{7/2}) \\
DF(\text{Cov}(T,T),p1,12) &= 3*A*B*Co(T)*(- 2*DF(C,p1,12)*C + 5*DF(C,p1)*DF(C,12))/(4*C^{7/2}) \\
DF(\text{Cov}(T,T),p1,r2) &= 3*A*Co(T)*(- 2*DF(B,r2)*DF(C,p1)*C - 2*DF(C,p1,r2)*B*C \\
&\quad + 5*DF(C,p1)*DF(C,r2)*B)/(4*C^{7/2}) \\
DF(\text{Cov}(T,T),p1,r2,2) &= 3*A*Co(T) \\
&\quad *(- 4*DF(B,r2,2)*DF(C,p1)*C^2 - 8*DF(B,r2)*DF(C,p1,r2)*C^2 \\
&\quad + 20*DF(B,r2)*DF(C,p1)*DF(C,r2)*C - 4*DF(C,p1,r2,2)*B*C^2 \\
&\quad + 20*DF(C,p1,r2)*DF(C,r2)*B*C \\
&\quad + 10*DF(C,p1)*DF(C,r2,2)*B*C - 35*DF(C,p1)*DF(C,r2)^2*B) \\
&\quad / (8*C^{9/2})
\end{aligned}$$

$$\begin{aligned}
DF(\text{Cov}(T,T),11) &= - 3*DF(C,11)*A*B*Co(T)/(2*C^{5/2}) \\
DF(\text{Cov}(T,T),11,p2) &= 3*A*B*Co(T) \\
&\quad *(- 2*DF(C,11,p2)*C + 5*DF(C,11)*DF(C,p2))/(4*C^{7/2}) \\
DF(\text{Cov}(T,T),11,12) &= 3*A*B*Co(T) \\
&\quad *(- 2*DF(C,11,12)*C + 5*DF(C,11)*DF(C,12))/(4*C^{7/2}) \\
DF(\text{Cov}(T,T),11,r2) &= 3*A*Co(T)*(- 2*DF(B,r2)*DF(C,11)*C \\
&\quad - 2*DF(C,11,r2)*B*C + 5*DF(C,11)*DF(C,r2)*B)/(4*C^{7/2}) \\
DF(\text{Cov}(T,T),11,r2,2) &= 3*A*Co(T) \\
&\quad *(- 4*DF(B,r2,2)*DF(C,11)*C^2 - 8*DF(B,r2)*DF(C,11,r2)*C^2 \\
&\quad - 4*DF(C,11,r2,2)*B*C^2 + 20*DF(C,11,r2)*DF(C,r2)*B*C \\
&\quad + 10*DF(C,11)*DF(C,r2,2)*B*C - 35*DF(C,11)*DF(C,r2)^2*B \\
&\quad + 20*DF(B,r2)*DF(C,11)*DF(C,r2)*C)/(8*C^{9/2})
\end{aligned}$$

$$DF(\text{Cov}(T,T),r1) = A*Co(T)*(2*DF(B,r1)*C - 3*DF(C,r1)*B)/(2*C^{5/2})$$

$$DF(\text{Cov}(T,T),r1,p2) = 3*A*Co(T)*(-2*DF(B,r1)*DF(C,p2)*C - 2*DF(C,r1,p2)*B*C + 5*DF(C,r1)*DF(C,p2)*B)/(4*C^{7/2})$$

$$DF(\text{Cov}(T,T),r1,12) = 3*A*Co(T)*(-2*DF(B,r1)*DF(C,12)*C - 2*DF(C,r1,12)*B*C + 5*DF(C,r1)*DF(C,12)*B)/(4*C^{7/2})$$

$$DF(\text{Cov}(T,T),r1,r2) = A*Co(T) * (4*DF(B,r1,r2)*C^2 - 6*DF(B,r1)*DF(C,r2)*C - 6*DF(B,r2)*DF(C,r1)*C - 6*DF(C,r1,r2)*B*C + 15*DF(C,r1)*DF(C,r2)*B)/(4*C^{7/2})$$

$$DF(\text{Cov}(T,T),r1,r2,2) = A*Co(T) * (8*DF(B,r1,r2,2)*C^3 - 24*DF(B,r1,r2)*DF(C,r2)*C^2 - 12*DF(B,r1)*DF(C,r2,2)*C^2 + 30*DF(B,r1)*DF(C,r2)^2 *C - 12*DF(B,r2,2)*DF(C,r1)*C^2 - 24*DF(B,r2)*DF(C,r1,r2)*C^2 + 60*DF(B,r2)*DF(C,r1)*DF(C,r2)*C - 12*DF(C,r1,r2,2)*B*C^2 + 60*DF(C,r1,r2)*DF(C,r2)*B*C + 30*DF(C,r1)*DF(C,r2,2)*B*C - 105*DF(C,r1)*DF(C,r2)^2 *B)/(8*C^{9/2})$$

$$DF(\text{Cov}(T,T),r1,2) = A*Co(T)*(4*DF(B,r1,2)*C^2 - 12*DF(B,r1)*DF(C,r1)*C - 6*DF(C,r1,2)*B*C + 15*DF(C,r1)^2 *B)/(4*C^{7/2})$$

$$\begin{aligned}
& DF(\text{Cov}(T,T), r1, 2, p2) - 3*A*Co(T) \\
& \quad * (- 4*DF(B, r1, 2)*DF(C, p2)*C^2 - 8*DF(B, r1)*DF(C, r1, p2)*C^2 \\
& \quad + 20*DF(B, r1)*DF(C, r1)*DF(C, p2)*C \\
& \quad + 20*DF(C, r1, p2)*DF(C, r1)*B*C - 4*DF(C, r1, 2, p2)*B*C^2 \\
& \quad + 10*DF(C, r1, 2)*DF(C, p2)*B*C - 35*DF(C, r1)^2 *DF(C, p2)*B) \\
& \quad / (8*C^{9/2})
\end{aligned}$$

$$\begin{aligned}
& DF(\text{Cov}(T,T), r1, 2, 12) - 3*A*Co(T) \\
& \quad * (- 4*DF(B, r1, 2)*DF(C, 12)*C^2 - 8*DF(B, r1)*DF(C, r1, 12)*C^2 \\
& \quad + 20*DF(B, r1)*DF(C, r1)*DF(C, 12)*C \\
& \quad + 20*DF(C, r1, 12)*DF(C, r1)*B*C - 4*DF(C, r1, 2, 12)*B*C^2 \\
& \quad + 10*DF(C, r1, 2)*DF(C, 12)*B*C - 35*DF(C, r1)^2 *DF(C, 12)*B) \\
& \quad / (8*C^{9/2})
\end{aligned}$$

$$\begin{aligned}
& DF(\text{Cov}(T,T), r1, 2, r2) - A*Co(T) \\
& \quad * (- 24*DF(B, r1, r2)*DF(C, r1)*C^2 + 8*DF(B, r1, 2, r2)*C^3 \\
& \quad - 12*DF(B, r1, 2)*DF(C, r2)*C^2 - 24*DF(B, r1)*DF(C, r1, r2)*C^2 \\
& \quad + 60*DF(B, r1)*DF(C, r1)*DF(C, r2)*C \\
& \quad - 12*DF(B, r2)*DF(C, r1, 2)*C^2 + 30*DF(B, r2)*DF(C, r1)^2 *C \\
& \quad + 60*DF(C, r1, r2)*DF(C, r1)*B*C - 12*DF(C, r1, 2, r2)*B*C^2 \\
& \quad + 30*DF(C, r1, 2)*DF(C, r2)*B*C - 105*DF(C, r1)^2 *DF(C, r2)*B) \\
& \quad / (8*C^{9/2})
\end{aligned}$$

$$DF(\text{Cov}(T,T), r1, 2, r2, 2) - A*Co(T)$$

$$\begin{aligned}
 & * (- 48*DF(B, r1, r2, 2)*DF(C, r1)*C^3 \\
 & - 96*DF(B, r1, r2)*DF(C, r1, r2)*C^3 \\
 & + 240*DF(B, r1, r2)*DF(C, r1)*DF(C, r2)*C^2 \\
 & + 16*DF(B, r1, 2, r2, 2)*C^4 \\
 & - 48*DF(B, r1, 2, r2)*DF(C, r2)*C^3 \\
 & - 24*DF(B, r1, 2)*DF(C, r2, 2)*C^3 \\
 & + 60*DF(B, r1, 2)*DF(C, r2)^2 *C^2 \\
 & - 48*DF(B, r1)*DF(C, r1, r2, 2)*C^3 \\
 & + 240*DF(B, r1)*DF(C, r1, r2)*DF(C, r2)*C^2 \\
 & + 120*DF(B, r1)*DF(C, r1)*DF(C, r2, 2)*C^2 \\
 & - 420*DF(B, r1)*DF(C, r1)*DF(C, r2)^2 *C^2 \\
 & - 24*DF(B, r2, 2)*DF(C, r1, 2)*C^3 \\
 & + 60*DF(B, r2, 2)*DF(C, r1)^2 *C^2 \\
 & + 240*DF(B, r2)*DF(C, r1, r2)*DF(C, r1)*C^2 \\
 & - 48*DF(B, r2)*DF(C, r1, 2, r2)*C^3 \\
 & + 120*DF(B, r2)*DF(C, r1, 2)*DF(C, r2)*C^2 \\
 & - 420*DF(B, r2)*DF(C, r1)^2 *DF(C, r2)*C^2 \\
 & + 120*DF(C, r1, r2, 2)*DF(C, r1)*B*C^2 \\
 & + 120*DF(C, r1, r2)^2 *B*C^2 \\
 & - 840*DF(C, r1, r2)*DF(C, r1)*DF(C, r2)*B*C^3 \\
 & - 24*DF(C, r1, 2, r2, 2)*B*C^3 \\
 & + 120*DF(C, r1, 2, r2)*DF(C, r2)*B*C^2 \\
 & + 60*DF(C, r1, 2)*DF(C, r2, 2)*B*C^2 \\
 & - 210*DF(C, r1, 2)*DF(C, r2)^2 *B*C^2 \\
 & - 210*DF(C, r1)^2 *DF(C, r2, 2)*B*C^2 \\
 & + 945*DF(C, r1)^2 *DF(C, r2)^2 *B)
 \end{aligned}$$

$$\begin{aligned}
 & \frac{11}{2} \\
 & / (16 * C^2)
 \end{aligned}$$

Asymptotic relations (flat earth model)

For local applications the asymptotic form (6-21) is used for the autocovariance function of the disturbing potential

$$\text{Cov}(T,T)(r_1,r_2,\text{Psi}) = 4 D \frac{A}{B^{3/2}} \text{Co}(T) ,$$

with

$$A = 2D + z_1 + z_2$$

$$B = S^2 + A$$

$$S^2 = U^2 + V^2$$

$$U = x_2 - x_1$$

$$V = y_2 - y_1 .$$

For the functionals of the gravity field in P we get the following asymptotic forms

- | | |
|--|---|
| 1) geoidal height | $N_1 = T_1/G$ |
| 2) gravity disturbance | $d g_1 = - DF(T_1, z_1)$ |
| 3) gravity anomaly | $D g_1 = - DF(T_1, z_1)$ |
| 4) radial gravity gradient | $= - DF(T_1, z_1, 2)$ |
| 5) second radial derivative of T | $= + DF(T_1, z_1, 2)$ |
| 6) N-S-component of the deflection of the vertical | $X_{11} = - DF(T_1, x_1)/G$ |
| 7) E-W-component of the deflection of the vertical | $E_{11} = - DF(T_1, y_1)/G$ |
| 8) density contrast | $d \rho = - DF(T_1, z_1) * \text{DIRAC}(z_1) / (4 * \pi * k)$ |

To get the functionals in Q substitute T_1, x_1, y_1, z_1 by T_2, x_2, y_2, z_2 .

Noteworthy is that the covariances of the gravity disturbance and the gravity anomaly become identical.

The covariances between the functionals are

$$\begin{aligned}
 \text{Cov}(1,1) &= + \text{Cov}(T,T) / G^2 \\
 \text{Cov}(1,2) &= - \text{DF}(\text{Cov}(T,T), z2) / G \\
 \text{Cov}(1,3) &= - \text{DF}(\text{Cov}(T,T), z2) / G \\
 \text{Cov}(1,4) &= - \text{DF}(\text{Cov}(T,T), z2, 2) / G \\
 \text{Cov}(1,5) &= + \text{DF}(\text{Cov}(T,T), z2, 2) / G \\
 \text{Cov}(1,6) &= - \text{DF}(\text{Cov}(T,T), x2) / G^2 \\
 \text{Cov}(1,7) &= - \text{DF}(\text{Cov}(T,T), y2) / G^2 \\
 \text{Cov}(1,8) &= - \text{DF}(\text{Cov}(T,T), z2) * \text{DIRAC}(z2) / (4*\text{Pi}*k*G) \\
 \\
 \text{Cov}(2,1) &= - \text{DF}(\text{Cov}(T,T), z1) / G \\
 \text{Cov}(2,2) &= + \text{DF}(\text{Cov}(T,T), z1, z2) \\
 \text{Cov}(2,3) &= + \text{DF}(\text{Cov}(T,T), z1, z2) \\
 \text{Cov}(2,4) &= + \text{DF}(\text{Cov}(T,T), z1, z2, 2) \\
 \text{Cov}(2,5) &= - \text{DF}(\text{Cov}(T,T), z1, z2, 2) \\
 \text{Cov}(2,6) &= + \text{DF}(\text{Cov}(T,T), x2, z1) / G \\
 \text{Cov}(2,7) &= + \text{DF}(\text{Cov}(T,T), y2, z1) / G \\
 \text{Cov}(2,8) &= + \text{DF}(\text{Cov}(T,T), z1, z2) * \text{DIRAC}(z2) / (4*\text{Pi}*k) \\
 \\
 \text{Cov}(3,1) &= - \text{DF}(\text{Cov}(T,T), z1) / G \\
 \text{Cov}(3,2) &= + \text{DF}(\text{Cov}(T,T), z1, z2) \\
 \text{Cov}(3,3) &= + \text{DF}(\text{Cov}(T,T), z1, z2) \\
 \text{Cov}(3,4) &= + \text{DF}(\text{Cov}(T,T), z1, z2, 2) \\
 \text{Cov}(3,5) &= - \text{DF}(\text{Cov}(T,T), z1, z2, 2) \\
 \text{Cov}(3,6) &= + \text{DF}(\text{Cov}(T,T), x2, z1) / G \\
 \text{Cov}(3,7) &= + \text{DF}(\text{Cov}(T,T), y2, z1) / G \\
 \text{Cov}(3,8) &= + \text{DF}(\text{Cov}(T,T), z1, z2) * \text{DIRAC}(z2) / (4*\text{Pi}*k)
 \end{aligned}$$

$$\begin{aligned}
\text{Cov}(4,1) &= - \text{DF}(\text{Cov}(T,T),z1,2) / G \\
\text{Cov}(4,2) &= + \text{DF}(\text{Cov}(T,T),z1,2,z2) \\
\text{Cov}(4,3) &= + \text{DF}(\text{Cov}(T,T),z1,2,z2) \\
\text{Cov}(4,4) &= + \text{DF}(\text{Cov}(T,T),z1,2,z2,2) \\
\text{Cov}(4,5) &= - \text{DF}(\text{Cov}(T,T),z1,2,z2,2) \\
\text{Cov}(4,6) &= + \text{DF}(\text{Cov}(T,T),x2,z1,2) / G \\
\text{Cov}(4,7) &= + \text{DF}(\text{Cov}(T,T),y2,z1,2) / G \\
\text{Cov}(4,8) &= + \text{DF}(\text{Cov}(T,T),z1,2,z2) * \text{DIRAC}(z2) / (4*\text{Pi}*k)
\end{aligned}$$

$$\begin{aligned}
\text{Cov}(5,1) &= + \text{DF}(\text{Cov}(T,T),z1,2) / G \\
\text{Cov}(5,2) &= - \text{DF}(\text{Cov}(T,T),z1,2,z2) \\
\text{Cov}(5,3) &= - \text{DF}(\text{Cov}(T,T),z1,2,z2) \\
\text{Cov}(5,4) &= - \text{DF}(\text{Cov}(T,T),z1,2,z2,2) \\
\text{Cov}(5,5) &= + \text{DF}(\text{Cov}(T,T),z1,2,z2,2) \\
\text{Cov}(5,6) &= - \text{DF}(\text{Cov}(T,T),x2,z1,2) / G \\
\text{Cov}(5,7) &= - \text{DF}(\text{Cov}(T,T),y2,z1,2) / G \\
\text{Cov}(5,8) &= - \text{DF}(\text{Cov}(T,T),z1,2,z2) * \text{DIRAC}(z2) / (4*\text{Pi}*k)
\end{aligned}$$

$$\begin{aligned}
\text{Cov}(6,1) &= - \text{DF}(\text{Cov}(T,T),x1) / G^2 \\
\text{Cov}(6,2) &= + \text{DF}(\text{Cov}(T,T),x1,z2) / G \\
\text{Cov}(6,3) &= + \text{DF}(\text{Cov}(T,T),x1,z2) / G \\
\text{Cov}(6,4) &= + \text{DF}(\text{Cov}(T,T),x1,z2,2) / G \\
\text{Cov}(6,5) &= - \text{DF}(\text{Cov}(T,T),x1,z2,2) / G \\
\text{Cov}(6,6) &= + \text{DF}(\text{Cov}(T,T),x1,x2) / G^2 \\
\text{Cov}(6,7) &= + \text{DF}(\text{Cov}(T,T),x1,y2) / G^2 \\
\text{Cov}(6,8) &= + \text{DF}(\text{Cov}(T,T),x1,z2) * \text{DIRAC}(z2) / (4*\text{Pi}*k*G)
\end{aligned}$$

$$\begin{aligned}
\text{Cov}(7,1) &= - \text{DF}(\text{Cov}(T,T),y1) / G^2 \\
\text{Cov}(7,2) &= + \text{DF}(\text{Cov}(T,T),y1,z2) / G \\
\text{Cov}(7,3) &= + \text{DF}(\text{Cov}(T,T),y1,z2) / G \\
\text{Cov}(7,4) &= + \text{DF}(\text{Cov}(T,T),y1,z2,2) / G \\
\text{Cov}(7,5) &= - \text{DF}(\text{Cov}(T,T),y1,z2,2) / G \\
\text{Cov}(7,6) &= + \text{DF}(\text{Cov}(T,T),x2,y1) / G^2 \\
\text{Cov}(7,7) &= + \text{DF}(\text{Cov}(T,T),y1,y2) / G^2 \\
\text{Cov}(7,8) &= + \text{DF}(\text{Cov}(T,T),y1,z2) * \text{DIRAC}(z2) / (4*\text{Pi}*k*G)
\end{aligned}$$

$$\begin{aligned}
\text{Cov}(8,1) &= - \text{DF}(\text{Cov}(T,T),z1) * \text{DIRAC}(z1) / (4*\text{Pi}*k*G) \\
\text{Cov}(8,2) &= + \text{DF}(\text{Cov}(T,T),z1,z2) * \text{DIRAC}(z1) / (4*\text{Pi}*k) \\
\text{Cov}(8,3) &= + \text{DF}(\text{Cov}(T,T),z1,z2) * \text{DIRAC}(z1) / (4*\text{Pi}*k) \\
\text{Cov}(8,4) &= + \text{DF}(\text{Cov}(T,T),z1,z2,2) * \text{DIRAC}(z1) / (4*\text{Pi}*k) \\
\text{Cov}(8,5) &= - \text{DF}(\text{Cov}(T,T),z1,z2,2) * \text{DIRAC}(z1) / (4*\text{Pi}*k) \\
\text{Cov}(8,6) &= + \text{DF}(\text{Cov}(T,T),x2,z1) * \text{DIRAC}(z1) / (4*\text{Pi}*k*G) \\
\text{Cov}(8,7) &= + \text{DF}(\text{Cov}(T,T),y2,z1) * \text{DIRAC}(z1) / (4*\text{Pi}*k*G) \\
\text{Cov}(8,8) &= + \text{DF}(\text{Cov}(T,T),z1,z2) * \text{DIRAC}(z1) * \text{DIRAC}(z2) / (16*\text{Pi}^2 * k^2)
\end{aligned}$$

In this case the derivatives of the autocovariance function Cov(T,T) of the disturbing potential can be given directly as

$$\begin{aligned}
\text{DF}(\text{Cov}(T,T),x2) &= - 12*D^2 * \text{Co}(T) * A * U / B^{5/2} \\
\text{DF}(\text{Cov}(T,T),y2) &= - 12*D^2 * \text{Co}(T) * A * V / B^{5/2} \\
\text{DF}(\text{Cov}(T,T),z2) &= 4*D^2 * \text{Co}(T) * (- 3*A^2 + B) / B^{5/2} \\
\text{DF}(\text{Cov}(T,T),z2,2) &= 12*D^2 * \text{Co}(T) * A * (5*A^2 - 3*B) / B^{7/2}
\end{aligned}$$

$$DF(\text{Cov}(T,T),x1) = 12 * D^2 * \text{Co}(T) * A * U / B^{5/2}$$

$$DF(\text{Cov}(T,T),x1,x2) = 12 * D^2 * \text{Co}(T) * A * (B - 5 * U^2) / B^{7/2}$$

$$DF(\text{Cov}(T,T),x1,y2) = - 60 * D^2 * \text{Co}(T) * A * U * V / B^{7/2}$$

$$DF(\text{Cov}(T,T),x1,z2) = 12 * D^2 * \text{Co}(T) * U * (- 5 * A^2 + B) / B^{7/2}$$

$$DF(\text{Cov}(T,T),x1,z2,2) = 60 * D^2 * \text{Co}(T) * A * U * (7 * A^2 - 3 * B) / B^{9/2}$$

$$DF(\text{Cov}(T,T),y1) = 12 * D^2 * \text{Co}(T) * A * V / B^{5/2}$$

$$DF(\text{Cov}(T,T),y1,x2) = - 60 * D^2 * \text{Co}(T) * A * U * V / B^{7/2}$$

$$DF(\text{Cov}(T,T),y1,y2) = 12 * D^2 * \text{Co}(T) * A * (B - 5 * V^2) / B^{7/2}$$

$$DF(\text{Cov}(T,T),y1,z2) = 12 * D^2 * \text{Co}(T) * V * (- 5 * A^2 + B) / B^{7/2}$$

$$DF(\text{Cov}(T,T),y1,z2,2) = 60 * D^2 * \text{Co}(T) * A * V * (7 * A^2 - 3 * B) / B^{9/2}$$

$$DF(\text{Cov}(T,T),z1) = 4 * D^2 * \text{Co}(T) * (- 3 * A^2 + B) / B^{5/2}$$

$$DF(\text{Cov}(T,T),z1,x2) = 12 * D^2 * \text{Co}(T) * U * (5 * A^2 - B) / B^{7/2}$$

$$DF(\text{Cov}(T,T),z1,y2) = 12 * D^2 * \text{Co}(T) * V * (5 * A^2 - B) / B^{7/2}$$

$$DF(\text{Cov}(T,T),z1,z2) = 12 * D^2 * \text{Co}(T) * A * (5 * A^2 - 3 * B) / B^{7/2}$$

$$DF(\text{Cov}(T,T),z1,z2,2) = 12 * D^2 * \text{Co}(T) * (- 35 * A^4 + 30 * A^2 * B - 3 * B^2) / B^{9/2}$$

$$DF(\text{Cov}(T,T),z1,2) = 12 * D^2 * Co(T) * A * (5 * A^2 - 3 * B) / B^{7/2}$$

$$DF(\text{Cov}(T,T),z1,2,x2) = 60 * D^2 * Co(T) * A * U * (-7 * A^2 + 3 * B) / B^{9/2}$$

$$DF(\text{Cov}(T,T),z1,2,y2) = 60 * D^2 * Co(T) * A * V * (-7 * A^2 + 3 * B) / B^{9/2}$$

$$DF(\text{Cov}(T,T),z1,2,z2) = 12 * D^2 * Co(T) * (-35 * A^4 + 30 * A^2 * B - 3 * B^2) / B^{9/2}$$

$$DF(\text{Cov}(T,T),z1,2,z2,2) = 60 * D^2 * Co(T) * A * (63 * A^4 - 70 * A^2 * B + 15 * B^2) / B^{11/2}$$

REFERENCES

- AKI, K. (1973): *Scattering of P Waves Under the Montana Lasa*. J. Geophys. Res., Vol. 78, pp. 1334–1346.
- AKIMA, H. (1978): *A Method of Bivariate Interpolation and Smooth Surface Fitting for Irregularly Distributed Data Points*. ACM Trans. Math. Software, 4/2, pp. 148–159.
- ALPINE EXPLOSION SEISMOLOGY GROUP (Reporter: Miller, H.) (1976): *A Lithospheric Seismic Profile Along the Axis of the Alps 1975 I: First Results*. Pageoph. 114, pp. 1109–1130.
- ANDERSON, D.L. (1967): *A Seismic Equation of State*. Geoph. J. R. astr. Soc. 13, pp. 9–30.
- ANDERSON, D.L. (1970): *Velocity–Density Relations*. J. Geophys. Res. Vol. 75, pp. 1623–1624.
- ANDERSON, O.L. (1973): *Comments on the Power Law Representation of Birch's Law*. J. Geophys. Res., Vol. 78B, pp. 4901–4914.
- ANSORGE, J. (1968): *Die Struktur der Erdkruste an der Westflanke der Zone von Ivrea*. Schweiz. Mineral. Petrol. Mitteilungen 48/1, pp. 247–254.
- ANSORGE, J., S. MÜLLER, E. KISSLING, I. GUERRA, C. MORELLI, S. SCARASCIA (1979): *Crustal Section Across the Zone of Ivrea–Verbano From the Valais to the Lago Maggiore*. Bolletino di Geof. Theor. ed Appl. Vol XXI, No. 83, pp. 149–157.
- ARIC, K. (1987): *Geschwindigkeits–Tiefenfunktionen an diskreten Punkten und Mohotiefen in Österreich*. Private communication.
- BABUŠKA, V., J. PLOMEROVÁ, J. ŠÍLENÝ, M. BAER (1985): *Deep Structure of the Lithosphere and Seismicity of the Alps*. Symposium Czegiskivajia, June 17–26, 1985.
- BARAZANGI, M., L. BROWN (Eds., 1986): *Reflection Seismology: A Global Perspective*. Geodynamics Series Vol. 13, AGU Washington DC.
- BERCKHEMER, H. (1968): *Topographie des Ivrea–Körpers aus seismischen und gravimetrischen Daten*. Schweiz. Mineral. Petrol. Mitteilungen, 48/1, pp. 235–246.
- BIRCH, F. (1958): *Interpretation of the Seismic Structure of the Crust in the Light of Experimental Studies of Wave Velocities in Rocks*. In: Contributions in Geophysics 1, pp. 158–170, Pergamon Press, New York.
- BIRCH, F. (1960): *The Velocity of Compressional Waves in Rocks to 10 Kilobars, 1*. J. Geophys. Res., Vol. 65B, pp. 1083–1102.
- BIRCH, F. (1961): *The Velocity of Compressional Waves in Rocks to 10 Kilobars, 2*. J. Geophys. Res., Vol. 66B, pp. 2199–2224.
- BIRCH, F. (1979): *Density and Composition of the Upper Mantle: First Approximation as an Olivine Layer*. In: Hart (Ed.): The Earth's Crust and Upper Mantle, Geophys. Monograph No.13, pp. 18–36.
- BOTT, M.H.P. (1971): *The Interior of the Earth*. Edward Arnold, London.

- BRANDSTÄTTER, G. (1987): *The Role of Geodetic Astronomy in the Determination of the Austrian Geoid*. In: Sünkel, H. (Ed.): *The Gravity Field in Austria, Geodätische Arbeiten Österreichs für die Internationale Erdmessung, Neue Folge, Vol. IV*, Graz.
- BULLEN, K.E. (1975): *The Earth's Density*. Chapman & Hall, London.
- BUNTEBARTH, G. (1982): *Density and Seismic Velocity in Relation to Mineralogical Constitution Based on an Ionic Model for Minerals*. *Earth and Planetary Science Letters* 57, pp. 358–366.
- CAPON, J. (1974). *Characterization of Crust and Upper Mantle Structure Under Lasa as a Random Medium*. *Bull. Seism. Soc. Am.* 64, pp. 235–266.
- CASSINIS, R. (Ed., 1981): *The Solution of the Inverse Problem in Geophysical Interpretation*. Plenum Press, New York.
- ÇAĞSAK, H. (1988): *Ein FORTRAN Unterprogramm zur Berechnung von Geoid- und Schwereeffekt eines Tetraeders*. Personal communication.
- ČERMÁK, V. (1982): *Regional Pattern of Lithospheric Thickness in Europe*. In: Čermák, V., R. Hänel (Eds.) : *Geothermics and Geothermal Energy*, Schweizerbart'sche Verlagsbuchhandlung, Stuttgart, pp. 1–10.
- CHAPMAN, M.E. (1979): *Techniques for Interpretation of Geoid Anomalies*. *J. Geophys. Res.*, Vol. 84, No. B8, pp. 3793–3801.
- CHERNOV, L.A. (1960): *Wave Propagation in a Random Medium*. McGraw-Hill, New York.
- CLOSS, H., Y. LABROUSTE (Eds., 1963): *Recherches Seismologiques dans les Alpes Occidentales au Moyen de Grandes Explosions en 1956, 1956 et 1960*. *Année Geophysique International, Participation Française, Series XII, Fascicule 2, Seismologie, Centre National de la Recherches Scientifiques*.
- ČOLIĆ, K.N., N. VUČETIĆ, S. PETROVIĆ (1988): *The Geoid and the Mohorovičić Discontinuity*. *Proc. 6th Intern. Symposium "Geodesy and Physics of the Earth"*, Potsdam.
- DEBELMAS, J., A. ESCHER, R. TRUMPY (1983): *Profiles through the Western Alps*. In: Rast, Delany (Eds.): *Profiles of Orogenic Belts*, pp. 83–96.
- DEICHMANN, N., J. ANSORGE, S. MÜLLER (1986): *Crustal Structure of the Southern Alps beneath the Intersection with the European Geotraverse*. *Tectonophysics*, 126, pp. 57–83.
- De MARCHI, F. (1983): *Project RIMINI – Kurze Beschreibung der Datenbank und der Anwendungsprogramme*. Gruppe für Rüstungsdienste, Internal Report, Bern.
- DORMAN, L.M., B.T.R. LEWIS (1970): *Experimental Isostasy. 1. Theory of the Determination of the Earth's Isostatic Response to a Concentrated Load*. *J. Geophys. Res.*, Vol. 75, pp. 3357–3365.
- DRISLER, J., W.R. JACOBY (1983): *Gravity Anomaly and Density Distributions of the Rhenish Massif*. In: Fuchs, v. Gehlen, Mälzer, Murawski, Semmel (Eds): *Plateau Uplift, the Rhenish Shield – A Case History*. Springer Verlag, Berlin, Heidelberg, New York, Tokyo, pp. 366–380.

- DZIEWONSKI, A.M. (1984): *Mapping of the Lower Mantle: Determination of Lateral Heterogeneity in P Velocity up to Degree and Order 6*. J. Geophys. Res., Vol. 89, pp. 5929-5952.
- EEG, J., T. KRARUP (1973): *Integrated Geodesy*. The Danish Geodetic Institute, Internal Report No. 7, Copenhagen.
- EGLOFF, R. (1979): *Sprengseismische Untersuchungen der Erdkruste in der Schweiz*. Dissertation Nr. 6502, ETH Zürich, Switzerland.
- FINCKH, P., W. FREI, B. FULLER, R. JOHNSON, S. MÜLLER, S. SMITHSON, C. SPRECHER (1986): *Detailed Crustal Structure from a Seismic Reflection Survey in Northern Switzerland*. In: Barazangi, Brown (Eds.): *Reflection Seismology: A Global Perspective*. Geodynamics Series Vol. 13, AGU Washington DC, pp. 43-54.
- FLEITOUT, L., C. FROIDEVAUX (1982): *Tectonics and Topography for a Lithosphere Containing Density Heterogeneities*. Tectonics 1, pp. 21-56, American Geophysical Union.
- FORSBERG, R. (1984): *A Study of Terrain Reduction, Density Anomalies and Geophysical Inversion Methods in Gravity Field Modelling*. Reports of the Department of Geodetic Science and Surveying, No. 355, The Ohio State University, Columbus, OH. AFGL-TR-84-0174, ADA150788.
- FORSBERG, R., C.C. TSCHERNING (1981): *The Use of Height Data in Gravity Field Approximation by Collocation*. J. Geophys. Res., Vol. 86, No. B9, pp. 7843-7854.
- FOTIOU, A., E. LIVIERATOS, I.N. TZIAVOS (1988): *The GRS80 Combined Geoid for the Hellenic Area and Upper Crust Density Anomalies Corresponding to its High Frequency Representations*. Manuscripta geodaetica, Vol. 13, pp.267-274.
- GEISS, E. (1987): *Die Lithosphäre im mediterranen Raum – ein Beitrag zu Struktur, Schwerefeld und Deformation*. Deutsche Geodät. Kommission, Reihe C, Nr. 332, Bayerische Akademie der Wissenschaften, München.
- GIESE, P. (1968a): *Versuch einer Gliederung der Erdkruste im nördlichen Alpenvorland, in den Ostalpen und in Teilen der Westalpen mit Hilfe charakteristischer Refraktions-Laufzeit-Kurven sowie eine geologische Deutung*. Berliner Geowissenschaftliche Abhandlungen, Band I, Heft 2, Verlag Dietrich Reimer, Berlin.
- GIESE, P. (1968b): *Die Struktur der Erdkruste im Bereich der Ivrea-Zone*. Schweiz. Mineral. Petrol. Mitteilungen 48/1, pp. 262-284.
- GIESE, P. (1976): *Result of the Generalized Interpretation of Deep Seismic Sounding Data*. In: Giese, Prodehl, Stein (Eds.): *Explosion Seismology in Central Europe – Data and Results*, Springer Verlag, Berlin, Heidelberg, New York, pp. 201-214.
- GIESE P. (1985): *The Structure of the Upper Lithosphere between the Ligurian Sea and the Southern Alps*. Second EGT Workshop Venice Febr. 7-9, 1985, European Science Foundation, pp. 143-153.
- GIESE, P., R. NICOLICH (1981): *Explosion Seismic Crustal Studies in the Alpine Mediterranean Region and their Implications to Tectonic Processes*. In: Berckhemer, Hsü (Eds.): *Alpine Mediterranean Geodynamics*, Geodynamics Series Vol. 7, AGU Washington DC, pp. 39-70.

- GIESE, P., C. PRODEHL (1976): *Main Features of Crustal Structures in the Alps*. In: Giese, Prodehl, Stein (Eds): *Explosion Seismology in Central Europe - Data and Results*, Springer Verlag, Berlin, Heidelberg, New York, pp. 347-375.
- GIESE, P., K. J. REUTTER (1978): *Crustal and Structural Features of the Adria Microplate*. In: Closs, Roeder, Schmidt (Eds.): *Alps, Apennines, Hellenides, Schweizerbart'sche Verlagsbuchhandlung, Stuttgart*, pp. 565-588.
- GÖPFERT, W. (1977): *Interpolationsergebnisse mit der multiquadratischen Methode*. Zeitschr. f. Vermessungswesen, Vol. 102, pp. 457-460.
- GRAFAREND, E.W. (1989): *The Geoid and the Gravimetric Boundary Value Problem*. Rep. No. 18, Department of Geodesy, The Royal Institute of Technology, Stockholm.
- GURTNER, W. (1978): *Das Geoid in der Schweiz*. In: Schweizerische Geodätische Kommission (Eds.): *Astronomisch-geodätische Arbeiten in der Schweiz*, Vol. 32.
- HAITZMANN, H. (1983): *Ein digitales Höhenmodell von Österreich*. In: *Geodätische Arbeiten Österreichs für die Internationale Erdmessung, Neue Folge, Band III*, pp. 147-152.
- HEHL, K., G.W. HEIN (1988): *Computation of Density Anomalies within the Earth's Crust Using the Integrated Geodesy Approach*. Proceedings of the International Symposium on Instrumentation, Theory and Analyses for Integrated Geodesy, Sopron, Hungary, May 16-20, 1988.
- HEIN, G.W. (1986): *Integrated Geodesy. State-of-the-Art 1986 Reference Text*. In: Sünkel, H. (Ed.): *Mathematical and Numerical Techniques in Physical Geodesy, Lecture Notes in Earth Sciences*, Vol. 7, pp. 505-548, Springer-Verlag, Berlin, Heidelberg.
- HEIN, G.W., F. SANSONE, G. STRYKOWSKI, C.C. TSCHERNING (1988): *On the Choice of Norm and Base Functions for the Solution of the Inverse Gravimetric Problem*. Presented at the 17th Conference on Mathematical Geophysics, Blanes, Cataluna, Spain, June 1988.
- HEISKANEN, W.A., H. MORITZ (1967): *Physical Geodesy*. W.H. Freeman & Co., San Francisco.
- HELLER, W.G., S.K. JORDAN (1979): *Attenuated White Noise Statistical Gravity Model*. J. Geophys. Res., Vol. 84, pp. 4680-4688.
- ITALIAN EXPLOSION SEISMOLOGY GROUP (1981): *Crust and Upper Mantle Structures in the Southern Alps from Deep Seismic Sounding Profiles (1977, 1978) and Surface Wave Dispersion Analyses*. Bolletino Geof. Theor. ed Appl., Vol. XIII, No. 92, pp. 297-330.
- JACOBY, W.R. (1973): *Isostasie und Dichteverteilung in Kruste und oberem Mantel*. Zeitschr. f. Geophysik, Nr. 39, pp. 79-86.
- JACOBY, W.R. (1975): *Velocity-Density Systematics from Seismic and Gravity Data*. Veröff. Zentr. Institut Physik d. Erde, Nr. 31, pp. 323-333.
- JORDAN, S. (1978): *Statistical Model for Gravity, Topography, and Density Contrasts in the Earth*. J. Geophys. Res., Vol. 83, pp. 1816-1824.
- JORDAN, S.K., W.G. HELLER (1978): *Upward Continuation of Gravity Disturbance Covariance Functions*. J. Geophys. Res., Vol. 83, pp. 3382-3388.

- JUNG, K. (1961): *Schwerkraftverfahren in der angewandten Geophysik*. Geophysikalische Monographien, Band 2, Akademische Verlagsgesellschaft Geest & Portig KG, Leipzig.
- KAHLE, H.G., S. MÜLLER, E. KLINGELE, E. EGLOFF, E. KISSLING (1980): *Recent Dynamics, Crustal Structure and Gravity in the Alps*. In: Mörner (Ed.): *Earth's Rheology, Isostasy and Eustasy*, John Wiley & Sons, New York, pp. 377-388.
- KEARSLEY, A.K.W., M.G. SIDERIS, J. KRYNSKI, R. FORSBERG, K.-P. SCHWARZ (1985): *White Sands Revisited - A Comparison of Techniques to Predict Deflections of the Vertical*. Report 30007, Division of Surveying Engineering, University of Calgary.
- KHAN, M.A. (1977): *Depth of Sources of Gravity Anomalies*. Geophys. J. R. astr. Soc., Vol. 48, pp. 197-209.
- KHAN, M.A. (1982): *Geodynamical and Geodetic Consistency Tests of Earth Density Models*. Physics of the Earth and Planetary Interiors, Vol. 28, pp. 291-301.
- KISSLING, E. (1982): *Aufbau der Kruste und des oberen Mantels in der Schweiz*. In: Schweiz. Geodätische Kommission (Ed.): *Geodätische Arbeiten in der Schweiz*, Band 35, Schwereanomalien und isostatische Modelle in der Schweiz, pp. 42-126.
- KISSLING, E., S. MÜLLER, D. WERNER (1983): *Gravity Anomalies, Seismic Structure and Geothermal History in the Central Alps*. Ann. Geophys. 1/1, pp. 37-46.
- KLINGELE, E., E. KISSLING (1982): *Zum Konzept der isostatischen Modelle in Gebirgen am Beispiel der Schweizer Alpen*. In: Schweiz. Geodätische Kommission (Ed.): *Geodätische Arbeiten in der Schweiz*, Band 35, Schwereanomalien und isostatische Modelle in der Schweiz, pp. 3-36.
- KNOPOFF, L., J.A. HUDSON (1964): *Scattering of Elastic Waves by Small Inhomogeneities*. The Journal of the Acoustical Soc. Am., Vol. 36, pp. 338-343.
- KNOPOFF, L., S. MUELLER, L. PILANTOW (1966): *Structure of the Crust and the Upper Mantle in the Alps from Phase Velocity of Rayleigh Waves*. Bulletin of the Seismologic Society of America, Vol. 56, Nr. 5, pp. 1009-1044.
- KORN, M. (1987): *Computation of Wavefields in Vertically Inhomogeneous Media by a Frequency Domain Finite-Difference Method and Application to Wave Propagation in Earth Models with Random Velocity and Density Perturbations*. Geophys. J. R. astr. Soc., Vol. 88, pp. 245-377.
- KRARUP, T. (1969): *A Contribution to the Mathematical Foundation of Physical Geodesy*. Report No. 44, Geodetic Institute, Copenhagen.
- KRARUP, T. (1970): *On Determination of Reasonable Distribution of Masses Corresponding to a Potential Harmonic Outside a Closed Surface*. Letter to the Members of IAG Special Study Group 4.31.
- LAMBECK, K. (1976): *Lateral Density Anomalies in the Upper Mantle*. J. Geophys. Res., Vol. 81, pp. 6333-6340.
- LAMBECK, K. (1988): *Geophysical Geodesy*. Clarendon Press, Oxford.
- LANDAU, H., K. HEHL, B. EISSFELLER, G.W. HEIN (1988): *OPERA 2.4 - User's Guide*. In: Landau, H., K. Hehl, B. Eissfeller, G.W. Hein, W.I. Reilly (Eds.): *Operational Geodesy Software Packages*. Schriftenreihe Studiengang Vermessungswesen, Universität der Bundeswehr München, Vol. 34, pp. 5-250, Neubiberg.

- LANDOLT-BÖRNSTEIN (1982): *Gruppe V: Geophysik und Weltraumforschung*. Ed.: G. Angenheister. Springer-Verlag, Berlin, Heidelberg, New York.
- LEWIS, B.T.R., L.M. DORMAN (1970): *Experimental Isostasy. 2. An Isostatic Model for the U.S.A. Derived from Gravity and Topographic Data*. J. Geophys. Res., Vol. 75, pp. 3367-3386.
- LIEBERMANN, R.C., A.E. RINGWOOD (1973): *Birch's Law and Polymorphic Phase Transformations*. J. Geophys. Res., Vol. 78, pp. 6926-6932.
- MARTINEC, Z., K. PĚČ (1986a): *Normal Earth Models*. Studia geoph. et geod., Vol. 30, pp. 129-147.
- MARTINEC, Z., K. PĚČ (1986b): *Three-Dimensional Density Distribution Generating the Observed Gravity Field of Planets. Part I. The Earth*. Proc. Int. Symp. Figure and Dynamics of the Earth, Moon, and Planets, Prague, Czechoslovakia, Sept. 15-20, 1986, pp. 129-152.
- MATYSKA, C. (1987): *The Inverse Gravimetric Problem: Existence, Uniqueness, and Stability of the Solution*. Studia geoph. et geod., Vol. 31, pp. 252-257.
- McNUTT, M. (1980): *Implications of Regional Gravity for State of Stress in the Earth's Crust and Upper Mantle*. J. Geophys. Res., Vol. 85, pp. 6377-6396.
- MEISSNER, R. (1986): *The Continental Crust - A Geophysical Approach*. Int. Geophys. Ser. 34, Academic Press, Orlando.
- MEISSNER, R., T. WEVER, E.R. FLÜH (1987): *The Moho in Europe - Implications for Crustal Development*. Annales Geophysicae 5B (4), pp. 357-364.
- MESHCHERYAKOV, G.A., N.F. AGEYEV, M.M.FYS (1986): *On the Spheroidal Normal Earth*. Proc. Int. Symp. Figure and Dynamics of the Earth, Moon, and Planets, Prague, Czechoslovakia, Sept. 15-20, 1986, pp. 95-117.
- MILLER, H., J. ANSORGE, K. ARIC, G. PERRIER (1978): *Preliminary Result of the Lithospheric Seismic Alpine Longitudinal Profile 1975, from France to Hungary*. In: Closs, Roeder, Schmidt (Eds.): Alps, Apeninnes, Hellenides, Schweizerbart'sche Verlagsbuchhandlung, Stuttgart, pp. 33-39.
- MILLER, H., S. MÜLLER, G. PERRIER (1982): *Structure and Dynamics of the Alps*. In: Berckhemer, Hsü (Eds.): Alpine Mediterranean Geodynamics, Geodynamics Series Vol. 7, AGU Washington DC, pp. 175-203.
- MÖRNER, N.A. (Ed., 1980): *Earth's Rheology, Isostasy and Eustasy*. John Wiley and Sons, New York.
- MORELLI, C. (1986): *Deep Crustal Knowledge in Italy*. In: Baranzangi, Brown (Eds.): Reflection Seismology: A Global Perspective, Geodynamics Series Vol. 13, AGU Washington DC, pp. 161-165.
- MORITZ, H. (1977): *Least-Squares Collocation and the Gravitational Inverse Problem*. J. Geophys., Vol. 43, pp. 153-162.
- MORITZ, H. (1989): *The Gravitational Inverse Problem. General Aspects and a Solution for the Sphere*. Presented at the II. Hotine-Marussi Symposium on Mathematical Geodesy, Pisa, Italy, June 5-8, 1989.

- MOSTAANPOUR, M.M. (1984): *Einheitliche Auswertung krustenseismischer Daten in Westeuropa – Darstellung von Krustenparametern und Laufzeitanomalien*. Berliner Geowissenschaftliche Abhandlungen, Series B, No. 10, Verlag Dietrich Reimer, Berlin.
- MÜLLER, S. (1982): *Deep Structure and Recent Dynamics in the Alps*. In: Hsü (Ed.): *Mountain Building Processes*, Academic Press, London, New York, pp. 181–199.
- MÜLLER, S. (1984): *Tiefenstruktur, Dynamik und Entwicklung des Mittelmeer- und Alpenraumes*. Vierteljahresschrift d. Naturforschenden Gesellschaft in Zürich, 129/3, pp. 217–245.
- MÜLLER, S., J. ANSORGE (1986): *Long-Range Seismic Refraction Profiles in Europe*. In: Baranzangi, Brown (Eds.): *Reflection Seismology: A Global Perspective*, Geodynamics Series Vol. 13, AGU Washington DC, pp. 167–182.
- MÜLLER, S., J. ANSORGE, R. EGLOFF, E. KISSLING (1980): *A Crustal Cross Section Along the Swiss Geotraverse from the Rhinegraben to the Po-Plain*. *Eclogae Geol. Helvet.*, Vol. 73/2, pp. 463–485.
- MÜLLER, S., R. EGLOFF, J. ANSORGE (1976): *Struktur des tieferen Untergrundes entlang der Schweizer Geotraverse*. *Schweiz. Mineral.-Petrol. Mitteilungen*, No. 56, pp. 685–692.
- MÜLLER, S., W. LOWRIE (1980): *Die geodynamische Entwicklung des westlichen Mittelmeerraumes und der Alpen*. *Vermessung, Photogrammetrie, Kulturtechnik*, 12/80, pp. 469–495.
- MÜLLER, S., C. SPRECHER (1978): *Upper Mantle Structure Along a Profile Through the Eastern Alps from Rayleigh Wave Dispersion*. In: Closs, Roeder, Schmidt (Eds.): *Alps, Apennines, Hellenides*, Schweizerbart'sche Verlagsbuchhandlung, Stuttgart, pp. 40–44.
- PANZA, G.F. (1981): *The Resolving Power of Seismic Surface Waves*. In: Cassinis (Ed.): *The Solution of the Inverse Problem in Geophysical Interpretation*, Plenum Press, New York, pp. 39–77.
- PANZA, G.F., S. MÜLLER (1979): *The Plate Boundary Between Eurasia and Africa in the Alpine Area*. *Mem. Sci. geol.* 33, pp. 43–50.
- PANZA, G.F., S. MÜLLER, G. CALCAGNILE (1980): *The Gross Features of the Lithosphere-Asthenosphere System in Europe from Seismic Surface Waves and Body Waves*. *Pageoph.* 118, pp. 1209–1213.
- PĚČ, K., Z. MARTINEC (1984): *Constraints to the Three-Dimensional Non-Hydrostatic Density Distribution in the Earth*. *Studia geoph. et geod.*, Vol. 28, pp. 264–379.
- PĚČ, K., Z. MARTINEC (1985): *An Analytical Model of Seismic Travel Times for a Spherically Asymmetric Earth*. *Studia geoph. et geod.*, Vol. 29, pp. 220–227.
- PĚČ, K., Z. MARTINEC (1988): *Gravitational Potential Inside 3-D Inhomogeneous Earth: A Boundary-Value Problem for the Poisson Equation*. *Studia geoph. et geod.*, Vol. 32, pp. 32–46.
- PERRIER, G., J.C. RUEGG (1973): *Structure profonde du Massiv Central Française*. *Ann. Geophys.*, Vol. 29, pp. 435–502.
- PLAUMANN, S. (1987): *Karte der Bouguer-Anomalien in der BRD*. *Geolog. Jahrbuch*, Reihe E, No. 40, pp. 3–7 & map.

- PRESS, W.H., B.P. FLANNERY, S.A. TEUKOLSKY, W.T. VETTERLING (1986): *Numerical Recipes – the Art of Scientific Computing*. Cambridge University Press, Cambridge, New York, New Rochelles, Melbourne, Sidney.
- RAPP, R.H., J.Y. CRUZ (1986): *Spherical Harmonic Expansions of the Earth's Gravitational Potential to Degree 360 using 30' Mean Anomalies*. Dept. of Geodetic Science and Surveying, Rep. No. 376, The Ohio State University, Columbus, OH.
- RAST, N., F.U. DELANY (Eds., 1983): *Profiles of Orogenic Belts*. Geodynamics Series Vol. 10, AGU, Washington DC.
- RAYNA, G. (1987): *REDUCE. Software for Algebraic Computation*. Springer Verlag, New York, Berlin, Heidelberg.
- RICARD, Y., L. FLEITOUT, C. FROIDEVAUX (1984): *Geoid Heights and Lithospheric Stresses for a Dynamic Earth*. Annales Geophysicae, Vol. 2, pp. 267–286.
- RUMMEL, R., R.H. RAPP, H. SÜNKEL, C.C. TSCHERNING (1988): *Comparisons of Global Topographic Isostatic Models to the Earth's Observed Gravity Field*. Dept. of Geodetic Science and Surveying, Rep. No. 388, The Ohio State University, Columbus, OH.
- RYBACH, L., G. BUNTEBARTH (1982): *Relationships Between the Petrophysical Properties Density, Seismic Velocity, Heat Generation, and Mineralogical Constitution*. Earth and Planetary Science Letters, Vol. 57, pp. 367–376.
- SANSÒ, F. (1980): *Internal Collocation*. Mem. Atti. Accad. Naz. Lincei, Ser. VIII, XVI, Fasc. 1.
- SANSÒ, F., C.C. TSCHERNING (1982): *Mixed Collocation: A Proposal*. Quaterniones Geodaesiae, Vol. 3/1, pp. 1–15.
- SANSÒ, F., R. BARZAGHI, C.C. TSCHERNING (1986): *Choice of Norm for the Density Distribution of the Earth*. Geophys. J. R. astr. Soc., Vol. 87, pp. 123–141.
- SCHWENDENER, M., S. MÜLLER (1985): *New Evidence for a Density Anomaly in the Upper Mantle below the Southern Alps*. In: Second EGT Workshop: The Southern Segment, Strasbourg, pp. 115–120.
- SCHMIDT, R., D. EHLERT (1982): *Die Diagnoseausgleichung 1980 des Deutschen Hauptdreiecksnetzes, Bd. I Problemstellung, Richtungen*. Deutsche Geodätische Kommission, Reihe B, No. 262.
- SIDERIS, M.G. (1984): *Computation of Gravimetric Terrain Correction Using Fast Fourier Transform Techniques*. Report 20007, Department of Surveying Engineering, University of Calgary.
- STEINHAUSER, P., H. GRANSER, K. HÖSCH, D. ZYCH (1983): *Über das Dichtemodell in Österreich*. In: Geodätische Arbeiten Österreichs für die Intern. Erdmessung, Neue Folge, Band III, pp. 159–183.
- STEINHAUSER, P., A. PUSTIZEK (1987): *Estimation of the Mass Deficit of the Eastern Alps*. Geodätische Arbeiten Österreichs für die Intern. Erdmessung, Neue Folge, Band IV, pp. 111–125.

- STRYKOWSKI, G. (1989): *A Study of Statistical Properties of the Earth's Density Distribution Based on Density Logs from the North Sea*. Pres. at the II Hotine-Marussi Symposium on Mathematical Geodesy, Pisa, Italy, June 5-8, 1989.
- SÜNKEL, H. (1986): *Konventionelle und moderne Verfahren zur Ableitung orthometrischer Höhen*. Österr. Zeitschrift für Vermessungswesen und Photogrammetrie, Vol. 74, pp. 77-93.
- SÜNKEL, H. (1986): *Global Topographic-Isostatic Models*. In: Sünkel, H. (Ed.): *Mathematical and Numerical Techniques in Physical Geodesy*, Lecture Notes in Earth Sciences, Vol. 7, pp. 417-462, Springer-Verlag, Berlin, Heidelberg, New York.
- SÜNKEL, H., N. BARTELME, H. FUCHS, M. HANAFY, W.-D. SCHUH, M. WIESER (1987): *The Gravity Field in Austria*. In: *Geodätische Arbeiten Österreichs für die Intern. Erdmessung*, Neue Folge, Band IV, pp. 47-75.
- SUHADOLC, P., G.F. PANZA (1988): *Physical Properties of the Lithosphere-Asthenosphere System in Europe from Geophysical Data*. Preprint, private communication.
- SZABO, B. (1986): *The Estimation of the Earth's Gravity Field*. Dept. of Geodetic Science and Surveying, Rep. No. 369, The Ohio State University, Columbus, OH. AFGL-TR-86-0125, ADA172177.
- TARANTOLA, A. (1987): *Inverse Problem Theory*. Elsevier, Amsterdam.
- TORGE, W., G. WEBER, H.-G. WENZEL (1983): *6' x 10' Free Air Gravity Anomalies of Europe Including Marine Areas*. Paper presented at the XVIII IUGG General Assembly, Hamburg, F.R.Germany.
- TSCHERNING, C.C. (1974): *Some Simple Methods for the Unique Assignment of a Density Distribution to a Harmonic Function*. Dept. of Geodetic Science and Surveying, Rep. No. 213, The Ohio State University, Columbus, OH. AFCRL-TR-74-0506, ADA006026.
- TSCHERNING, C.C. (1976): *A Mass Density Covariance Function Consistent with the Covariance Function of the Anomalous Potential*. Boll. Geod. Sci. Aff., Vol. XXXV, No. 2, pp. 161-172.
- TSCHERNING, C.C. (1977): *Models for the Auto- and Cross Covariances between Mass Density Anomalies and First and Second Order Derivatives of the Anomalous Potential of the Earth*. Proc. 3rd Int. Symp. "Geodesy and Physics of the Earth", Weimar, Oct. 1976, pp. 261-268, Potsdam.
- TSCHERNING, C.C. (1979): *Gravity Prediction Using Collocation and Taking Known Mass Density Anomalies into Account*. Geophys. J. R. astr. Soc., Vol. 59, pp. 147-153.
- TSCHERNING, C.C. (1989): *Density-Gravity Covariance Functions Produced of Overlapping Rectangular Blocks of Constant Density*. Presented at the II. Hotine-Marussi Symposium on Mathematical Geodesy, Pisa, Italy, June 5-8, 1989.
- TSCHERNING, C.C., R. RAPP (1974): *Closed Covariance Expression for Gravity Anomalies, Geoid Undulations, and Deflections of the Vertical Implied by Anomaly Degree Variance Models*. The Ohio State University, Department of Geodetic Sciences, Report No. 208, Columbus, OH. AFCRL-TR-74-0231, AD786417.

- TSCHERNING, C.C., G. STRYKOWSKI (1988): *Quasi-Harmonic Inversion of Gravity Field Data*. In: Vogel, A. (Ed.): *Model Optimization in Exploration Geophysics 2*, pp. 137–154, Friedrich Vieweg & Sohn, Braunschweig, Wiesbaden.
- TSCHERNING, C.C., H. SÜNKEL (1981): *A Method for the Construction of Spheroidal Mass Distributions Consistent with the Harmonic Part of the Earth's Gravity Field*. *Manuscripta Geodaetica*, Vol. 6, pp. 131–156.
- TURCOTTE, D.L., G. SCHUBERT (1982): *Geodynamics*. John Wiley & Sons, New York.
- VASSILIOU, A.A., SCHWARZ, K.P. (1987): *On the Combination of Gravity Data with other Geophysical Data for the Solution of the Inverse Gravimetric Problem*. Paper presented at the XIX IUGG General Assembly, Vancouver, Canada
- VIEL, L. (1987): *Untersuchung der Lithosphärenwurzel unter den Alpen mit Hilfe teleseismischer Laufzeitresiduen*. Diplomarbeit Di203, Inst. f. Meteorologie und Geophysik, Universität Frankfurt.
- VIGNY, R.Y., C. FROIDEVAUX (1988): *Mantle Heterogeneities, Geoid and Plate Motion. A Monte-Carlo Inversion*. Submitted to *J. Geophys. Res.*
- WALACH, G. (1987): *A Digital Model of Surface Rock Densities of Austria and the Alpine Realm*. In: *Geodät. Arbeiten Österreichs für die Intern. Erdmessung, Neue Folge, Band IV*, pp. 3–9.
- WIESER, M. (1987): *Das Globale Digitale Höhenmodell TUG87 – Aufbau, Entstehung und Merkmale*. Internal Report of the Institute of Mathematical Geodesy, Technical University Graz, Austria.
- WIGGER, P.J. (1984): *Die Krustenstruktur des Nordappennins und angrenzender Gebiete mit besonderer Berücksichtigung der geothermischen Anomalie der Toskana*. *Berliner geowissenschaftliche Abhandlungen, Reihe B, Heft 9*, Verlag Dietrich Reimer, Berlin.
- WILCOX, L.E. (1974): *An Analysis of Gravity Prediction Methods for Continental Areas*. DMAAC Reference Publication, No. 74-001.
- WILL, M., H. MILLER, H. GEBRANDE (1978): *Upper Crustal Structure in the Northern Alps Derived from Seismic Refraction Measurements*. In: Closs, Roeder, Schmidt (Eds.): *Alps, Apennines, Hellenides*, Schweizerbart'sche Verlagsbuchhandlung, Stuttgart, pp. 80–82.
- WOODHOUSE, J.H., A.M. DZIEWONSKI (1984): *Mapping the Upper Mantle: Three-Dimensional Modeling of Earth Structure by Inversion of Seismic Waveforms*. *J. Geophys. Res.*, Vol. 89, pp. 5953–5986.
- WOOLLARD, G.P. (1975): *Regional Changes in Gravity and their Relation to Crustal Parameters*. *Bureau Gravimétric International., Bull. d'Information*, 36, pp. 106–110.